DAMAGE CONSIDERATIONS OF A FLEXIBLE MICRO AIR VEHICLE WING USING 3-D LASER VIBROMETRY

THESIS

Leo L. Mendoza Jr., ENS, USN

AFIT/GAE/ENY/07-J13

DEPARTMENT OF THE AIR FORCE
AIR UNIVERSITY

AIR FORCE INSTITUTE OF TECHNOLOGY

Wright-Patterson Air Force Base, Ohio

AFIT/GAE/ENY/07-J13

DAMAGE CONSIDERATIONS OF A FLEXIBLE MICRO AIR VEHICLE WING USING 3-D LASER VIBROMETRY

THESIS

Presented to the Faculty

Department of Aeronautical and Astronautical Engineering

Air Force Institute of Technology

Air University

Air Education and Training Command

In Partial Fulfillment of the Requirements for the

Degree of Master of Science in Aeronautical Engineering

Leo Lopez Mendoza Jr., BS

Ensign, USN

June 2007

AFIT/GAE/ENY/07-J13

DAMAGE CONSIDERATIONS OF A FLEXIBLE MICRO AIR VEHICLE WING USING 3-D LASER VIBROMETRY

Leo L. Mendoza Jr., B.S.
ENS, USN

Approved:

//SIGNED//	
Dr. Anthony N. Palazotto (Chairman)	date
//SIGNED//	
Dr. Richard G. Cobb (Member)	date
//SIGNED//	
Dr. Donald L. Kunz (Member)	date

Abstract

In recent years there has been a major push towards a new class of unmanned aerial vehicles: micro air vehicles. A great amount of research has been done towards the aerodynamics, aeroelasticity, construction, and flight characteristics of flexible wing micro air vehicles. However, there has not been much research done regarding possible structural deficiencies of a flexible micro air vehicle wing. The focus of this research is to evaluate the effects of damage on a flexible micro air vehicle wing, particularly its natural frequencies and mode shapes, using three dimensional laser vibrometry. The flexible micro air vehicle wing studied was based on a University of Florida micro air vehicle wing design and was examined using measurements from the Polytec 400-3D Scanning Vibrometer. Comparisons of the wing's natural frequencies and displacements were made between the wing's undamaged and damaged states.

Acknowledgements

I would like to express my gratitude to my thesis advisor, Dr. Anthony Palazotto, for his support throughout this endeavor and Dr. Philip Beran AFRL for sponsoring this project. I would also like to thank AFIT laboratory staff members John and Jay for their help through equipment malfunctions and setup. Additionally, I would like to thank Sean Hollands and Michael Stone of Polytec for their assistance in testing. Finally, I would like to thank my family and Christle for their constant support and words of encouragement.

Table of Contents

Page

Page

List of Figures

Page

Page

Page

List of Tables

Page

Nomenclature

AOA	Angle of Attack
FFT	Fast Fourier Transform
FRF	Frequency Response Function
LDV	Laser Doppler Vibrometer
MAV	Micro Air Vehicle
PSV	Polytec Scanning Vibrometer
UAV	Unmanned Aerial Vehicle

DAMAGE CONSIDERATIONS OF A FLEXIBLE MICRO
AIR VEHICLE WING USING 3-D LASER VIBROMETRY

1. Introduction

1.1 Background

In recent years, there has been a major push towards a new class of unmanned aerial vehicles (UAVS): micro air vehicles (MAV). MAVs have been defined by the Defense Advanced Research Projects Agency as "fully functional, military capable, small flight vehicles of size less than 15 cm in length, width, or height" (Malolan, 2004:1). Additionally, the gross takeoff weight (GTOW) must be approximately 200 g or less (Pines and Bohorquez, 2006:290). This restriction in size and weight puts MAVs, at the minimum, an order of magnitude smaller than traditional UAVs. In addition, the goal is to make these vehicles affordable and easy to produce (McMichael, 1997). With their size, capabilities, and price, MAVs are certainly deployable at platoon levels and capable of completing missions in surveillance, target acquisition, and bio-chemical sensing. Additionally, MAVs can operate in a variety of environments whether over wide open land and water or buildings, tunnels, or other confined areas (Pines and Bohorquez, 2006:291).

The design and development of MAVs is not without problems. One challenge facing MAVs is that they operate in a low, very sensitive Reynolds number regime, one more common to small birds and large insects (Pines and Bohorquez, 2006:290; McMichael, 1997). Various complex flow phenomena can occur within the boundary in this Reynolds number regime. Furthermore, separation, transition, and reattachment of the flow can all occur within short distances along the chord line of a wing. Since MAVs are so small, this can have a significant impact on the effectiveness of the lifting surface (Pines and Bohorquez, 2006:290). Another

challenge is the lack of knowledge on the flow physics in this Reynolds number regime. For example, small birds and large insects are able to generate forces from 2 to 12 times their bodyweight. Conventional steady-state aerodynamic theory cannot explain this phenomenon (Pines and Bohorquez, 2006:294). Another problem is lack of available analysis tools to assist MAV designers model the steady and unsteady flow MAVs encounter while flying (Pines and Bohorquez, 2006:290).

MAVs are expected to fly at speeds of 25 mph or less. At these flight speeds with an aircraft this small, a sudden gust of wind can change the flight Reynolds number more than 30%, resulting in a highly unsteady flight regime. Studies have shown that allowing the lifting surface to move and deform leads to more favorable aerodynamic performance in the unsteady low Reynolds number regime (Ifju and others, 2002:2). Because of this, a flexible wing MAV concept is desirable.

A great amount of research has been done towards the aerodynamics, aeroelasticity, construction, and flight characteristics of a flexible MAV wing. However, there has not been much research done from a structural point of view. Possible structural deficiencies of flexible micro air vehicle wings have not been investigated.

1.2 Research Objectives

This research investigates the changes of a flexible MAV wing's dynamic properties, particularly its natural frequencies and mode shapes, under damaged conditions. Modal data of the damaged wing will be evaluated against previous tests before damage was applied to the wing. The wing's natural frequencies and mode shapes will be measured with the Polytec PSV 400-3D Scanning Vibrometer.

2. Polytec Scanning Vibrometer Theory

The major component that will be used for evaluating the structural dynamic properties of the flexible MAV wing is the Polytec PSV 400-3D Scanning Vibrometer. The Polytec PSV 400-3D works by the principle of laser Doppler interferometry. A laser vibrometer measures the velocity of an object's movement by detecting the Doppler shift of coherent laser light as it is scattered from a test object (Polytec Vibrometry, 2007).

2.1 Laser Doppler Vibrometer

2.1.1 The Doppler Effect

The Doppler Effect is a change in frequency of a propagating wave perceived by the observer when there is relative movement between the source and receiver. The following is a graphical representation of the Doppler principle.

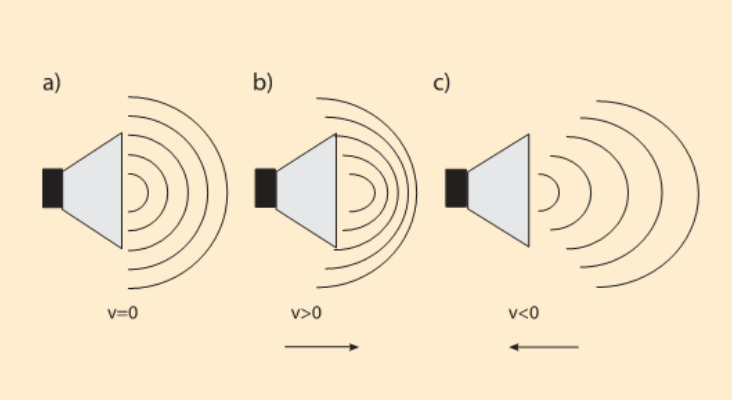

Figure 1: The Doppler Effect

In Figure 1, a wave source (loudspeaker) is shown in three cases: (a) at rest, (b) moving to the right, and (c) moving to the left. In the first case (a), an observer will hear a frequency corresponding to the frequency emitted by the loudspeaker. In the second case (b), an observer will hear a higher frequency as the waves are heard in shorter intervals. In the third case (c), the

observer will hear a lower frequency as the loudspeaker moves away. This change in frequency is the Doppler frequency shift. The frequency shift is calculated by the equation:

$$f_D = 2 \cdot \frac{|v|}{\lambda} \tag{1}$$

where v is the object's velocity and λ is the wavelength of the emitted wave. Therefore, if the Doppler frequency shift is known, as by the Laser Doppler Vibrometer, the velocity can be determined (Polytec Principles, 2003).

2.1.2 Optical Interferometry

Polytec's Laser-Doppler vibrometers work on the basis of optical interference, carried out using a modified Mach-Zehnder interferometer (Polytec Principles, 2003). Optical interference requires two coherent light beams and their respective light intensities to overlap. The resulting intensity of the two beams is determined by the equation:

$$I_{tot} = I_1 + I_2 + 2\sqrt{I_1 I_2}\cos\left[2\pi\left(r_1 - r_2\right)/\lambda\right] \tag{2}$$

where I_1 is the intensity of beam 1, I_2 is the intensity of beam 2, r_1 is the path length of beam 1, and r_2 is the path length of beam 2. In equation (2), the term $2\sqrt{I_1 I_2}\cos\left[2\pi\left(r_1 - r_2\right)/\lambda\right]$ is referred to as the "interference" term, which relates the difference between beams 1 and 2 (Polytec Principles, 2003). If the path length difference is an integer multiple of the laser wavelength, the overall intensity is four times a single intensity and the beams are said to interfere constructively. If the difference is half of one wavelength, the overall intensity is zero and the beams are said to interfere destructively. This physical law is manipulated in Polytec's Laser-Doppler vibrometer scanning heads (Polytec Principles, 2003). The schematic in Figure 2 shows the optical configuration of a PSV-I-400 Scanning head.

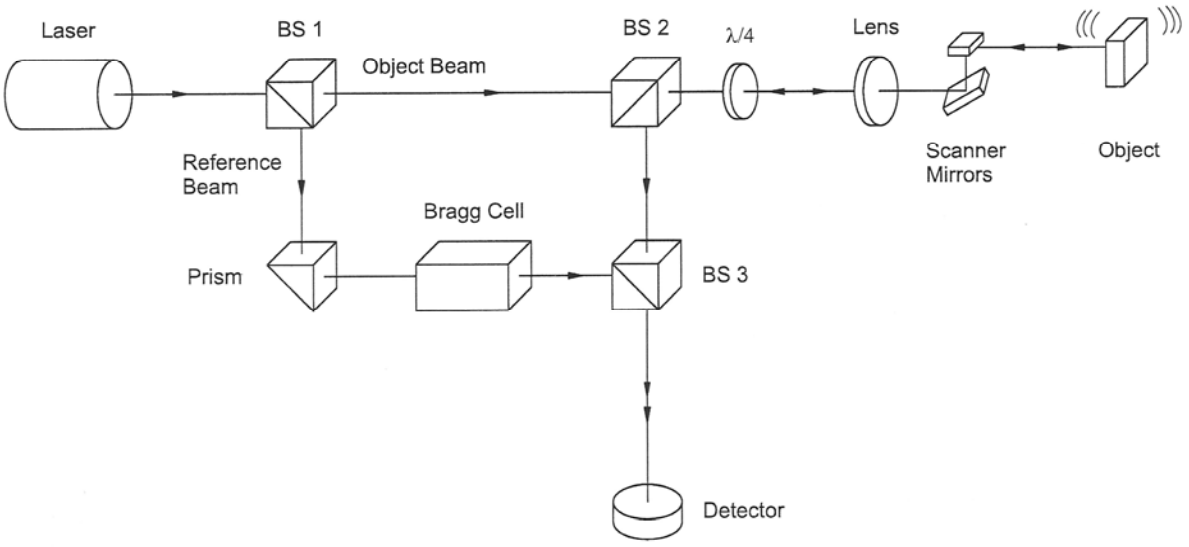

Figure 2: PSV-I-400 Scanning Head Optical Configuration (Polytec Hardware Manual)

The helium neon laser beam is split by the beam splitter (BS 1) into a reference beam and an object, or measurement, beam. After passing through the polarizing beam splitter (BS 2) and λ/4 plate, the object beam is focused by the lens onto the object being measured and is reflected back to the scanning head. The polarizing BS 2 then functions as an optical directional coupler along with the λ/4 plate, deflecting the reflected beam downwards to the third beam splitter (BS 3). This beam is then directed onto the detector (Polytec Hardware Manual:A-3). Since the path length of the reference beam is constant (r_2 = constant), any movement of the object being measured (r_1 = r(t)) generates a dark and bright fringe pattern on the detector. One full dark-bright cycle on the detector corresponds to an object displacement of exactly half of the wavelength of the helium neon laser, which is 316 nm. Therefore, changing the optical path length of the object beam per unit of time records itself as the Doppler frequency shift. As a result, the velocity of the object can be determined through the use of Equation 1 (Polytec Principles, 2003).

2.1.3 Determining the Direction of Movement

While it is possible to determine the magnitude of the velocity of an object, a problem arises with the direction of motion as object movement away from the interferometer generates the same interference pattern and Doppler frequency shift as object movement towards the interferometer. To alleviate this problem, a Bragg Cell is introduced. The Bragg Cell is an acoustico-optic modulator and is placed in the path of the reference beam, which shifts the light frequency by 40 MHz. Doing so generates a modulation frequency on the fringe pattern of 40 MHz when the object is still. If the object moves towards the interferometer, the modulation frequency is reduced. On the other hand, if the object moves away from the interferometer, the detector receives a frequency higher than 40 MHz. As a result, both the magnitude and direction of the object can now be measured (Polytec Hardware Manual:A-3).

2.2 Measuring 3-D Vibration

A single scanning head is only capable of measuring the vibrations of an object along the direction of its laser beam path. In this configuration, only "out-of-plane" movement is measured, shown in Figure 3.

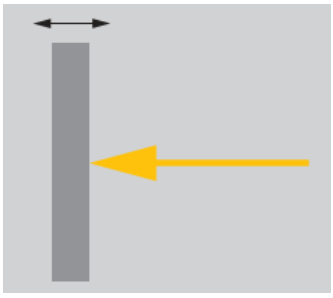

Figure 3: Single Point Vibration

With the PSV 400-3D Scanning Vibrometer, three scanning heads are used. In this configuration, three independent laser beams each measure the velocities of a scan point from

three different locations, shown in Figure 4. Through triangulation, the in-plane as well as out-of-plane vibration of an object is capable of being measured (Polytec Theory Manual:13-6).

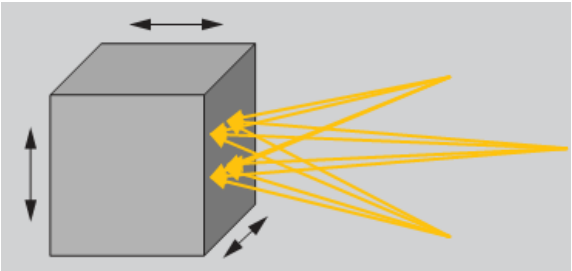

Figure 4: 3-D Vibration Measurement

3. Methodology

This chapter describes the equipment used to capture structural dynamic properties of the flexible MAV wing along with the procedures followed to evaluate how damage affected the wing.

3.1 Equipment

3.1.1 PSV 400-3D Scanning Vibrometer

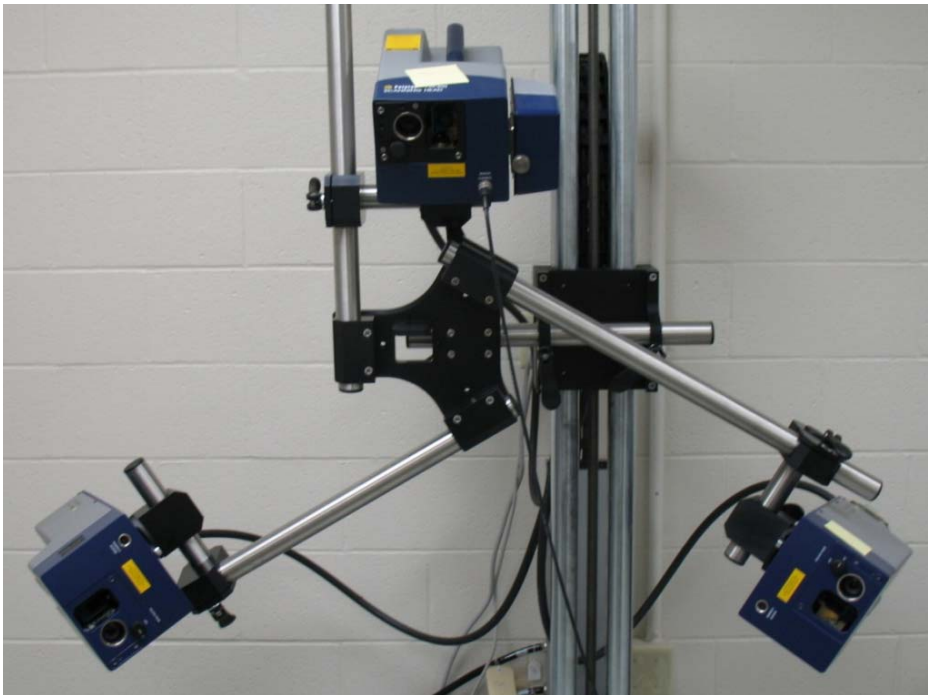

Figure 5: PSV-I-400 Scanning Heads on Motorized Tripod

The PSV 400-3D Scanning Vibrometer allows for precise structural vibration measurements using a non-contact three-dimensional measurement technique. The system consists of three (top, left, and right) PSV-I-400 scanning heads, three OFV-5000 controllers for each sensor head, one PSV-E-400-3D junction box, and one PSV-W-400-3D Data Management System.

The PSV-I-400 Scanning Head incorporates an eye-safe, Class II helium-neon laser with a wavelength of 633 nm and cavity length of 204 mm ± 1 mm. The OFV-5000 Controller has six velocity ranges: 1, 2, 50, 10, 100, and 1000 mm/s/V. It has a 3D Mode bandwidth that ranges from 0 kHz to 80 kHz and an output bandwidth of 1.5 MHz. The PSV-W-400-3D Data Management System has PSV Software 8, the program for data acquisition and presentation. The PSV-E-400-3D Junction Box is the central hub that allows the scanning heads, controllers, and data management system to communicate with one another.

Figure 6: PSV Controllers, Junction Box, and Data Management System

3.1.2 Micro Air Vehicle Flexible Wing

Figure 7: Flexible Micro Air Vehicle Wing

The wing shown in Figure 7 is based on the University of Florida's flexible MAV wing design. The leading edge and center of the wing are constructed of bi-directional composite carbon fiber. The battens, ribs attaching the membrane to the wing, are constructed of unidirectional carbon fiber. The wing has 19 battens on each span of the wing. The leading edge, center, and battens make up the skeleton of the wing. The membrane of the wing is constructed of Icarex, an extensible polyester fabric. The leading edge and battens of the wing have a Young's modulus of 83.85 GPa, Poisson's ratio of 0.0359, and shear modulus of 4.4 GPa. Icarex has a Young's modulus of 1.6 GPa and Poisson's ratio of 0.35.

Table 1: Summary of MAV Wing Dimensions

Span	607.8 mm
Root Chord	153.35 mm
Leading Edge Thickness	0.61 mm
Batten Thickness	0.54 mm
Membrane Thickness	0.19 mm

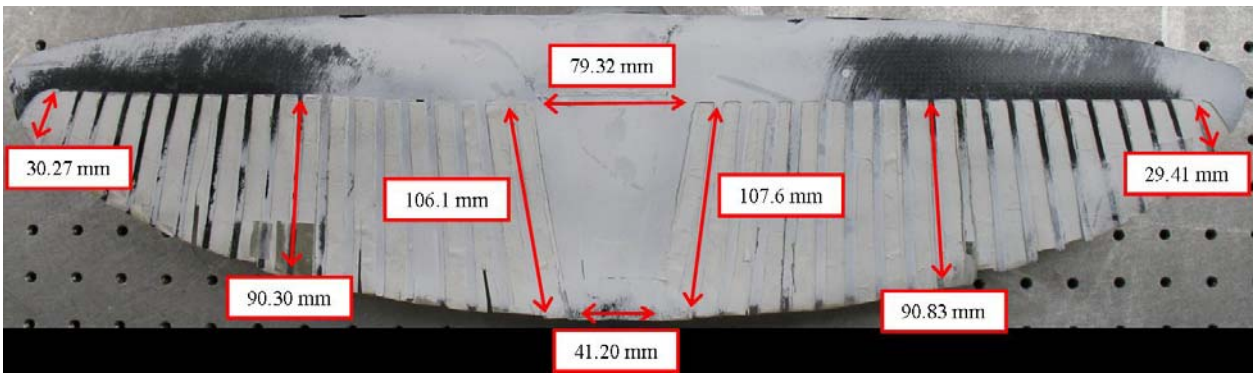

Figure 8: Additional Flexible MAV Wing Dimensions

The flexible MAV wing has a span of 607.8 mm and root chord length of 153.35 mm. The carbon fiber leading edge is 0.61 mm thick and the battens are 0.54 mm thick. The membrane of the wing is 0.19 mm thick. These dimensions are summarized in Table 1. Some additional dimensions of the wing are shown in Figure 8. The center of the wing is 79.32 mm wide at the top and 41.20 mm at the bottom. The first battens on each span are approximately 107 mm each. The ninth battens on each span are approximately 90 mm each. The last battens on each span are approximately 30 mm each. To easily identify areas on the wing the following notation is used: battens are first identified by the span on which they are located, either left (L) or right (R) followed by their number starting from the center of the wing. In addition, the following coordinate system is used: positive x-axis pointing out towards the right span of the

wing, positive y-axis pointing up on top of the wing, and positive z-axis coming out-of-plane towards the reader. The notation and coordinate system can be seen in Figure 9.

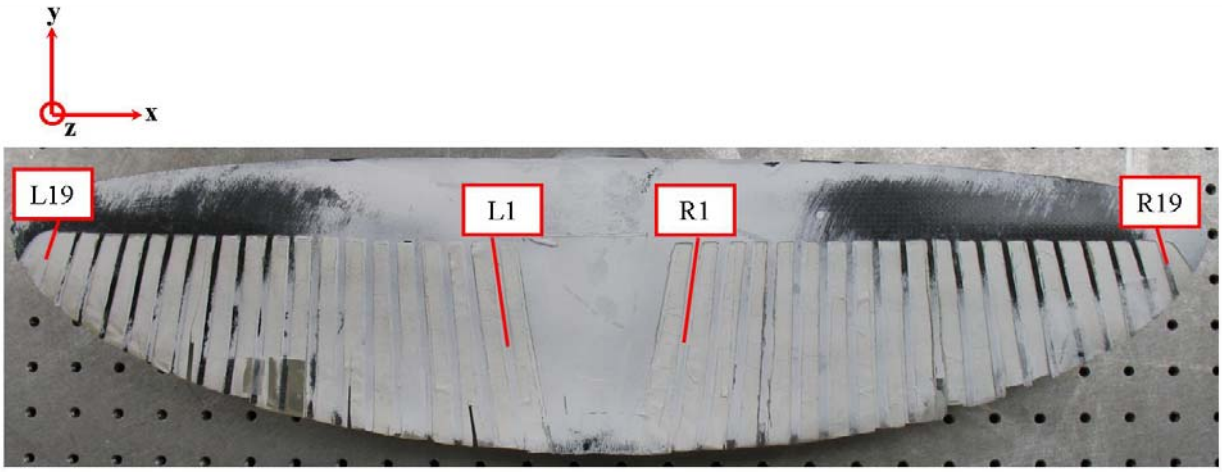

Figure 9: Wing Notation and Coordinate System

The MAV wing has a custom support for mounting on the APS 113 Shaker, shown in Figure 10. The support allows the MAV wing to slide onto the shaker arm and is secured by four bolts.

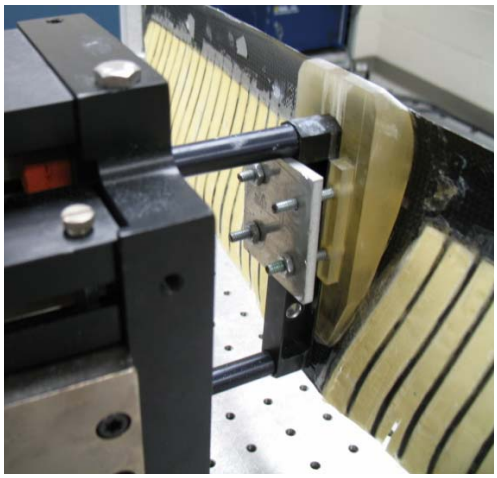

Figure 10: MAV Wing Support

3.1.3 APS 113 Electro-Seis Long Stroke Shaker

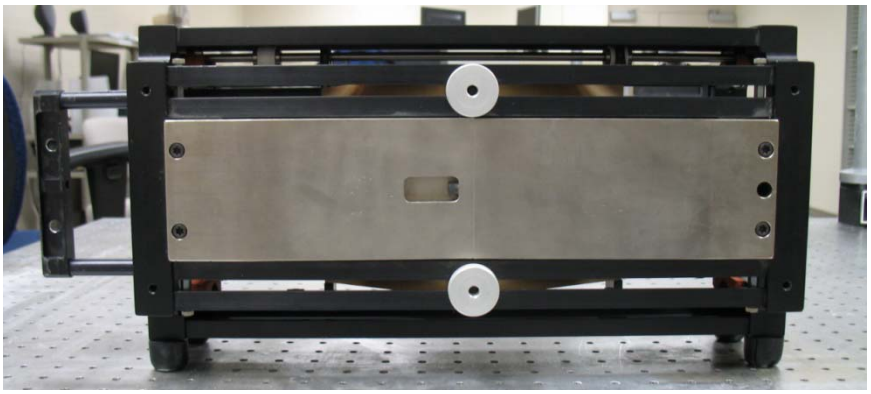

Figure 11: APS Model 113 Electro-Seis Shaker

The APS 113 Electro-Seis Long Stroke Shaker is an electrodynamic force generator for studying dynamic response characteristics of various structures in the seismic frequency range. The APS 113 Shaker can generate sine wave, swept sine wave, random, and impulse force waveforms. It has a maximum force vector of 30 lbs, maximum velocity of 30 in/s, and maximum stroke of 6.25 in. The APS 113 Shaker is rated for frequencies up to 200 Hz.

3.1.4 APS 114 Dual Mode Amplifier

Figure 12: APS Model 114 Dual Mode Amplifier

The APS 114 Dual Mode Amplifier is used to provide driver power for the APS 113 Shaker. It has a power output peak of 250 V and current output peak of 6 A. It also has a frequency range from 0 to 2000 Hz.

3.2 Setup

The MAV wing was secured onto the shaker arm and the shaker was placed approximately 1.8 m from the top scanning head. The APS shaker and amplifier were connected and linked to the PSV Junction Box. The generator output signal from the PSV Junction Box was split: one signal was sent to the amplifier while the other was returned back to the junction box as a reference signal, Ref 1. Figure 13 shows the wing, shaker, and amplifier setup.

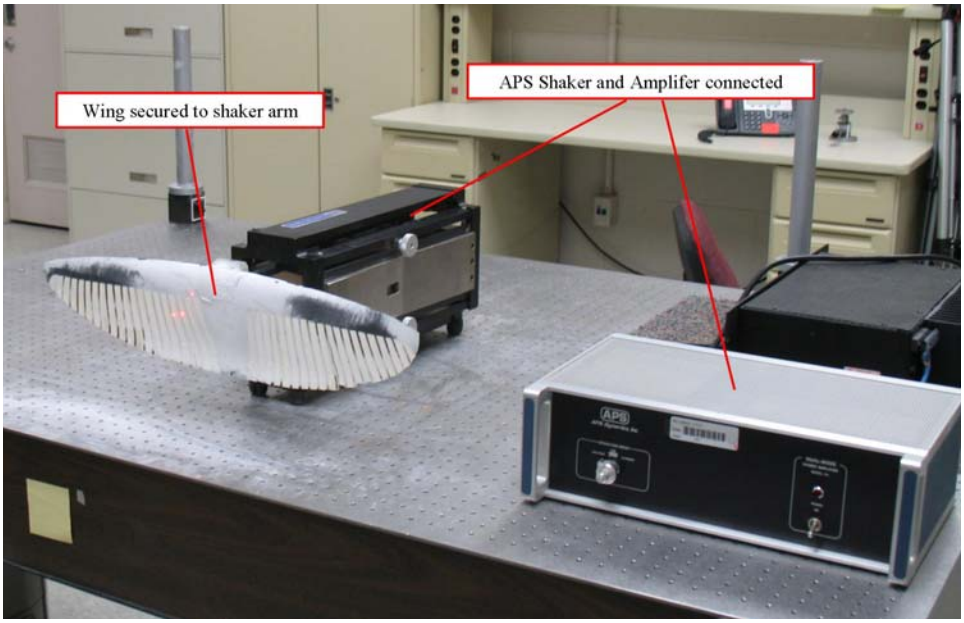

Figure 13: Wing, Shaker, and Amplifier Setup

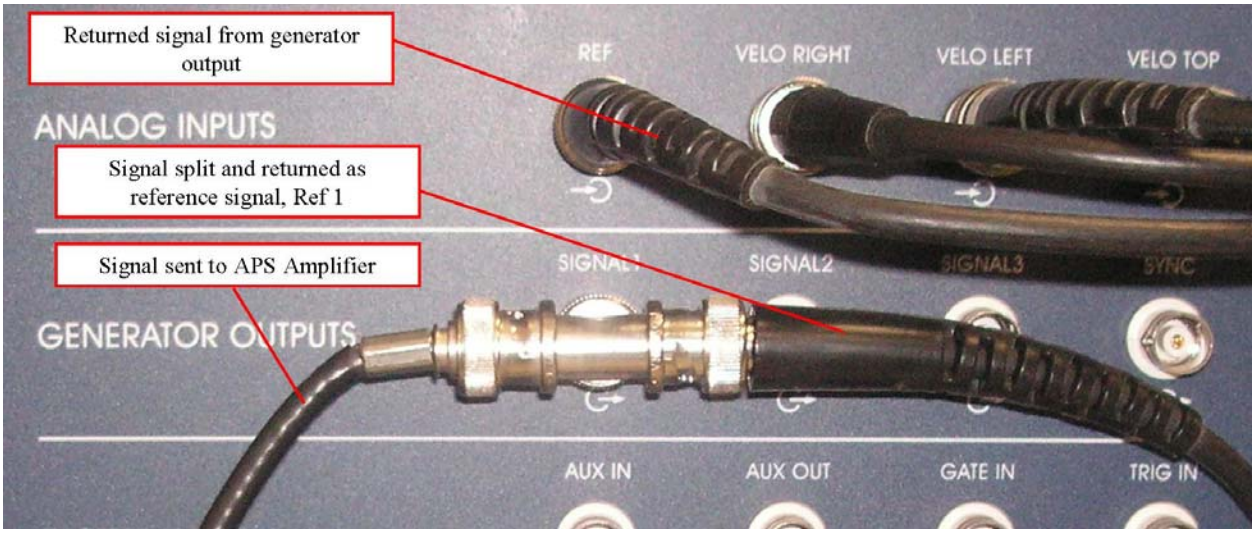

Figure 14: Generator and Reference Signal on Junction Box

Table 2: PSV Software Test Settings

Scan Points	96 (Test 1), 92 (Test 2)
Acquisition Mode	FFT
Averaging	Complex, 40
Bandwidth	100 Hz
FFT Lines	3200
Overlap	66%
Sample Time	32 s
Resolution	31.25 mHz
Window	Rectangle
Vibrometer Range	VD-03 10 mm/s/V
Signal	Periodic Chirp
Amplitude	10 mV

Table 2 shows a summary of the software settings used during testing. The acquisition mode was set to FFT during testing. For averaging, 40 complex averages were used. Averaging improves the clarity of data and accommodates for unwanted noise encountered during testing. 40 complex averages gave the best compromise between data quality and the length of time to perform a scan. 3200 FFT Lines were selected, which allowed for a resolution of 31.25 mHz. A Rectangle window was used in conjunction with a Periodic Chirp generator. A vibrometer range of 10 mm/s/V was selected. An over-range can occur if the magnitude of the velocity being measured is too large for the scanning head or junction box to register. A range of 10 mm/s/V was the smallest range possible to use during these tests without registering an over-range. A complete list of software settings can be found in Appendix A.

3.3 Procedure

Initially, the plan was to compare measurements taken from a completely undamaged flexible MAV wing to a wing that was intentionally damaged. Due to some equipment malfunctions, the next best scenario was to compare measurements from a "least damaged" wing to a wing with more significant damage. Two scans were performed: Test 1, the wing in its least damaged state, and Test 2, the wing after it was severely damaged.

3.3.1 Test 1 Wing Damage

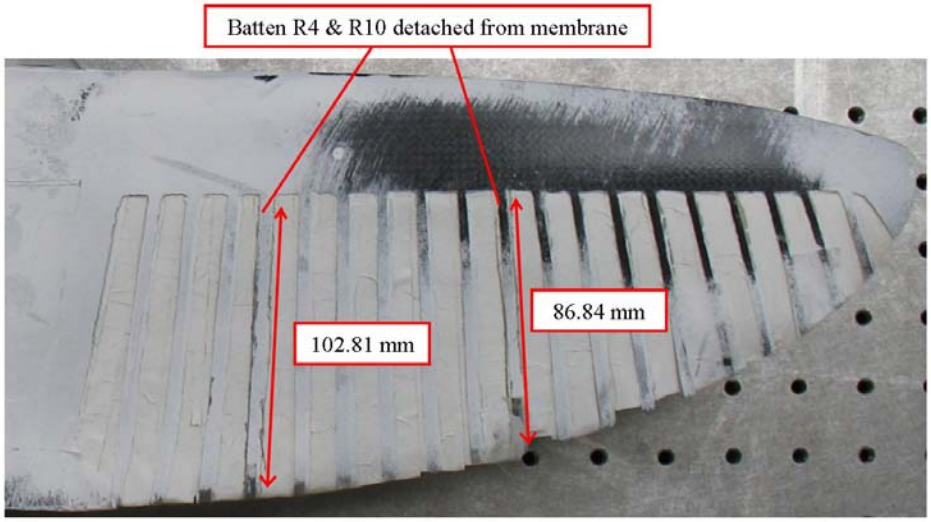

Figure 15: Test 1, Right Span Wing Damage

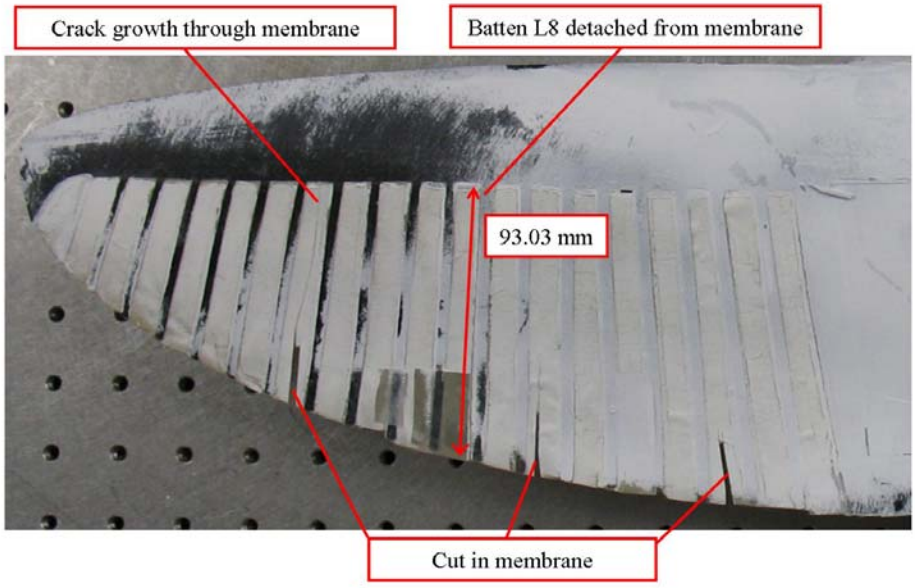

Figure 16: Test 1, Left Span Wing Damage

In Test 1, the right span of the wing had two battens that had detached from the membrane, R4 and R10. Batten R4 is 102.81 mm long and approximately 47 mm from the center of the wing. Batten R10 was 85.84 mm long and approximately 126 mm from the center of the wing. The left span of the wing also had a batten that detached, batten L8. Batten L8 is

93.03 mm long and approximately 93 mm from the center of the wing. There were also three on the membrane and a crack that extended during testing. These three cuts and the crack will be discussed further in Chapter 4. Figure 15 and Figure 16 show damage on the wing during Test 1.

3.3.2 Test 2 Wing Damage

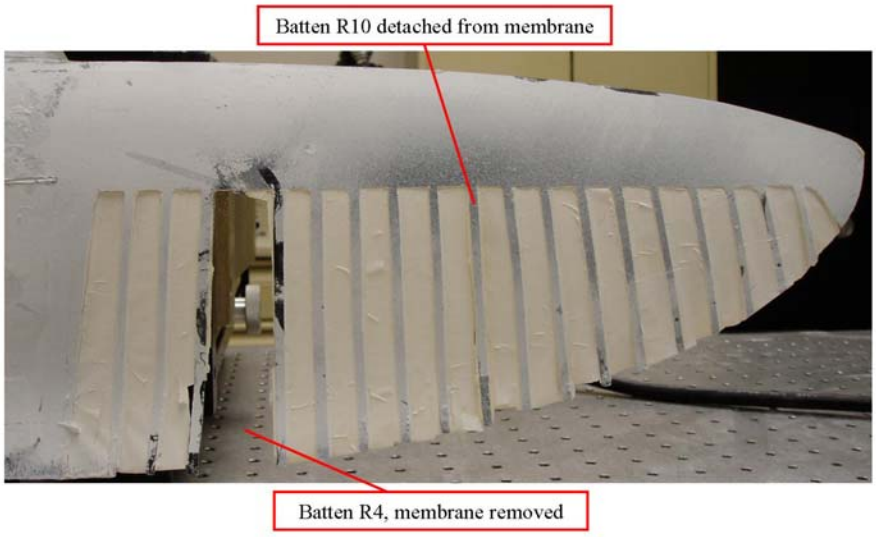

Figure 17: Test 2, Right Span Wing Damage

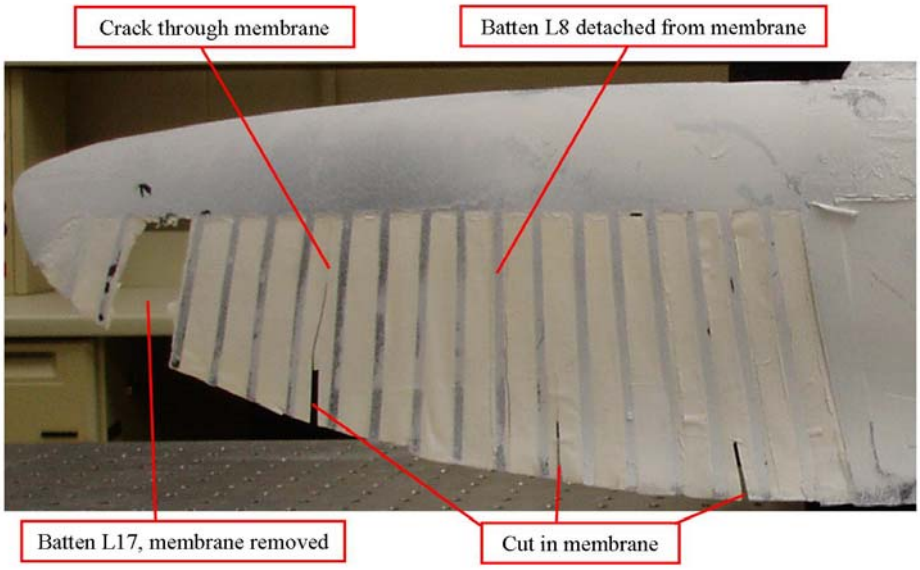

Figure 18: Test 2, Left Span Wing Damage

For Test 2, damage was intentionally applied to the wing. On the right span, batten R10 remained the same as in Test 1. Batten R4 was cut and removed from the wing along with its surrounding membrane. On the left span of the wing, the three cuts in the membrane, extended crack, and detached batten L8 remained the same as in Test 1. Near the tip of the left wing, batten L17 was cut and removed along with its surrounding membrane. Figure 17 and Figure 18 show the damage on the wing during Test 2.

3.4 Data Analysis

PSV Software 8.41 stored the scanning files and was used to carry out the analysis of the modal data. The average spectrum data of the wing between the two tests was used to evaluate the effects of damage on the wing overall. In addition, selected scanning points were used to compare velocities between the wing in Test 1 and Test 2. These scanning points selected will be shown in Chapter 4.

4. Results and Analysis

This chapter will discuss the results from Tests 1 and 2. First, the crack growth and extension on the left span of the wing in Test 1 will be examined. Next, frequency comparisons will be made. Comparisons will be made between the wings in Test 1 and Test 2 as well as individual spans. The third section will involve velocity comparisons between scanning points, giving a more detailed understanding of the damage characteristics.

4.1 Membrane Crack Growth

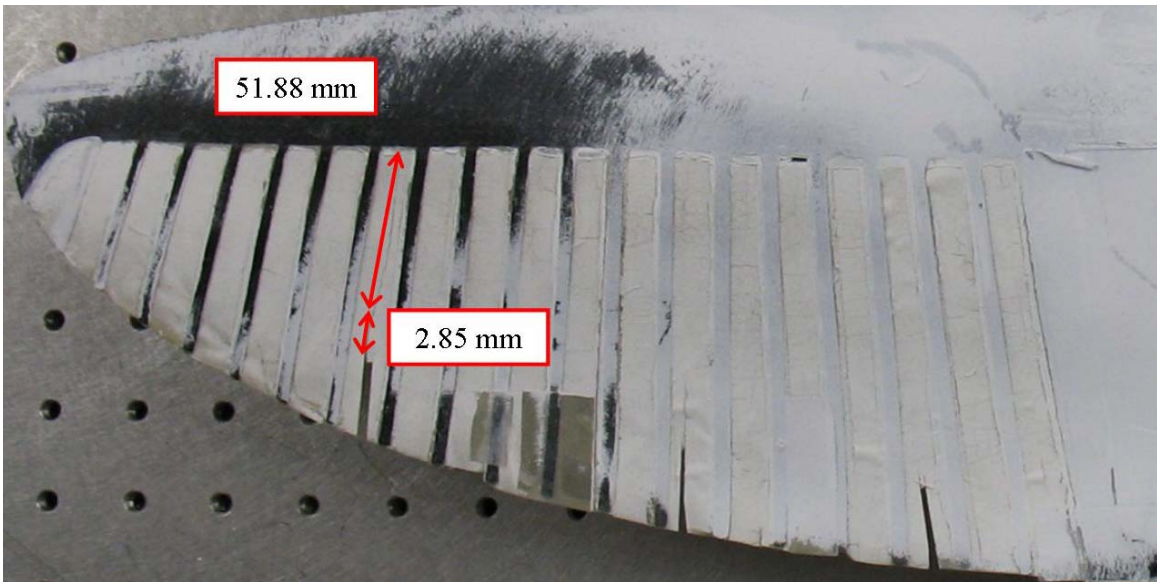

Figure 19: Membrane Crack Dimensions

Before testing, the crack in the membrane was originally 2.85 mm long, a short extension of the intentional cut made into the wing. However, during testing the crack grew to 54.73 mm long, extending all the way to the top of the membrane up to the leading edge of the wing. Because of the complex three dimensional geometry of the wing, the wing encountered three modes of fracture mechanics: Mode I, Mode II, and Mode III.

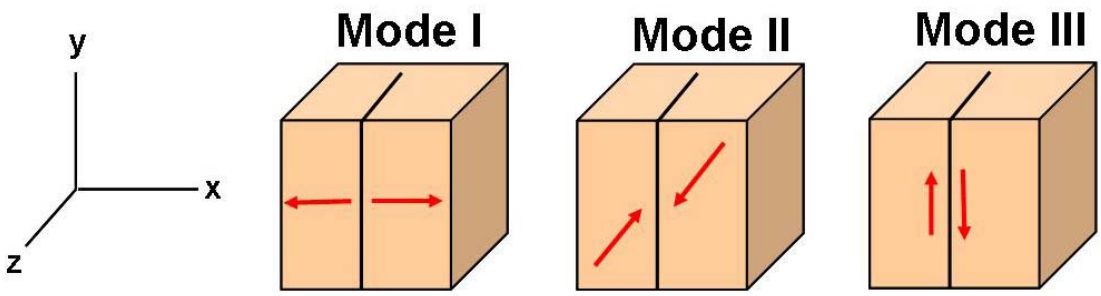

Figure 20: Fracture Mechanics Modes I, II, and III

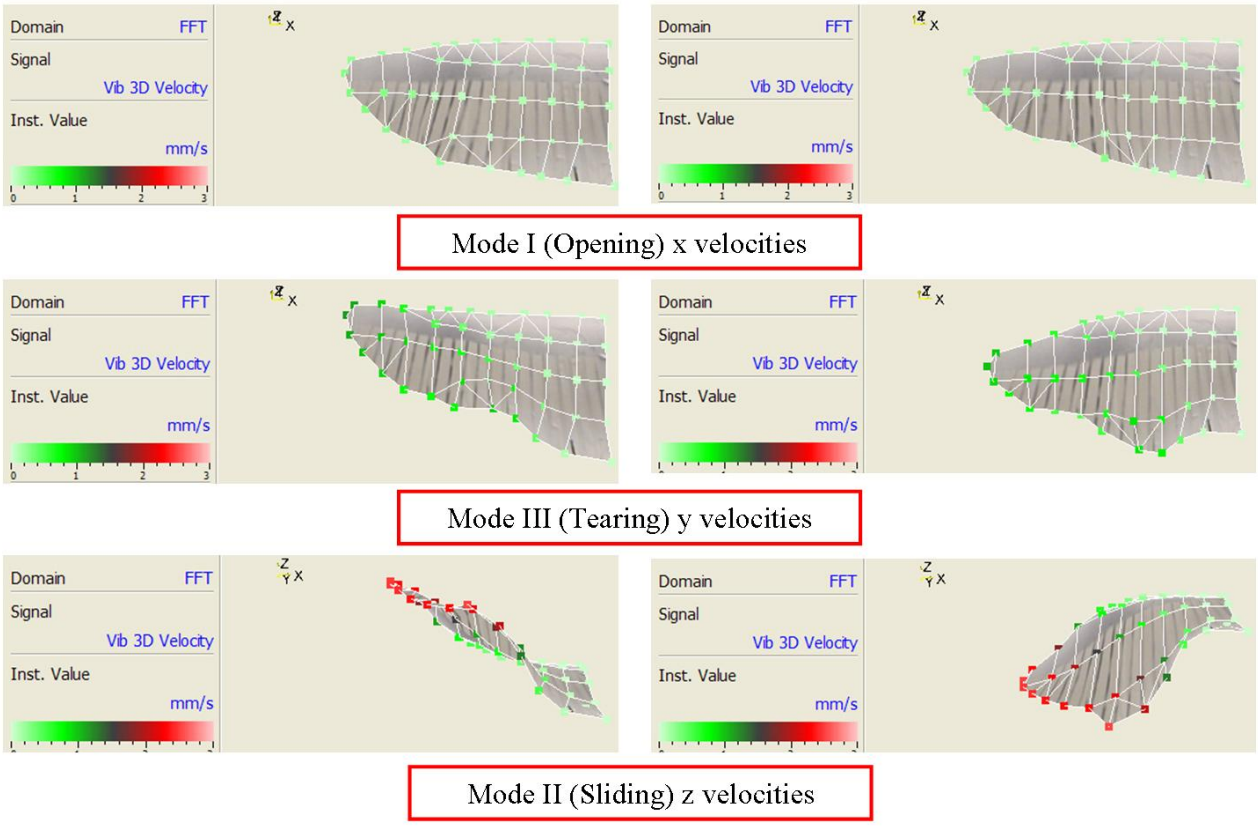

Figure 21: Fracture Mechanics Modes on Wing

Mode I is an opening or tensile mode with a tensile stress normal to the crack. In this mode, the crack faces are pulled apart. Mode II is a sliding or in-plane shear mode where shear stresses are acting parallel to the plane of the crack and perpendicular to the crack front. Mode III is a tearing or anti-plane shear mode with shear stresses acting parallel to the plane of the

crack and parallel to the crack front. These three modes are illustrated in Figure 20. During testing, the wing experienced a combination of the three modes shown in Figure 21. With velocities in the x-direction, Mode I opening can be seen as the membrane is pulled apart in opposite directions. Vibrations in the y-direction exhibited Mode II tearing where shear stresses acted parallel on the membrane of the wing. With z-vibrations, Mode II sliding can be seen as the wing's membrane flapped.

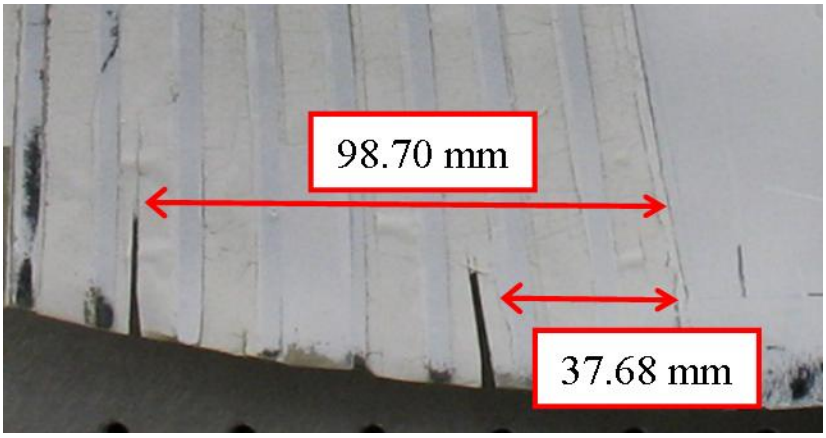

Figure 22: Two Cuts Near Center of Wing

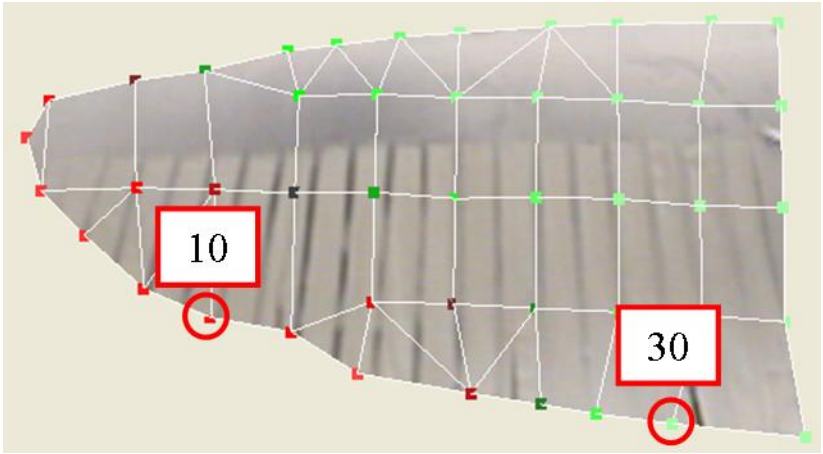

Figure 23: Scan Points by Center Wing and Left Wing Tip

The two cuts near the center of the wing were not affected. The nearest cut was 37.68 mm from the center of the wing and the second was 98.70 mm. The cut where the crack extended was 256.56 mm from the center of the wing. Examining velocities at two scan points,

Index 10 and Index 30, shows that velocities further from the center of the wing were much greater. Index 10, closer to the tip of the wing, experienced velocities that were multiple times greater in the x, y, and z-directions.

Table 3: Index 10 and Index 30 Scan Point Comparison

	Index 10	Index 30
x	184.4 µm/s	80.72 µm/s
y	749.6 µm/s	118.6 µm/s
z	1281 µm/s	165.8 µm/s

4.2 Frequency Comparisons

The following section will examine the frequency variation of the wing between its damaged states in Test 1 and Test 2. When referring to the global frequency, it is the natural frequencies found for the wing that were averaged across the entire wing.

4.2.1 Test 1 Global Frequency

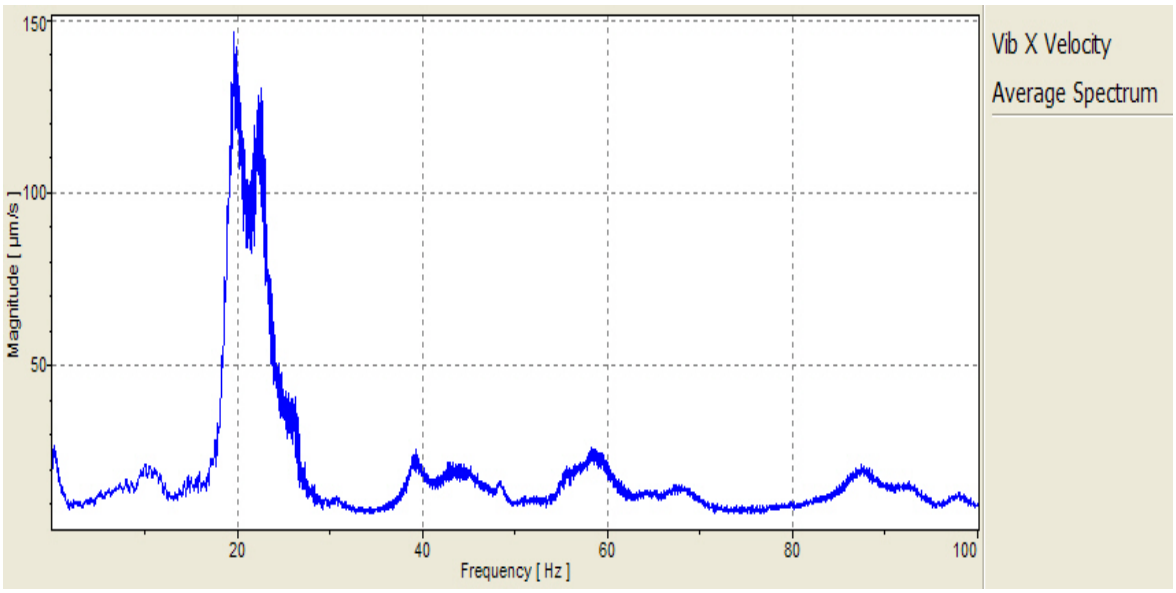

Figure 24: Test 1, Average Spectrum, Vib X Velocity

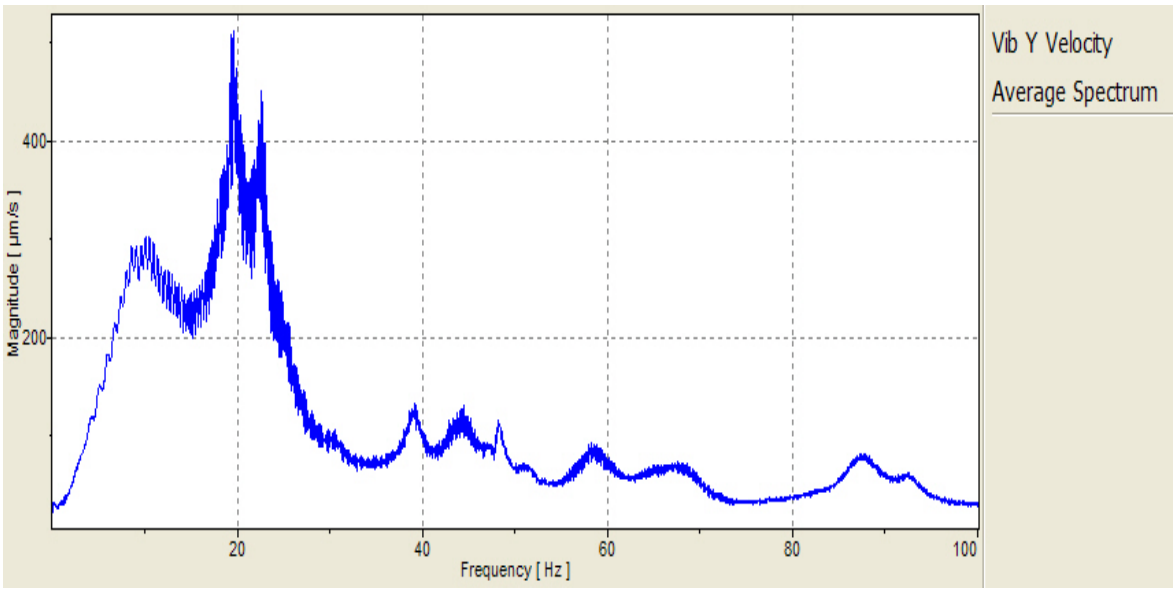

Figure 25: Test 1, Average Spectrum, Vib Y Velocity

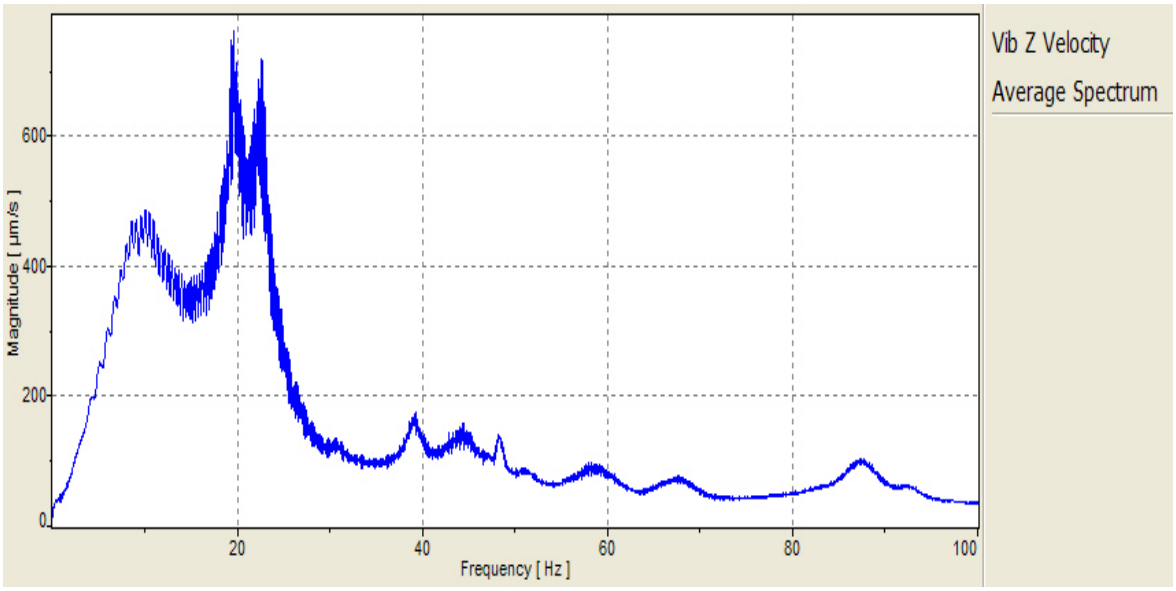

Figure 26: Test 1, Average Spectrum, Vib Z Velocity

Table 4: Test 1 Global Frequencies

Test 1 Frequencies (Hz)					
Mode	1	2	3	4	5
X	19.594	22.531	39.281	42.844	48.406
Y	19.594	22.531	39.094	44.438	48.094
Z	19.594	22.531	39.281	44.438	48.094

Figure 24 through Figure 26 show the frequency response functions for Test 1 averaged across the entire wing. Table 4 shows a summary of the natural frequencies of the wing in Test 1. The first mode of the wing is found at 19 Hz, the dominant frequency during testing. The second mode is found at 22 Hz. The third natural mode of the wing is found at 39 Hz. The fourth and fifth modes are found at 44 Hz and 48 Hz, respectively.

The first mode shape of the wing exhibited a somewhat asymmetric flapping motion with larger displacements found on the right span of the wing. The second mode was a symmetric flapping motion with larger displacements found on the left span of the wing. At 39 Hz, the right span of the wing had an s-bending mode shape with relatively little motion on the left span of the wing. At 44 Hz, the opposite occurred. The fourth mode exhibited an s-bending mode shape on the left span of the wing with relatively little motion on the right span. The fifth mode was dominated by motion on the right span of the wing around the area where batten R4 had detached. The five mode shapes of the wing in Test 1 are illustrated in Figure 27.

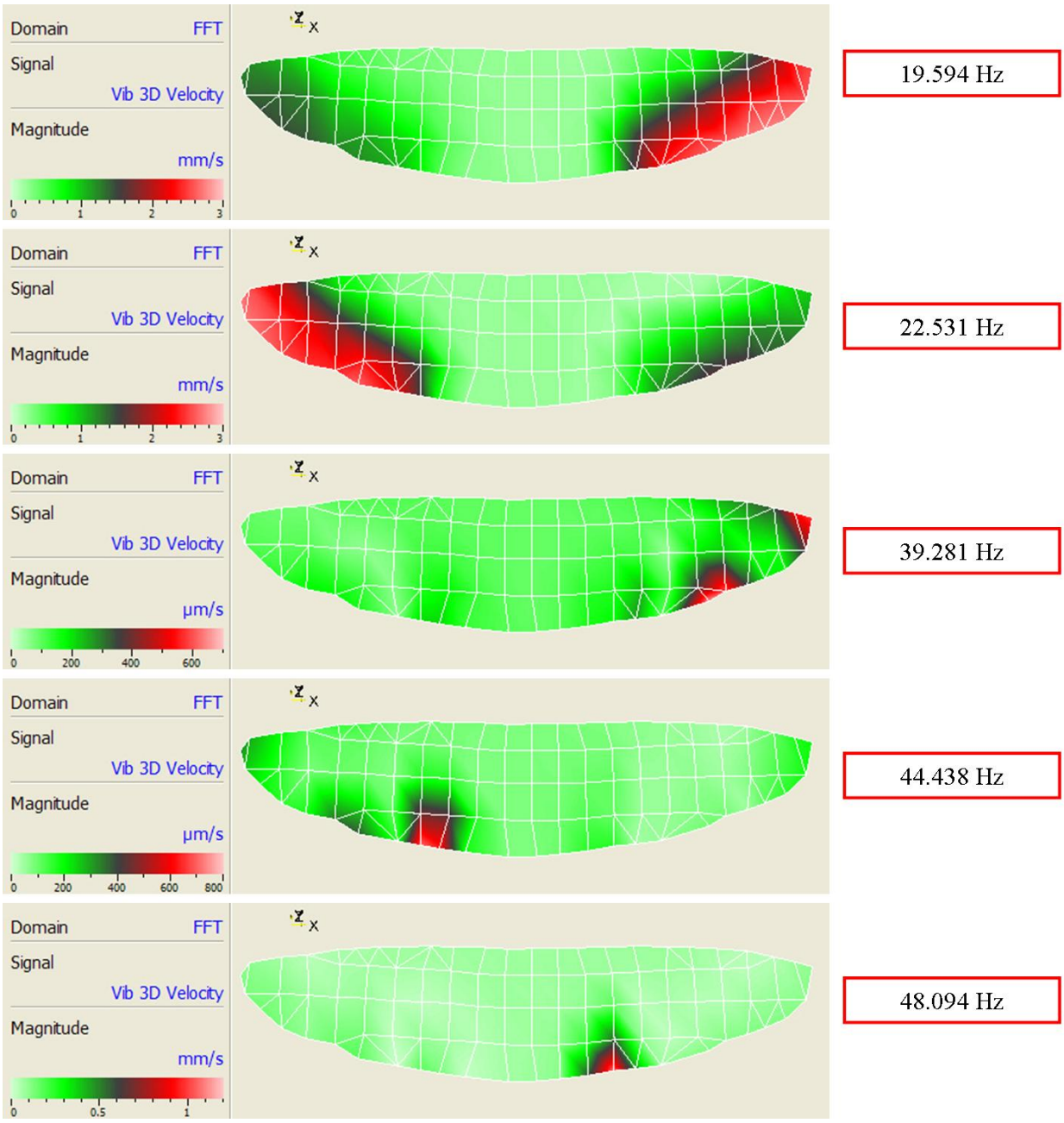

Figure 27: Test 1 Mode Shapes

4.2.2 Test 1 Left and Right Spans

Table 5: Test 1 Right Span Frequencies

Test 1 Right Span Frequencies (Hz)					
Band	1	2	3	4	5
X	19.594	22.500	39.281	48.313	58.656
Y	19.344	22.719	39.094	48.094	59.063
Z	19.344	22.719	39.281	48.219	59.063

Table 6: Test 1 Left Span Frequencies

Test 1 Left Span Frequencies (Hz)					
Band	1	2	3	4	5
X	22.531	30.719	44.438	-	68.000
Y	22.531	30.531	44.438	58.000	67.656
Z	22.531	30.688	44.438	58.000	67.656

Comparison between the left and right spans of the wing in Test 1 revealed differences in the initial damage applied to the wing. To do this, scan points were invalidated on the span of the wing to be removed. Doing so treats the span of the wing remaining as if it were the only section tested. The FRFs of the left and right spans for Test 1 can be found in Appendix B. The natural frequencies found from the FRFs for the left and right span are summarized in Table 5 and Table 6.

Overall, similar frequencies can be found between the individual spans and the global frequencies; however, some frequencies are missing or shifted. The first natural frequency of the right span of the wing is found at 19 Hz. This frequency, which was found in the global frequency, is not found on the left span of the wing. The right span of the wing is missing the global frequency found at 44 Hz, though it is found in the left span. In addition, the left span of the wing has an additional frequency at 30 Hz, which is not found on either the right span or the

global frequency. These changes in frequency between the right and left spans as well as the global frequency suggest a coupling of frequencies when data is averaged across the entire wing.

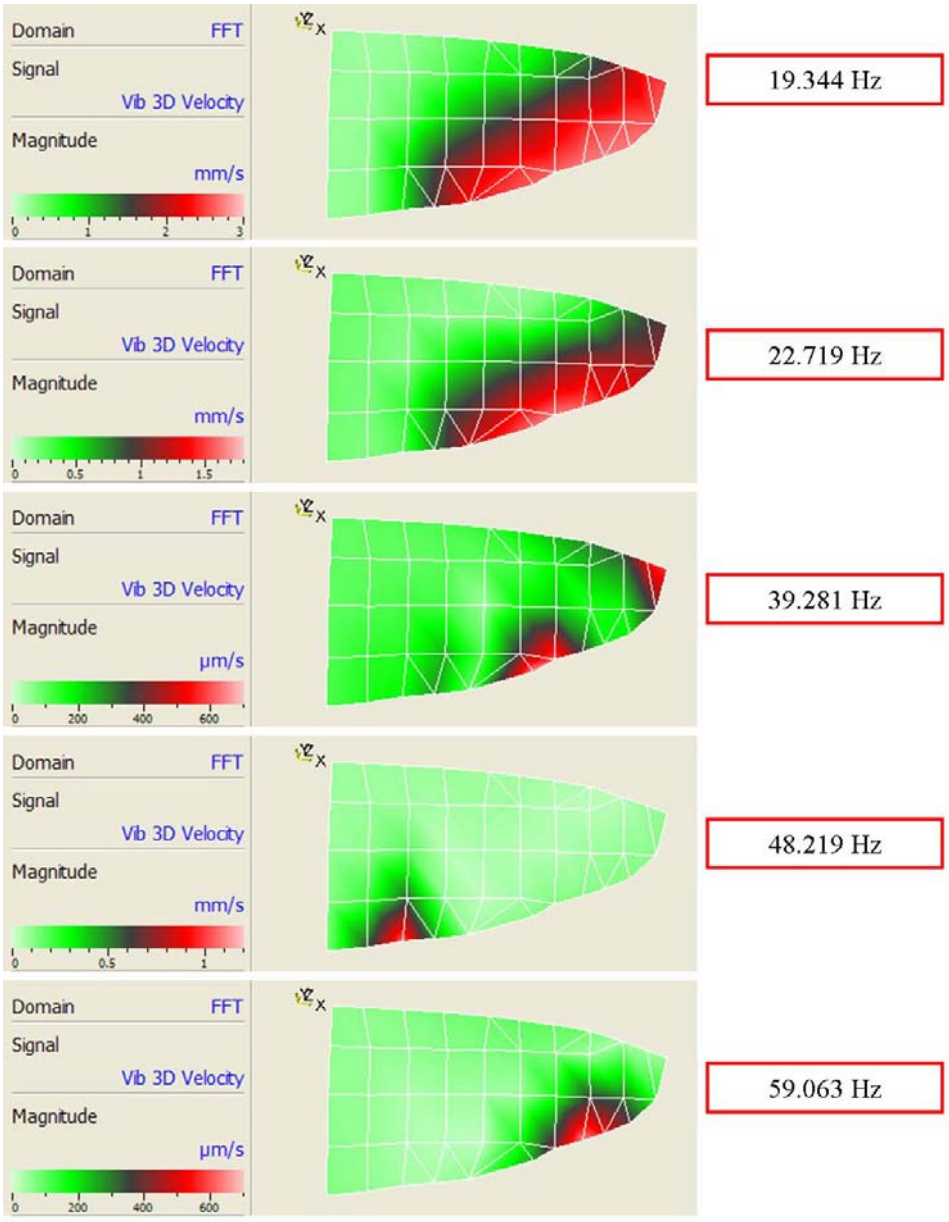

Figure 28: Test 1 Right Span Mode Shapes

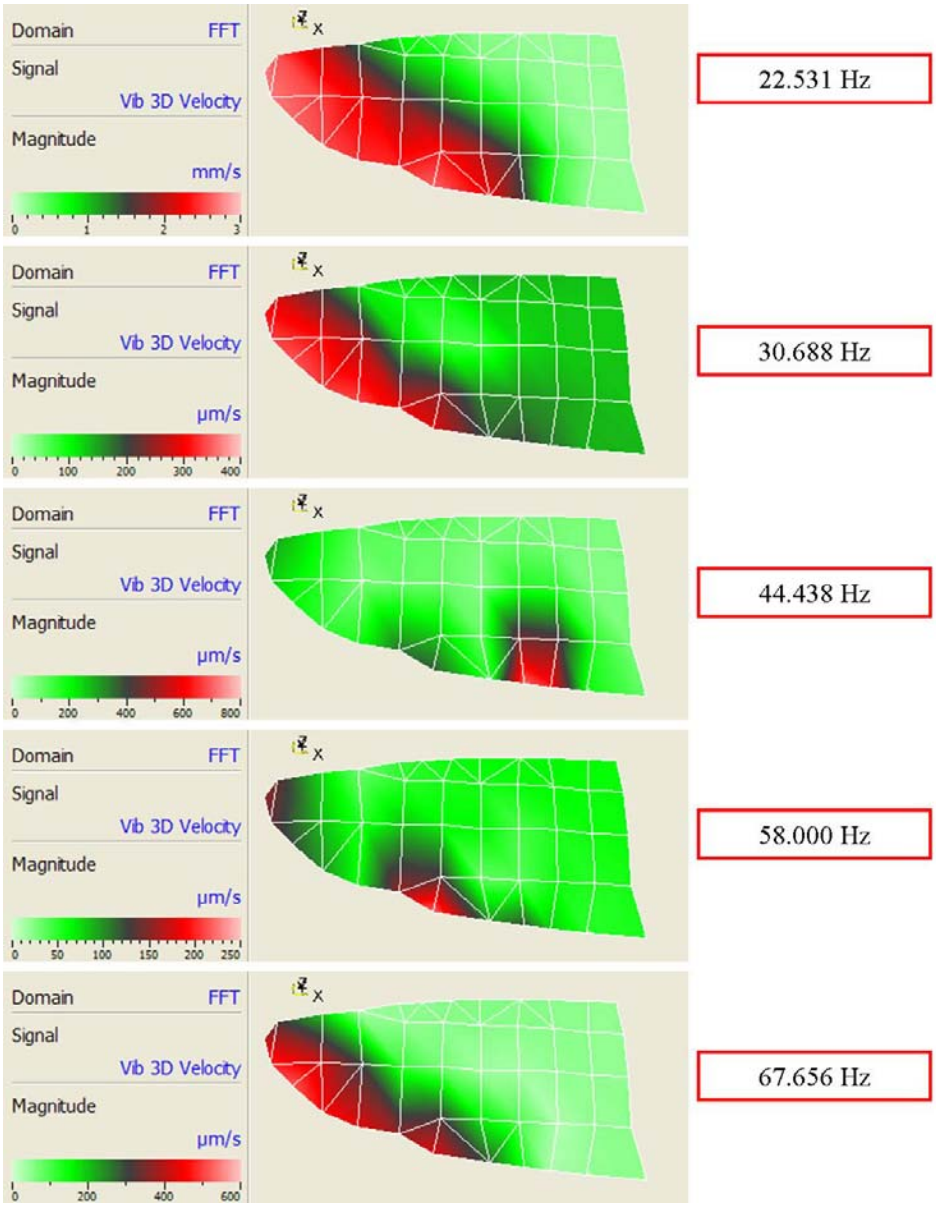

Figure 29: Test 1 Left Span Mode Shapes

The mode shapes of the left and right wing spans are shown in Figure 28 and Figure 29. The mode shapes of interest are those that occurred at or around the global natural frequencies for Test 1. The mode shapes for the right span of the wing at 19 Hz, 22 Hz, 39 Hz, and 48 Hz can all be seen in the global view. On the left span, the modes at 22 Hz and 44 Hz can be found in the global view. Overall, the mode shapes of the entire wire are a combination of the mode shapes of these spans averaged together.

4.2.3 Test 2 Global Frequencies

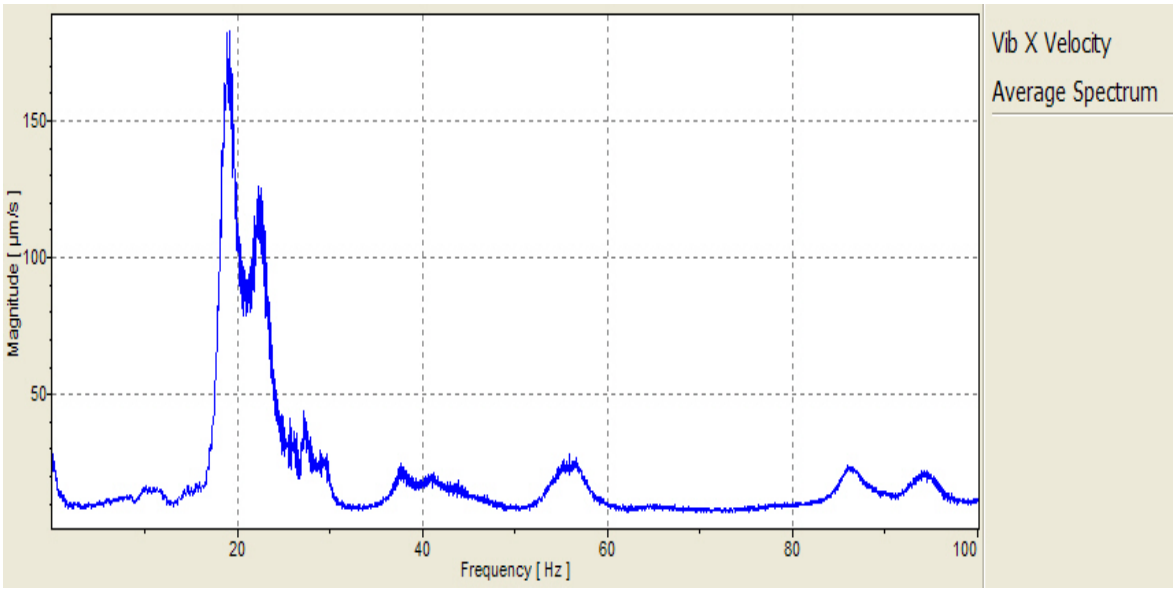

Figure 30: Test 2, Average Spectrum, Vib X Velocity

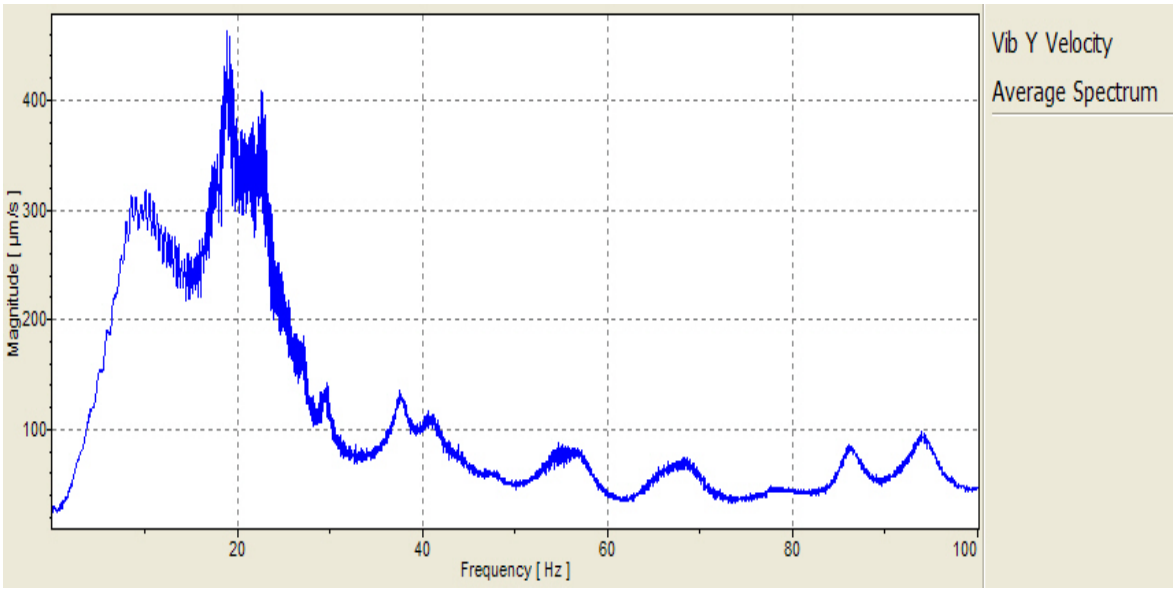

Figure 31: Test 2, Average Spectrum, Vib Y Velocity

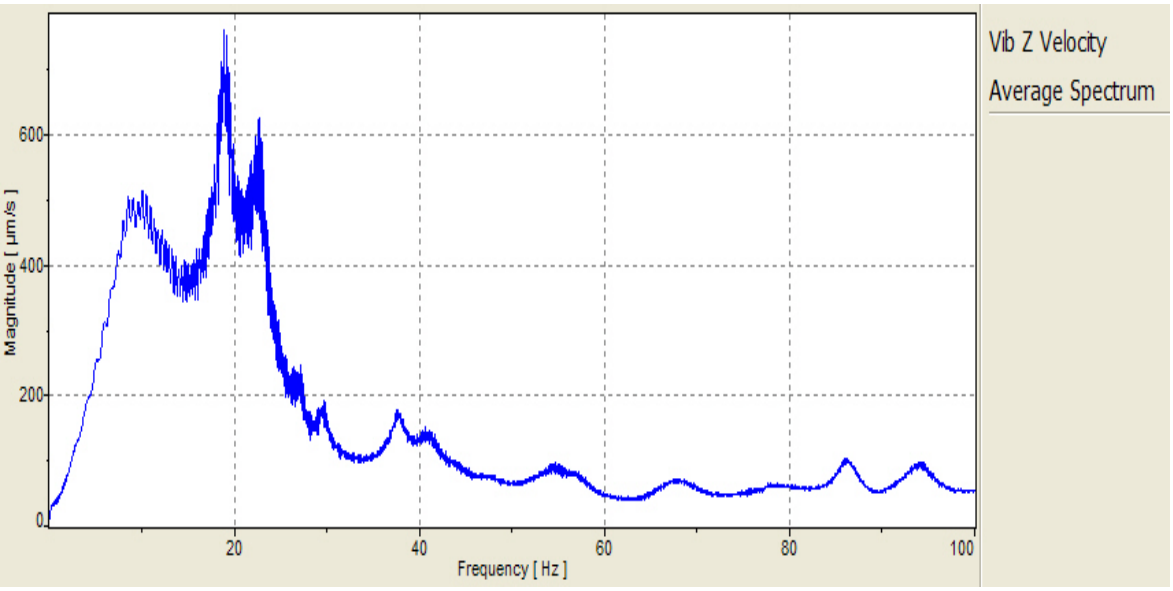

Figure 32: Test 2, Average Spectrum, Vib Z Velocity

Table 7: Test 2 Global Frequencies

Test 2 Frequencies (Hz)					
Mode	1	2	3	4	5
X	19.094	22.313	27.125	37.656	41.156
Y	18.844	22.531	29.594	37.469	40.563
Z	18.844	22.719	29.594	37.469	40.563

The FRFs of the wing in Test 2 are shown in Figure 30, Figure 31, and Figure 32. The natural frequencies found from these plots are summarized in Table 7. The first natural frequency for Test 2 was found at 18 Hz, very close to the first natural frequency in Test 1, which was found at 19 Hz. The second natural frequency was the same as in Test 1 at 22 Hz. A third natural frequency was found at 29 Hz, which did not appear in Test 1's global frequencies. The fourth mode occurred at 37 Hz and the fifth mode was found at 40 Hz.

The mode shapes of the wing in Test 2 are illustrated in Figure 33. The first two mode shapes for the wing in Test 2 stayed relatively the same. The first mode was an asymmetric flapping while the second mode exhibited a symmetric flapping motion. The third mode shape was an underdeveloped s-bending motion. At 37 Hz, the wing exhibited an s-bending mode

shape on the right span with very little movement on the left span. At 40 Hz, the left span exhibited an s-bending motion with very little movement on the right span. These two modes are similar to the third and fourth mode of the wing in Test 1.

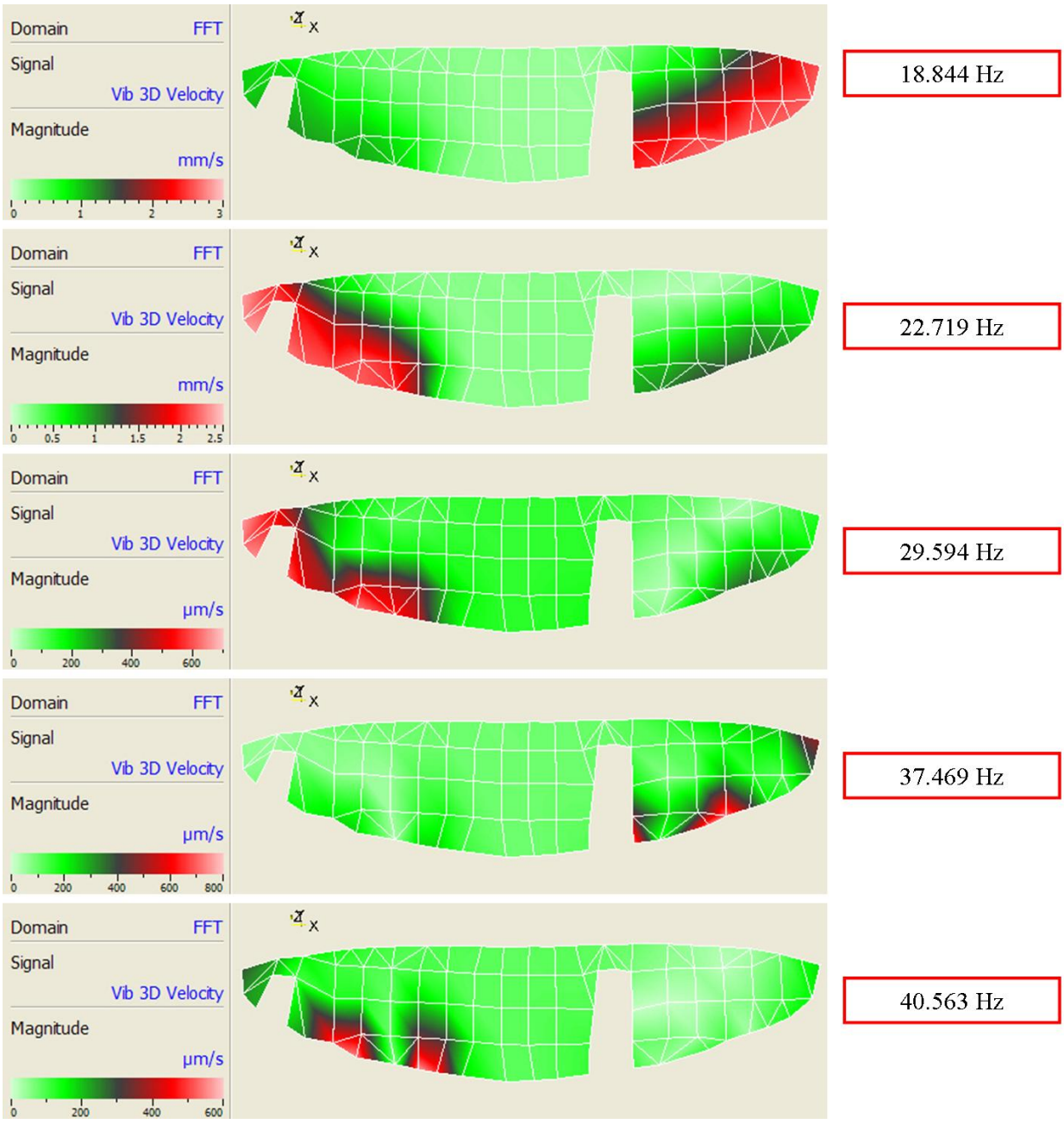

Figure 33: Test 2 Mode Shapes

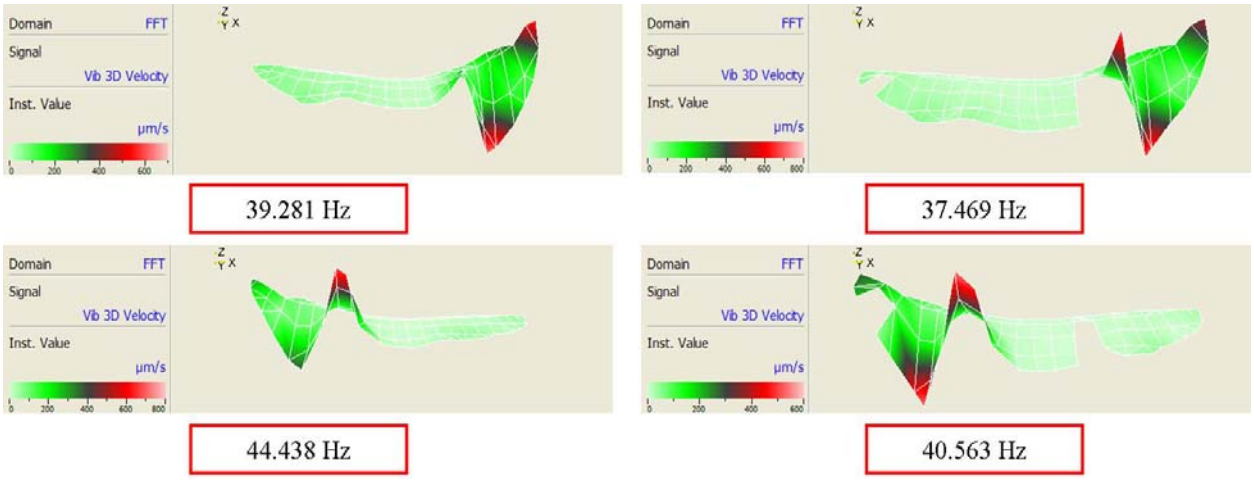

Figure 34: Mode Shape Comparison

In Test 1, the mode shape that exhibited an s-bending motion on the right span with little movement on the left span of the wing was found at 39.281 Hz. In Test 2, this same mode shape was found at 37.469 Hz. There is a drop of approximately 2 Hz after damage was applied to the wing. In Test 1, an s-bending motion on the left span with relatively little movement on the right span of the wing occurred at 44 Hz. In Test 2, the same mode shape was found at 40 Hz, approximately 4 Hz lower. The cause for the drop in frequency is a decrease in the stiffness of the wing after the membrane is removed. The natural frequency of the wing is function of the stiffness over the mass of the wing. With a drop in frequency, it is found that the stiffness has the dominant effect in changing the frequency of the wing.

4.2.4 Test 2 Left and Right Spans

Table 8: Test 2 Right Span Frequencies

Test 2 Right Span Frequencies (Hz)					
Mode	1	2	3	4	5
X	18.844	22.313	27.125	37.656	56.594
Y	18.844	22.906	27.125	37.469	57.125
Z	18.844	22.906	27.125	37.469	57.125

Table 9: Test 2 Left Span Frequencies

Test 2 Left Span Frequencies (Hz)					
Mode	1	2	3	4	5
X	19.094	22.500	-	41.156	55.844
Y	-	22.531	29.594	40.563	55.781
Z	-	22.500	29.594	40.563	55.250

The FRFs of the left and right span for Test 2 can be found in Appendix B. A summary of the natural frequencies found from these plots are found in Table 8 and Table 9. Test 2 showed some similar patterns as Test 1. In the global frequency, the first mode was found at a frequency of 18 Hz. This frequency is found in the right span of the wing but not in the left span, similar to what occurred in Test 1. Again, the second mode occurred at 22 Hz and was found for both spans of the wing. The third mode occurred around 27 Hz for the right span and 29 Hz for the left. The global frequency for the wing occurred at approximately 29 Hz. These frequency differences between the left and right spans show evidence of coupling of modes between the left and right span when the data is averaged across the entire wing.

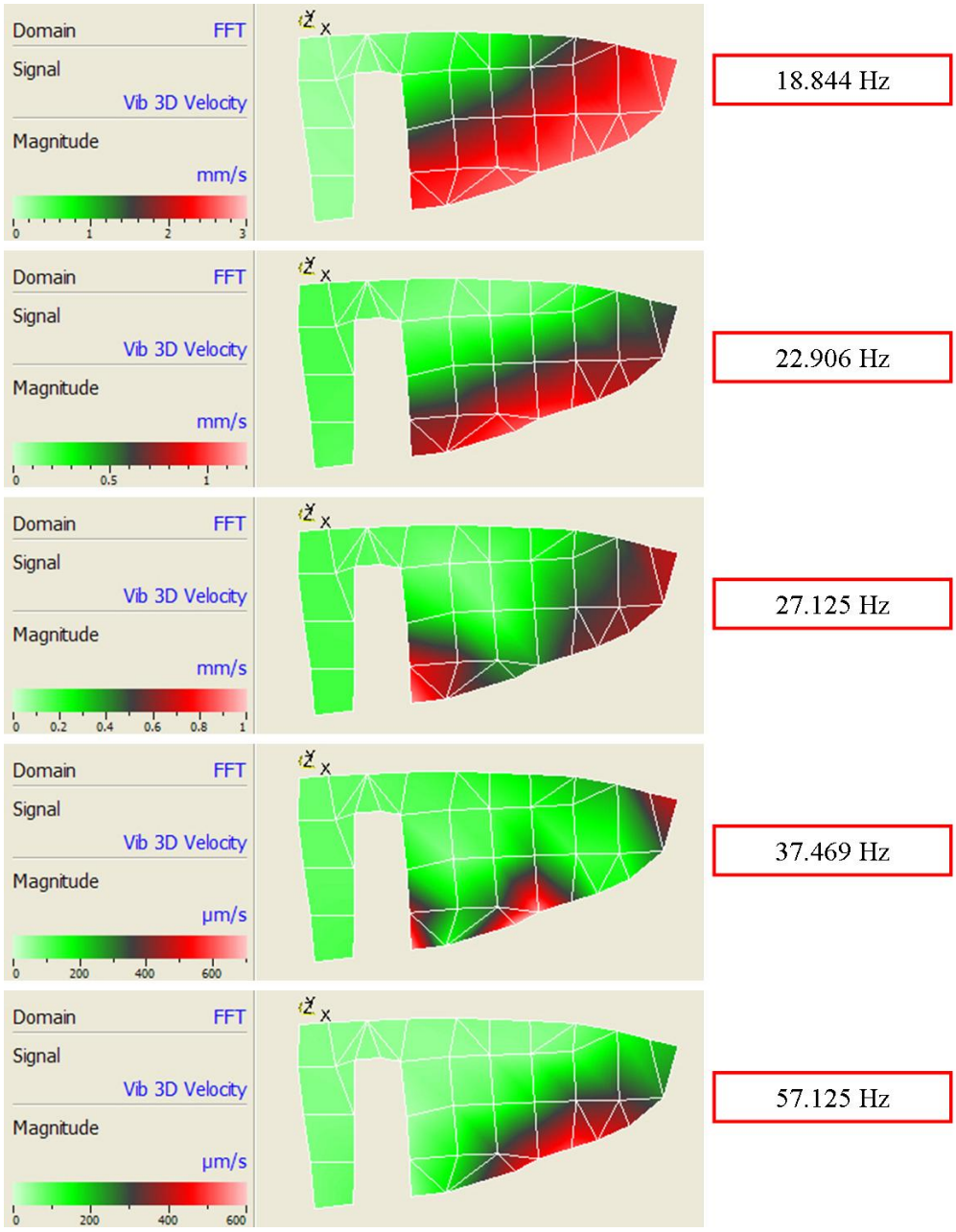

Figure 35: Test 2 Right Span Mode Shapes

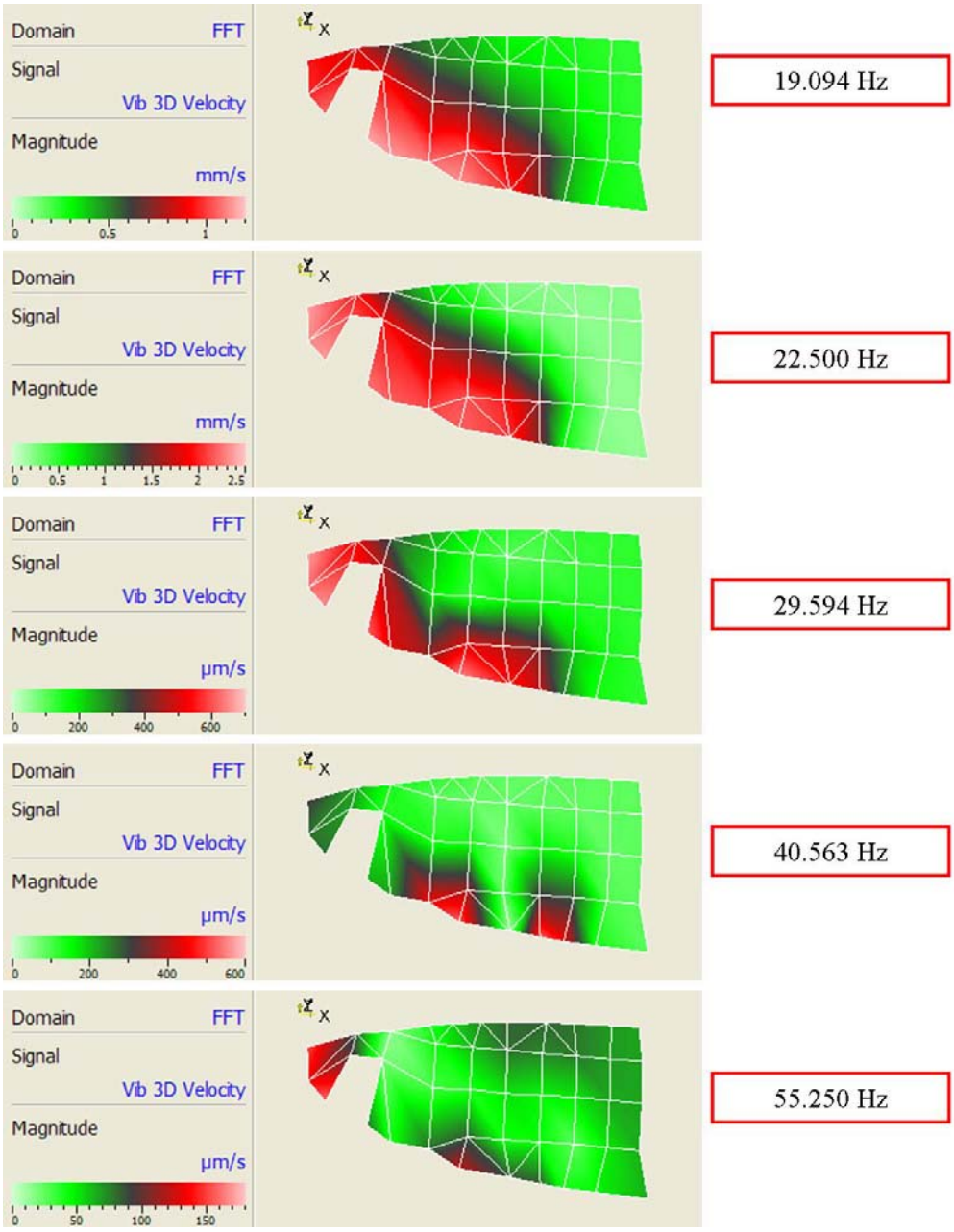

Figure 36: Test 2 Left Span Mode Shapes

The mode shapes for the left and right wing spans in Test 2 are shown in Figure 35 and Figure 36. Like the mode shapes examined in Test 1, the mode shapes of interest are those found at frequencies common to the global frequencies. As with Test 1, the mode shapes for the entire wing are a combination of the left and right spans as they are averaged together.

4.3 Velocity Comparisons

The following section presents a more detailed understanding of damage characteristics by examining velocities at single scan points. Four scanning points were selected to see the changes in their velocities after the wing was damaged. The four scanning points are: Index 4, 147, 103 and 76 shown in Figure 37. Index 4 is located near the tip of the left span of the wing. Index 76 is located on the opposite side on the right span of the wing. Index 147 is located on the membrane near the middle of the left span at the trailing edge. Similarly, Index 103 is at the trailing edge on the membrane near the middle of the right span.

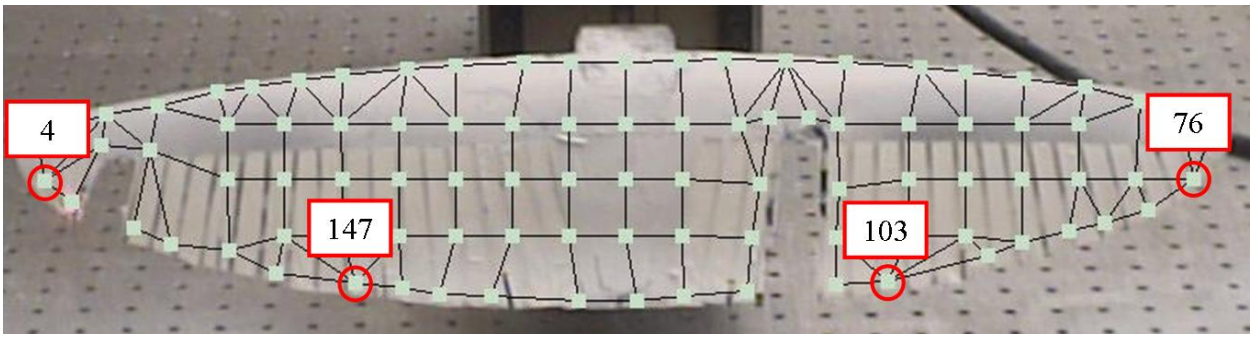

Figure 37: Selected Scan Points

4.3.1 Velocity Comparisons at 19 Hz (Test 1) and 18 Hz (Test 2)

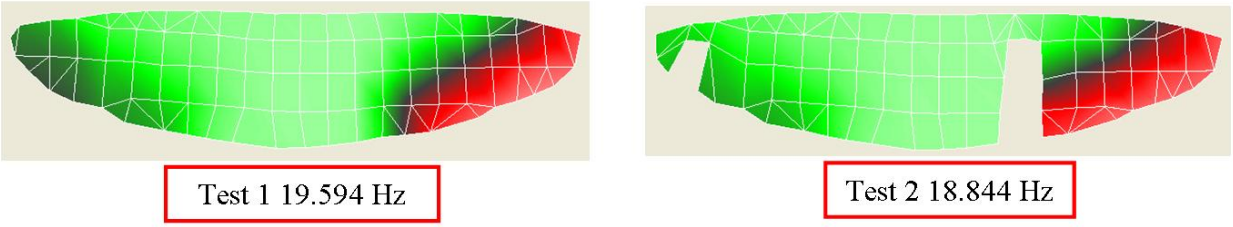

Figure 38: Velocity Comparisons for 19 Hz (Test 1) and 18 Hz (Test 2)

Table 10: Index Velocities for 19 Hz (Test 1) and 18 Hz (Test 2)

Index	Test 1 Velocity	Test 2 Velocity
4	971.2	1372
147	970.8	1053
103	2486	2351
76	2621	2626

The first frequency comparison is between the wing in Test 1 and 2 at the first natural global frequency for each respective test. The velocities at the selected scanning points can be found in Table 10. The first mode shape for both tests at these frequencies was an asymmetric flapping motion. On the left span of the wing, there is a noticeable increase in velocity for both Index 4 and 147. Index 4 near the tip of the wing had the greatest velocity change, nearly 1.5 times the velocity in Test 1. On the right span of the wing, the frequencies stayed relatively the same between the two tests. The right span of the wing had two detached battens during Test 1. It seems the removal of the membrane near the center of the wing did not change the effect of the removed battens significantly. However, with the battens removed, the membrane of the right span of the wing was allowed to displace larger distances resulting in greater velocities overall compared to the left span.

4.3.2 Velocity Comparisons at 22 Hz (Test 1 and Test 2)

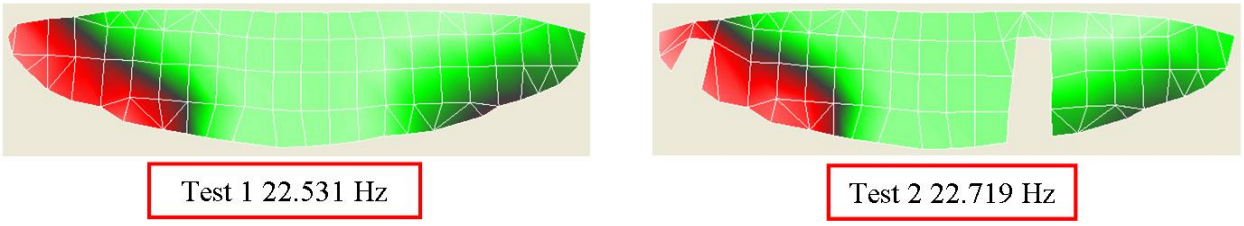

Figure 39: Velocity Comparisons for 22 Hz (Test 1 and Test 2)

Table 11: Index Velocities for 22 Hz (Test 1 and Test 2)

Index	Test 1 Velocity	Test 2 Velocity
4	2324	2712
147	2062	2235
103	1006	1245
76	712.4	1166

The following velocity comparison is at the second mode, which occurred at 22 Hz for both Test 1 and Test 2. The velocities for the scanning points at these frequencies can be found in Table 11. At 22 Hz, the mode shape exhibited by the wing was an asymmetric flapping motion with greater velocities found on the left span of the wing. The greatest velocity change occurred near the tip of the wing around Index 76. The velocity was approximately 1.6 times larger in Test 2 at Index 76. In the comparison of the first mode, the right span stayed relatively the same. The opposite occurred at 22 Hz. The magnitudes of velocity on the left span of the wing stayed somewhat the same while the right span experienced large changes in velocity. At these frequencies, the removal of the batten and its surrounding membrane near the center of the wing had a great effect in allowing the right span of the wing to displace larger distances. On the other hand, the removal of a batten and membrane near the tip of the wing at these frequencies did not have a significant effect.

4.3.3 Velocity Comparisons at 39 Hz (Test 1) and 37 Hz (Test 2)

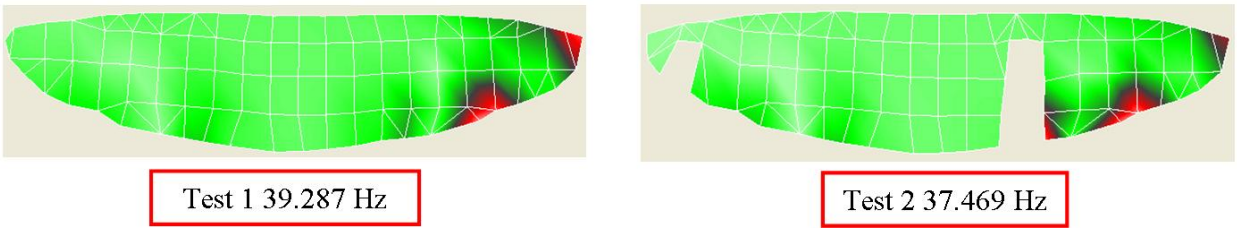

Figure 40: Velocity Comparisons for 39 Hz (Test 1) and 37 Hz (Test 2)

Table 12: Index Velocities for 39 Hz (Test 1) and 37 Hz (Test 2)

Index	Test 1 Velocity	Test 2 Velocity
4	66.47	111.7
147	46.99	60.68
103	171.6	100.3
76	334.1	386.7

This velocity comparison is at the frequencies where the wing's mode shape exhibited an s-bending motion on the right span of the wing with comparatively smaller velocities on the left span of the wing. Overall, the velocities at this mode were much smaller compared to the velocities for the first two modes compared. These velocities are summarized in Table 12. On the left span of the wing, the greater velocity change occurred near the tip of the wing. On the right span of the wing, the greater velocity change was not found near the tip but rather around Index 103. Moreover, this index point experienced a decrease in velocity. Index 103 is located between damaged areas where the largest velocities were encountered in Test 2. To the left, there is the area where a batten and membrane were removed. To the right is the area where a batten had detached from the membrane of the wing. Index 103 acted like the center of the wing where the two areas on its left and right side were "wings" that resulted in a reduction in velocity at Index 103 but greater velocities at its surrounding areas.

4.3.4 Velocity Comparisons at 44 Hz (Test 1) and 40 Hz (Test 2)

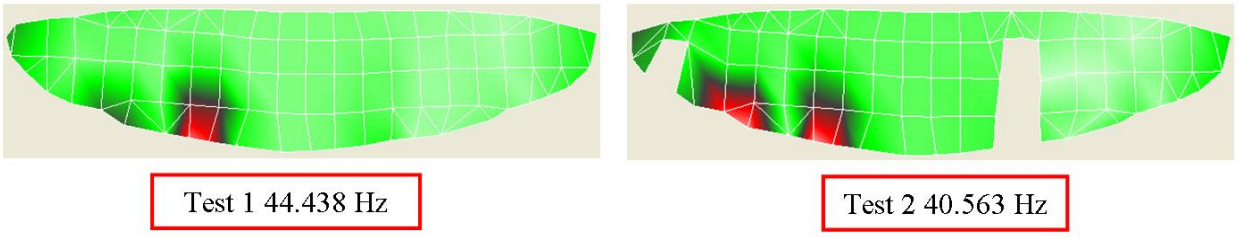

Figure 41: Velocity Comparisons for 44 Hz (Test 1) and 40 Hz (Test 2)

Table 13: Index Velocities for 44 Hz (Test 1) and 40 Hz (Test 2)

Index	Test 1 Velocity	Test 2 Velocity
4	242.1	260.2
147	60.46	160.9
103	49.32	60.58
76	159.1	187.4

The fourth velocity comparison is between the mode shape that exhibited s-bending motion on the left span with relatively little movement on the right span. This mode shape occurred at 44 Hz during Test 1 and 40 Hz during Test 2. As with the previous velocity comparisons, the velocities found at this mode are much smaller compared to velocities of the first two modes. The greatest velocity change occurred at Index 147, found on the membrane of the left span at the trailing edge. Although the damage was closer to the tip, the removal of the membrane at the tip allowed the rest of the wing to the right to flap more.

4.3.5 Velocity Comparisons by Damaged Areas

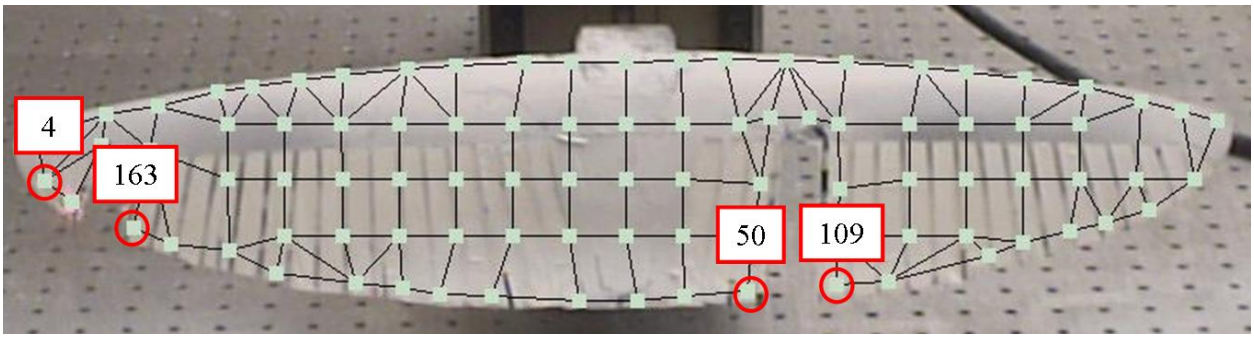

Figure 42: Selected Scanning Points by Damaged Areas

This section compares velocities directly by the damaged areas. The scanning points selected are shown in Figure 42. On the left span of the wing, Index 4 and 163 are located by the area where the batten and its surrounding membrane were removed. On the right wing span, Index 50 and 109 surround the area where the batten and membrane were removed on this span. Also, these two index points surround the area where a batten had detached from the membrane

during Test 1. Comparing velocities at directly at the damage on both sides will help determine which form of damage had a greater affect on the wing.

Table 14: Damage Near the Center of Wing

Index	50	109	Change in 109
Test 1 19.59 Hz	261.5	1635	6.25 x greater
Test 2 18.84 Hz	229.3	2386	10.41 x greater
Test 1 22.53 Hz	105.1	213.2	3.97 x greater
Test 2 22.72 Hz	213.2	913.8	4.28 x greater
Test 1 39.29 Hz	156.6	250.2	1.59 x greater
Test 1 37.47 Hz	119.3	412.8	3.46 x greater
Test 1 44.44 Hz	163.9	43.86	3.73 x less
Test 2 40.56 Hz	114.1	109.6	1.04 x less

Table 14 summarizes the velocities found at scanning points 50 and 109 for Test 1 and 2 at certain natural frequencies of the wing. At the first mode compared, there is a significant velocity difference between Index 50 and 109. During Test 1, these two scanning points were by a detached membrane. It seems the detachment of the batten from the membrane allowed the index point further from the center to move at greater velocities. After the batten and membrane were removed in Test 2, there is a significant change in velocities between Index 50 and 109. However, there is a decrease in the velocity at Index 50, closer to the center of the wing. Removing the membrane partitioned the wing's movement, creating larger velocities further away from the center of the wing. At 22 Hz, a similar pattern is found: during Test 1, Index 109 registered a larger velocity than Index 50; when damage is applied to the right span, there is another increase in velocity at the two scanning points. This pattern continues through the higher frequencies but there is a steep decline in the velocity differences found between the two scanning points. As the frequency increased, the velocity difference decreased between Index 50 and 109. This was the not expected result. With the wing moving at a higher frequency, a greater velocity difference was expected. The reason this did not happen because the energy in

the wing was greatest at lower frequencies. This is apparent by the higher velocities experienced at 19 Hz and 22 Hz. Additionally, the FRF for the wing in Test 1 and 2 show the greatest response at the first two natural frequencies.

Table 15: Damage Near the Tip of Left Wing

Index	4	163	Increase
Test 1 19.59 Hz	1372	1451	1.05 x greater
Test 2 18.84 Hz	971.2	1152	1.18 x greater
Test 1 22.53 Hz	2712	2545	1.06 x less
Test 2 22.72 Hz	2324	2243	1.03 x less
Test 1 39.29 Hz	111.7	141.7	1.26 x greater
Test 1 37.47 Hz	66.47	193.2	2.91 x greater
Test 1 44.44 Hz	260.2	156.1	1.67 x less
Test 2 40.56 Hz	242.1	191.3	1.26 x less

Table 15 summarizes the velocities found at Index 4 and 163 on the left span of the wing. By looking at changes in velocities overall between the two scanning points, it is immediately apparent that damage near the tip of the wing did not have as significant of an effect as damage near the center. Removing a batten and its surrounding membrane near the tip of the wing does not have a significant effect on velocity. One similar pattern that has been found throughout all comparisons is the significant decrease in velocity at higher frequencies.

5. Conclusions and Recommendations

5.1 Conclusions

- Cracks and their extension or growth become an area of concern for structural integrity when they are further away from the center of the wing. Through investigation of the membrane crack growth, it was seen that cracks near the center of the wing were unaffected during testing. However, the crack furthest from the center of the wing extended at the beginning of testing. Moreover, this crack extended even at the small velocities experienced by the wing.
- Frequency variation is a by-product of the damage applied to the wing. The wing experienced decreases in its natural frequencies, especially at higher frequencies. Damaging the wing by removing its battens and membranes changed the wing's structural dynamic properties. Using frequency comparisons, it was shown that the change in stiffness of the wing as the membrane was removed was the dominant affect in shifting the natural frequencies.
- From a frequency standpoint, the first two modes are largely unaffected. Damage affects higher modes more significantly. With the frequency comparisons, the first two modes for both Test 1 and Test 2 occurred at approximately 19 Hz and 22 Hz. When comparing mode shapes at higher frequencies, it was seen that the wing experienced decreases in natural frequencies. The third mode of Test 1 was 2 Hz lower in Test 2 while the fourth mode in Test 1 was 4 Hz lower.
- Frequency coupling was evident between the left and right wing spans when observing the global frequency. When the wing was split into two separate components as the left

and right wing span, it was seen that certain frequencies were missing or shifted in the frequency response function of individual spans. Looking at the global frequency spectrum, it could be seen that the natural frequencies found for the entire wing was a coupling of frequencies of the left and right wing as scanning points were averaged across the entire wing.

- Severe damage by removing a batten and its surrounding membrane near the center of the wing partitioned the wing's movement. Examining velocities directly at the damaged areas showed that much greater velocity differences were found by the damage near the center of the wing. The index point closer to the center experienced relatively little movement compared to the index point on the middle of the span of the wing at the trailing edge. When batten and membrane were removed near the center, a greater amount of the span was left intact that was free to displace larger distances. When the membrane was completely connected, movement of the membrane near the center of the wing was driven by flapping on the middle of the wing. With the membrane removed, the middle of the wing was allowed to move more freely without being tied down the by membrane attached to the stiff center of the wing.
- Relative movement between scanning points at damaged areas on the membrane is much greater near the center of the wing than at the tips.
- Greater velocity changes are brought about at lower resonant frequencies. When examining scanning points directly by the damaged areas, the velocity differences decreased at higher frequencies.
- Damage at the center of the wing creates larger velocity changes at the wing tips than damage near the wing tips. During the velocity comparisons, it was seen that overall, the

velocity at the index point near the tip of the right span was consistently higher than the velocity at the tip of the left span. Even with damage applied near the tip of the left span, the velocities did not match those reached on the right span.

5.2 Recommendations

- Perform vibrometer scans on a completely undamaged wing and then make comparisons as it is damaged. Because the wing tested during this project already had damage, the first scan did not give a true picture of the wing's natural frequencies and mode shapes.
- Perform similar tests conducted in this project using a finite element analysis program such as ABAQUS. Doing so can verify data between the experimental work and finite element software. In addition, given accurate results in the finite element software, several more damaged states of the wing can be examined while still maintaining an undamaged wing to use for comparison
- During testing, the shaker should be hard mounted to the table. Standing on rubber feet, the shaker is still able to slightly move. Also, the amplifier should be placed on the ground or any place off the table where the shaker is set. Unwanted noise introduced during testing will be reduced.
- During 3-D alignment of the scanning heads, only use the top scanning head for selecting an origin, axis and plane. This reduces the time needed for alignment. For the alignment points, use all three scanning heads and select points on the test object for the best target quality.

Bibliography

Abdulrahim, M., Garcia, H., & Lind, R. (2005). Flight Characteristics of Shaping the Membrane Wing of a Micro Air Vehicle. Journal of Aircraft , 42.

Blandino, J. R., Pappa, R. S., & Black, J. T. (2003). Modal Identification of Membrane Structures with Videogrammetry and Laser Vibrometry. AIAA 2003-1745 . Norfolk: American Institute of Aeronautics and Astronautics, Inc.

DeLuca, A. M. (2004). Experimental Investigation into the Aerodynamic Performance of Both Rigid and Flexible Wing Structured Micro-Air-Vehicles. Thesis, Air Force Institute of Technology, Wright-Patterson Air Force Base.

Deluca, A. M., Reeder, M. F., OL, M. V., Freeman, J., Bautista, I., & Simonich, M. (2004, July). Experimental Investigation into the Aerodynamic Properties of a Flexible and Rigid Wing Micro Air Vehicle. AIAA 2004-2396 . Portland, Oregon: American Institute of Aeronautics and Astronautics, Inc.

Gad-el-Hak, M. (2001). Micro-Air Vehicles: Can They be Controlled Better. Journal of Aircraft , 38 (3).

Ifju, P. G., Jenkins, D. A., Ettinger, S., Lian, Y., Shyy, W., & Waszak, M. R. (2002, January). Flexible-Wing-Based Micro Air Vehicles. AIAA 2002-0705 . American Institute of Aeronautics and Astronautics, Inc.

Ifju, P. G., Stanford, B., Sytsma, M., & Albertani, R. (2006, June). Analysis of A Flexible Wing Micro Air Vehicle. AIAA 2006-3311 . American Institute of Aeronautics and Astronautics, Inc.

Malolan, V., Dineshkumar, M., & Baskar, V. (2004, January). Design and Development of Flapping Wing Micro Air Vehicle. AIAA 2004-40 . American Institute of Aeronautics and Astronautics, Inc.

Mueller, T. J. (2001). Fixed and Flapping Wing Aerodynamics for Micro Air Vehicle Applications (Vol. 195). Reston, Virginia: American Institute of Aeronautics and Astronautics, Inc.

Pines, D. J., & Bohorquez, F. (2006). Challenges Facing Future Micro-Air-Vehicle Development. Journal of Aircraft , 43 (2).

Polytec. (2007). Laser Basics. Retrieved April 8, 2007, from Polytec: http://www.polytec.com/usa/158_1001.asp

Polytec Scanning Vibrometer Software Manual.

Polytec Scanning Vibrometer Theory Manual.

Polytec. (2003). Principles of Vibrometry. Polytec LM INFO Special, Issue 1 .

Polytec. (2007). Vibrometry Basics. Retrieved April 8, 2007, from Polytec: http://www.polytec.com/usa/158_942.asp

Stanford, B., Abdulrahim, M., Lind, R., & Ifju, P. (2006, May). Design and Optimization of Morphing Mechanisms for Highly Flexible Micro Air Vehicles. AIAA 2006-2162 . American Institute of Aeronautics and Astronautics, Inc.

Stults, J. A. (2005). Computational Aeroelastic Analysis of Micro Air Vehicle with Experimentally Determined Modes. Thesis, Air Force Institute of Technology, Wright-Patterson Air Force Base.

Stults, J. A., Maple, R. C., Cobb, R. G., & Parker, G. H. (2005, June). Computational Aeroelastic Analysis of a Micro Air Vehicle with Experimentally Determined Modes. AIAA 2005-4614 .

Appendix A

A.1 Test 1 Software Settings

```
Name:                        F:\Experimental Data\Test 1\test1.svd
 User:                        Administrator
 Created:                     Saturday, May 10, 2003
                              9:20:33 AM
 File version:                8.40
 Application version:         8.41
 ---------------------------------------------------------------------
 Comment

 ---------------------------------------------------------------------
 Scan Points

 Total:                       96
 Not measured:                0              0.0 %
 Valid:                       0              0.0 %
 Optimal:                     96             100.0 %
 Overrange:                   0              0.0 %
 Invalidated:                 0              0.0 %
 Disabled:                    0              0.0 %
 Not reachable:               0              0.0 %
 Hidden:                      0              0.0 %
 ---------------------------------------------------------------------
 Scanning Head:               PSV-I-400 LR  (OFV-505)
 Junction Box:                PSV-E-400-3D
 Acquisition Board:           National Instruments PCI-4452
 ---------------------------------------------------------------------
 General

 Acquisition  Mode:           FFT
 Averaging:                   Complex
 Averaging count:             40
 PCA (MIMO):                  Not active
 ---------------------------------------------------------------------
 Frequency

 Bandwidth:                   100 Hz
 Bandwidth from:              31.25 mHz
 Bandwidth to:                100 Hz
 ---------------------------------------------------------------------
 Sampling

 FFT  Lines:                  3200
 Overlap:                     66 %
 Sample frequency:            256 Hz
 Sample time:                 32 s
 Resolution:                  31.25 mHz
 ---------------------------------------------------------------------
 Trigger

 Source:                      Off
 ---------------------------------------------------------------------
 Channel Vibrometer 3D (connected to Vibrometer 1)

 Range:                       31.62 V
 Coupling:                    DC
 Impedance:                   1 MOhm
 Differential Input:          Off
 Quantity:                    Velocity
 Calibration factor:          10e-3  (m/s)/V
 Signal Delay:                0  s
 Filter Type:                 No Filter
```

```
Int/Diff Quantity:          Velocity
Window:                     Rectangle
Signal Enhancement:         Active

Channel Reference 1

Reference:                  Active
Reference point index:      0
Direction:                  +Z
Range:                      100 mV
Coupling:                   DC
Impedance:                  1 MOhm
ICP:                        Off
Differential Input:         Off
Quantity:                   Voltage
Calibration factor:         1
Signal Delay:               0  s
Filter Type:                No Filter
Int/Diff Quantity:          Voltage
Window:                     Rectangle
Signal Enhancement:         Not active
-------------------------------------------------------------------------
Signal Enhancement

Speckle Tracking:           Active
Mode:                       Fast
-------------------------------------------------------------------------
Vibrometer 1

Type:                       OFV-5000
Tracking filter:            Off

Velocity output

Range:                      VD-03  10 mm/s/V
Low pass filter:            1.5 MHz
High pass filter:           Off
-------------------------------------------------------------------------
Function Generator 1

Type:                       NI 671x
Signal:                     Periodic Chirp
Amplitude:                  100 mV
Offset:                     0 V
Amplitude correction:       None
-------------------------------------------------------------------------
```

A.2 Test 2 Software Settings

```
Name:                       F:\Experimental Data\Test 2\test2.svd
User:                       Administrator
Created:                    Sunday, May 11, 2003
                            9:00:44 AM
File version:               8.40
Application version:        8.41
-------------------------------------------------------------------------
Comment

-------------------------------------------------------------------------
Scan Points

Total:                      92
Not measured:               0              0.0 %
Valid:                      0              0.0 %
Optimal:                    92             100.0 %
Overrange:                  0              0.0 %
Invalidated:                0              0.0 %
Disabled:                   0              0.0 %
Not reachable:              0              0.0 %
```

```
Hidden:                      0             0.0 %
-----------------------------------------------------------------------
Scanning Head:               PSV-I-400 LR  (OFV-505)
Junction Box:                PSV-E-400-3D
Acquisition Board:           National Instruments PCI-4452
-----------------------------------------------------------------------
General

Acquisition  Mode:           FFT
Averaging:                   Complex
Averaging count:             40
PCA (MIMO):                  Not active
-----------------------------------------------------------------------
Frequency

Bandwidth:                   100 Hz
Bandwidth from:              31.25 mHz
Bandwidth to:                100 Hz
-----------------------------------------------------------------------
Sampling

FFT  Lines:                  3200
Overlap:                     66 %
Sample frequency:            256 Hz
Sample time:                 32 s
Resolution:                  31.25 mHz
-----------------------------------------------------------------------
Trigger

Source:                      Off
-----------------------------------------------------------------------
Channel Vibrometer 3D (connected to Vibrometer 1)

Range:                       31.62 V
Coupling:                    DC
Impedance:                   1 MOhm
Differential Input:          Off
Quantity:                    Velocity
Calibration factor:          10e-3  (m/s)/V
Signal Delay:                0  s
Filter Type:                 No Filter
Int/Diff Quantity:           Velocity
Window:                      Rectangle
Signal Enhancement:          Active

Channel Reference 1

Reference:                   Active
Reference point index:       0
Direction:                   +Z
Range:                       100 mV
Coupling:                    DC
Impedance:                   1 MOhm
ICP:                         Off
Differential Input:          Off
Quantity:                    Voltage
Calibration factor:          1
Signal Delay:                0  s
Filter Type:                 No Filter
Int/Diff Quantity:           Voltage
Window:                      Rectangle
Signal Enhancement:          Not active
-----------------------------------------------------------------------
Signal Enhancement

Speckle Tracking:            Active
Mode:                        Fast
-----------------------------------------------------------------------
Vibrometer 1

Type:                        OFV-5000
```

```
Tracking filter:             Off

Velocity output

Range:                       VD-03  10 mm/s/V
Low pass filter:             1.5 MHz
High pass filter:            Off
---------------------------------------------------------------------
Function Generator 1

Type:                        NI 671x
Signal:                      Periodic Chirp
Amplitude:                   100 mV
Offset:                      0 V
Amplitude correction:        None
-----------------------------------------------------------------
```

Appendix B

B.1 Test 1 Left Span Average Spectrum Graphs

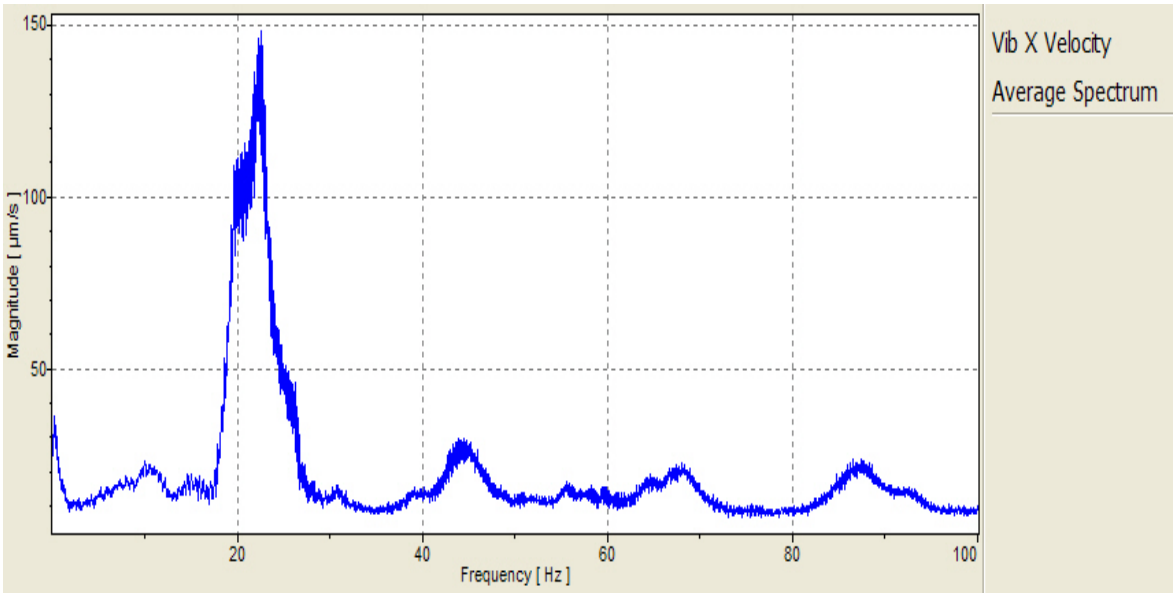

Figure 43: Test 1, Left Span, Average Spectrum, Vib X Velocity

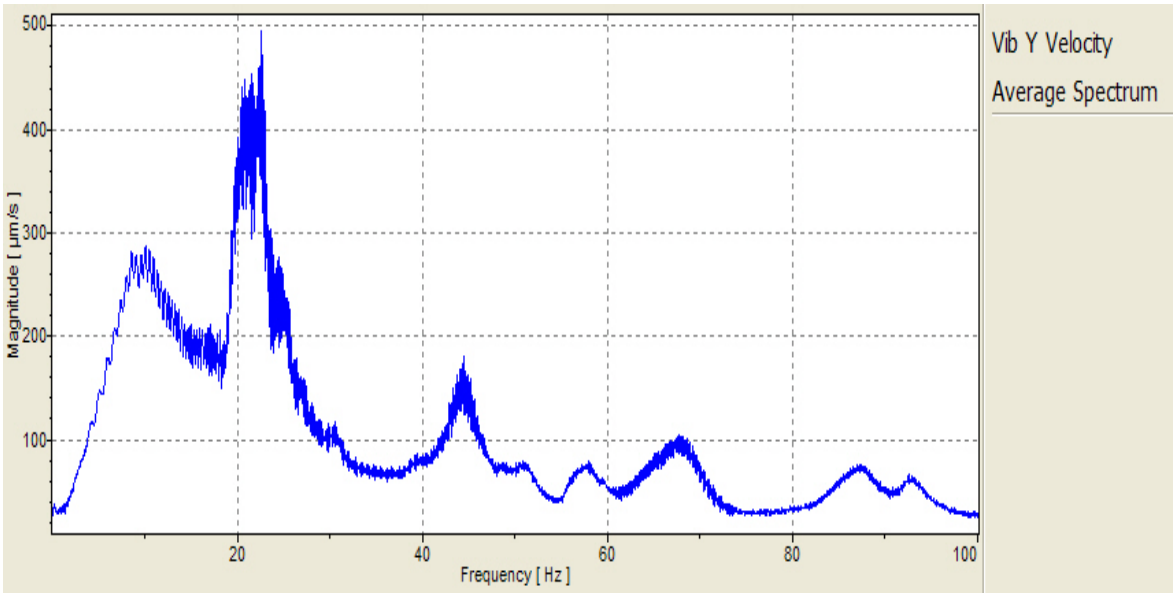

Figure 44: Test 1, Left Span, Average Spectrum, Vib Y Velocity

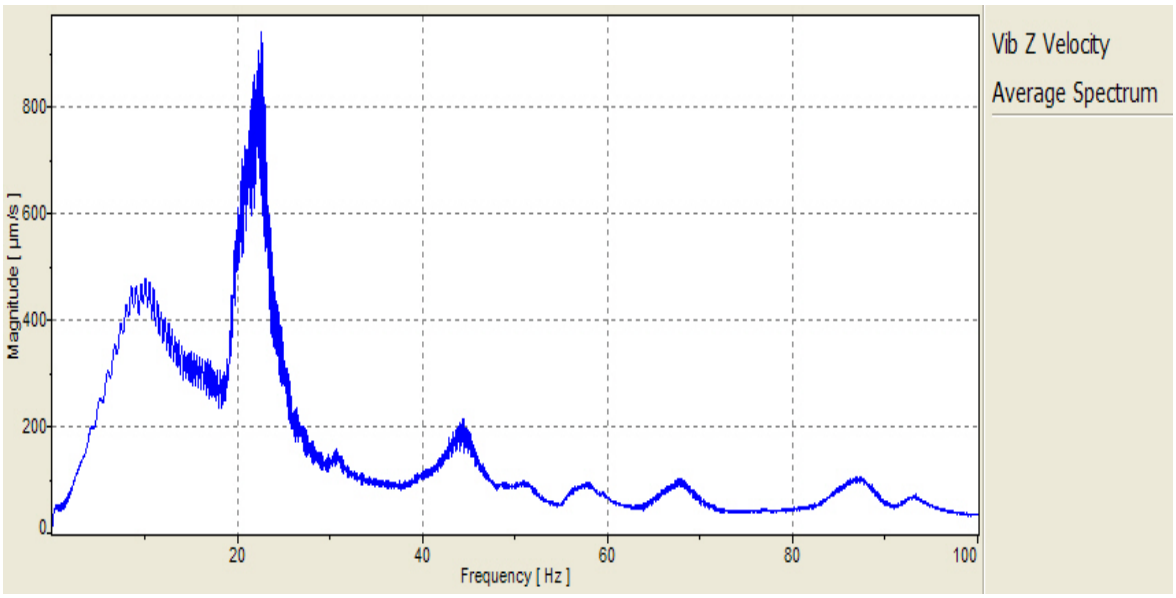

Figure 45: Test 1, Left Span, Average Spectrum, Vib Z Velocity

B.2 Test 1 Right Span Average Spectrum Graphs

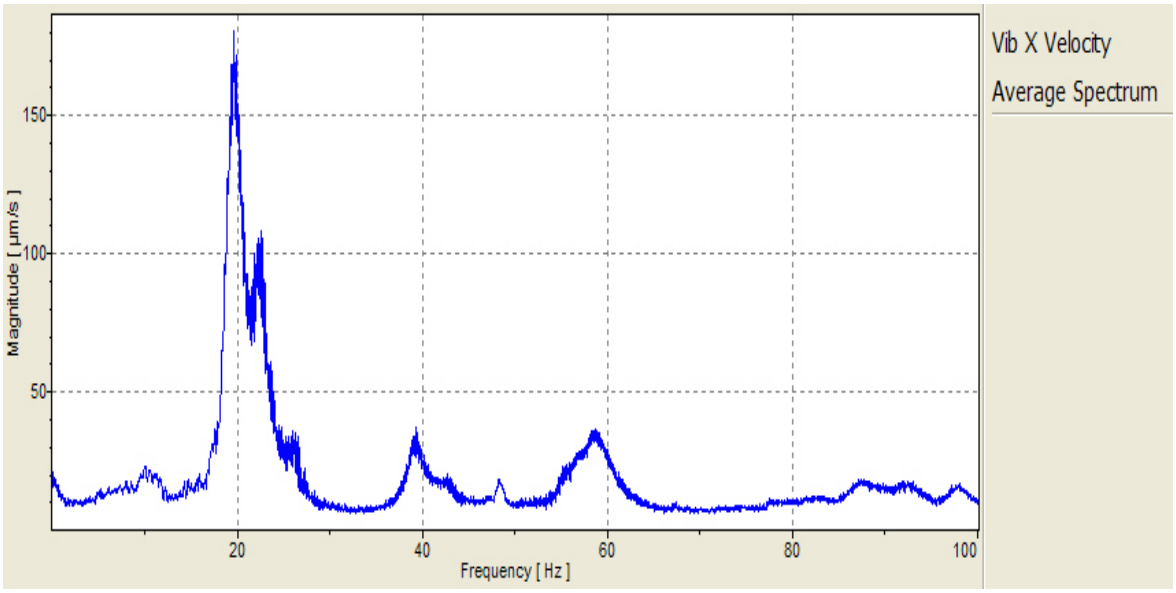

Figure 46: Test 1, Right Span, Average Spectrum, Vib X Velocity

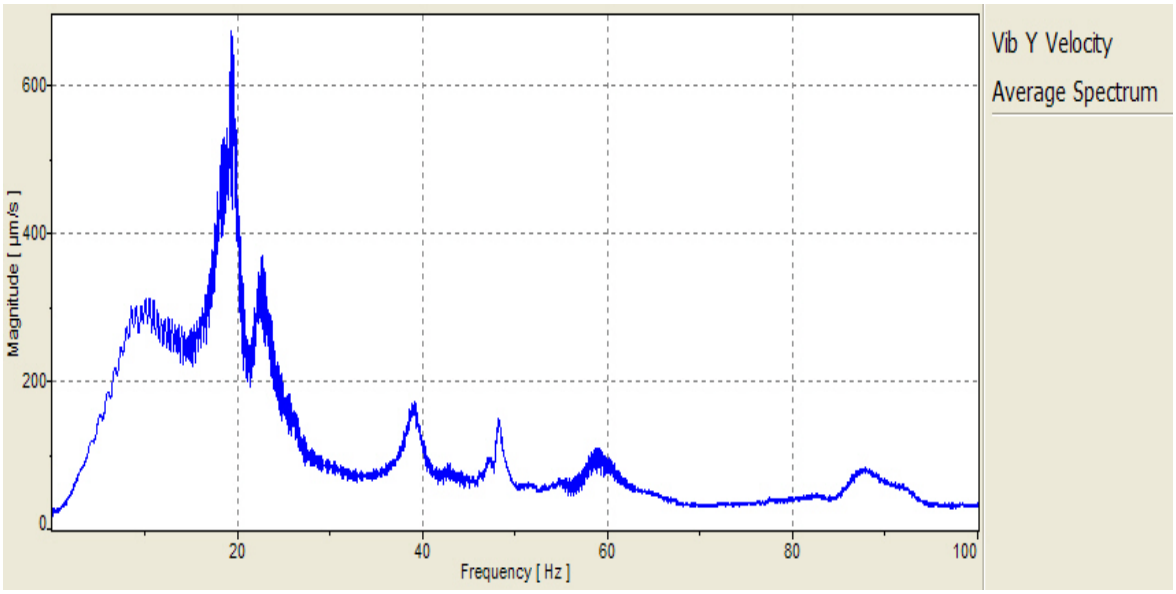

Figure 47: Test 1, Right Span, Average Spectrum, Vib Y Velocity

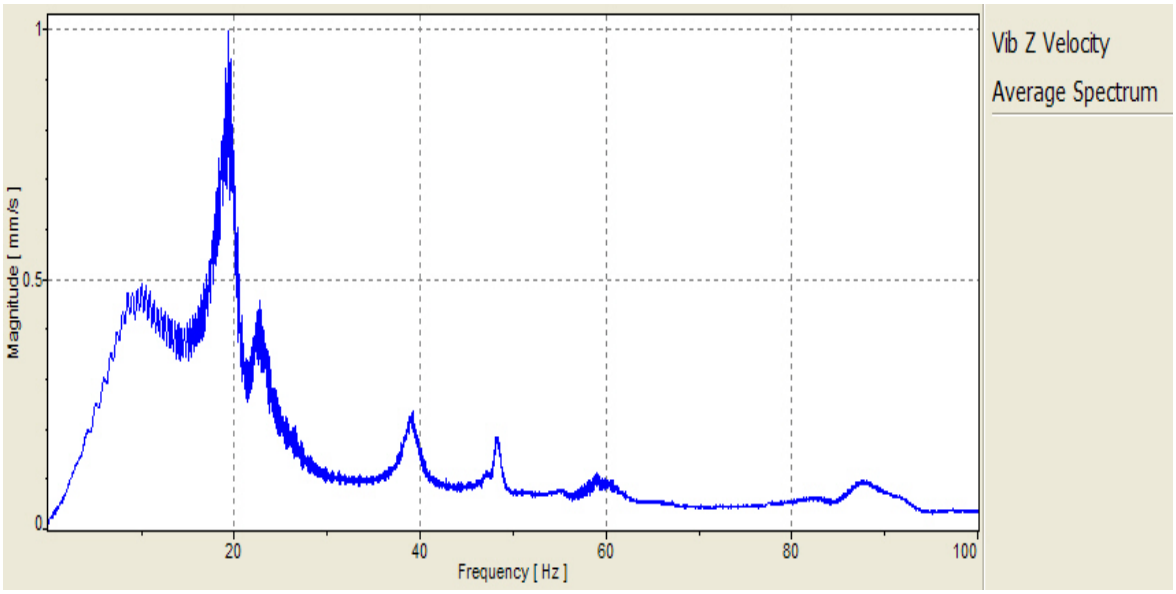

Figure 48: Test 1, Right Span, Average Spectrum, Vib Z Velocity

B.3 Test 2 Left Span Average Spectrum Graphs

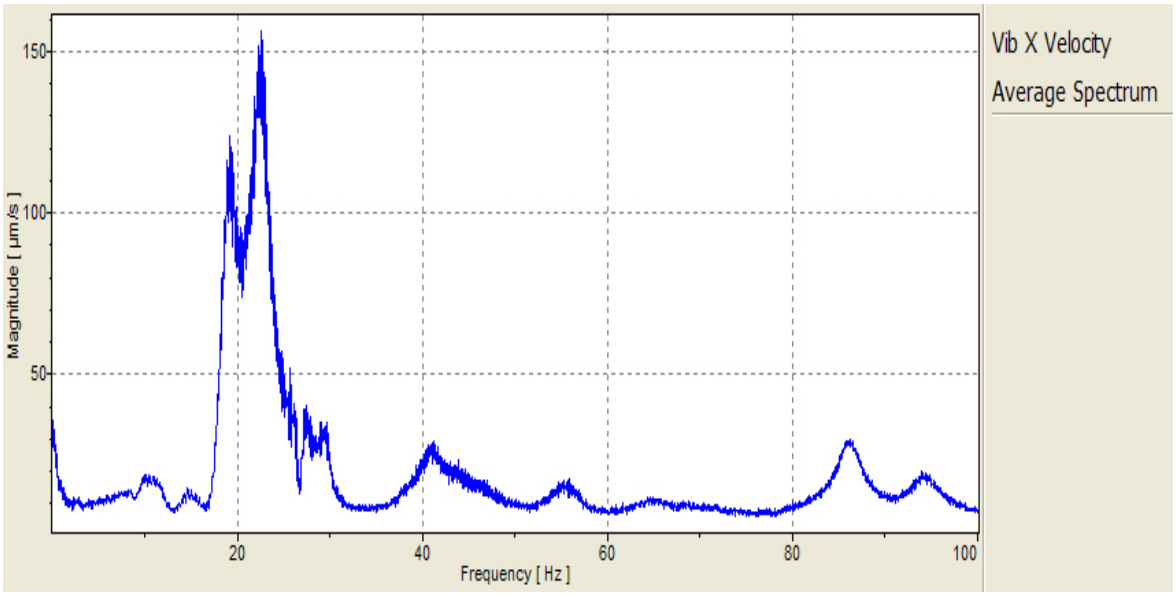

Figure 49: Test 2, Left Span, Average Spectrum, Vib X Velocity

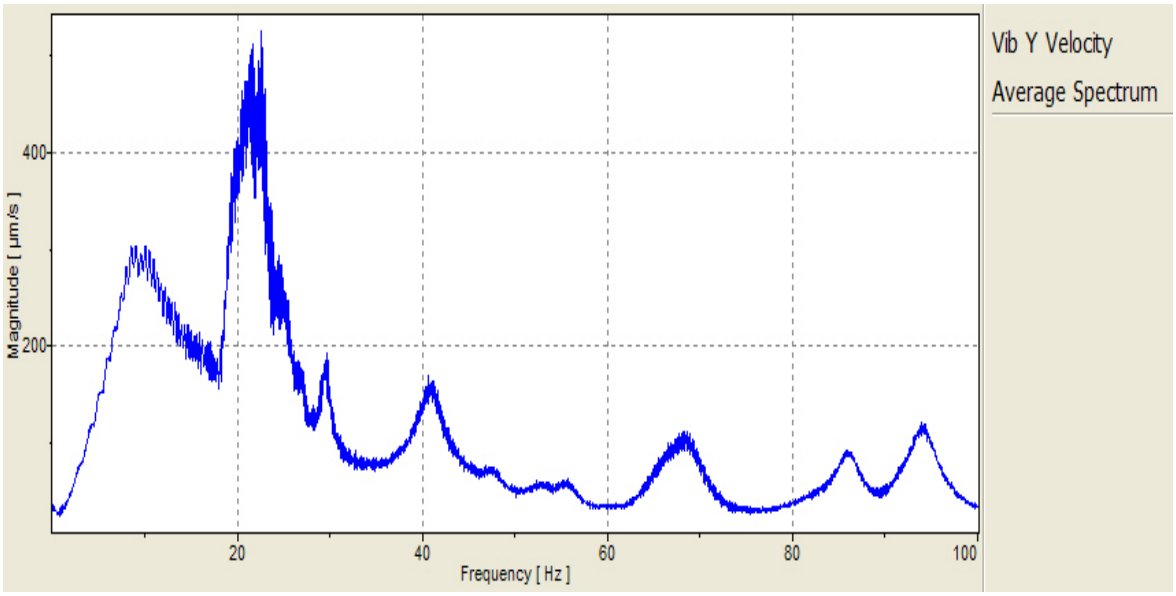

Figure 50: Test 2, Left Span, Average Spectrum, Vib Y Velocity

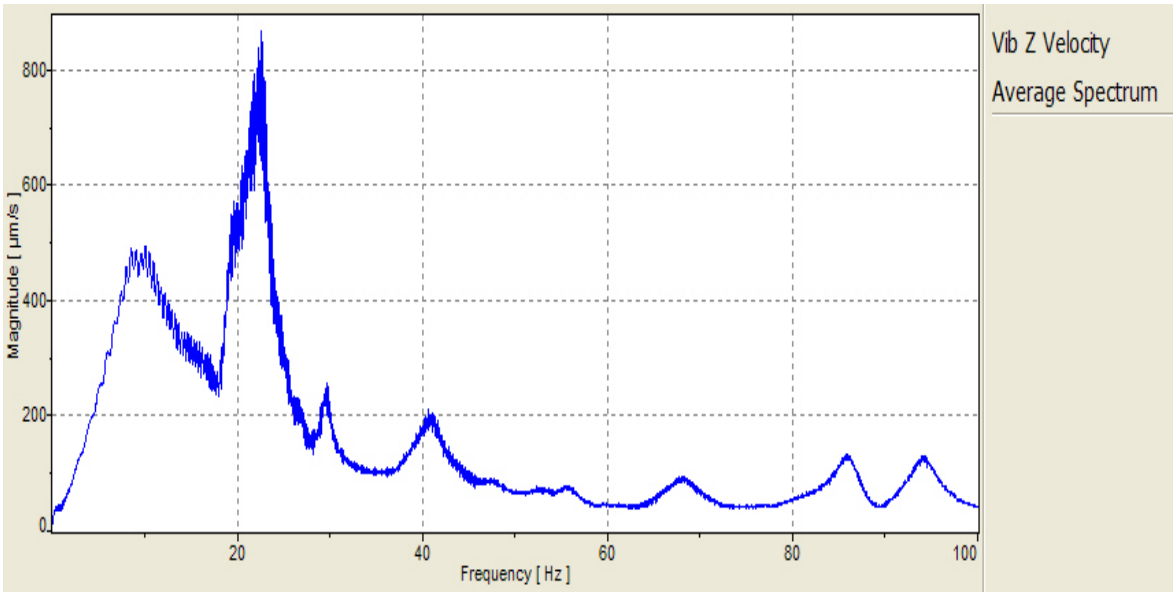

Figure 51: Test 2, Left Span, Average Spectrum, Vib Z Velocity

B.4 Test 2 Right Span Average Spectrum Graphs

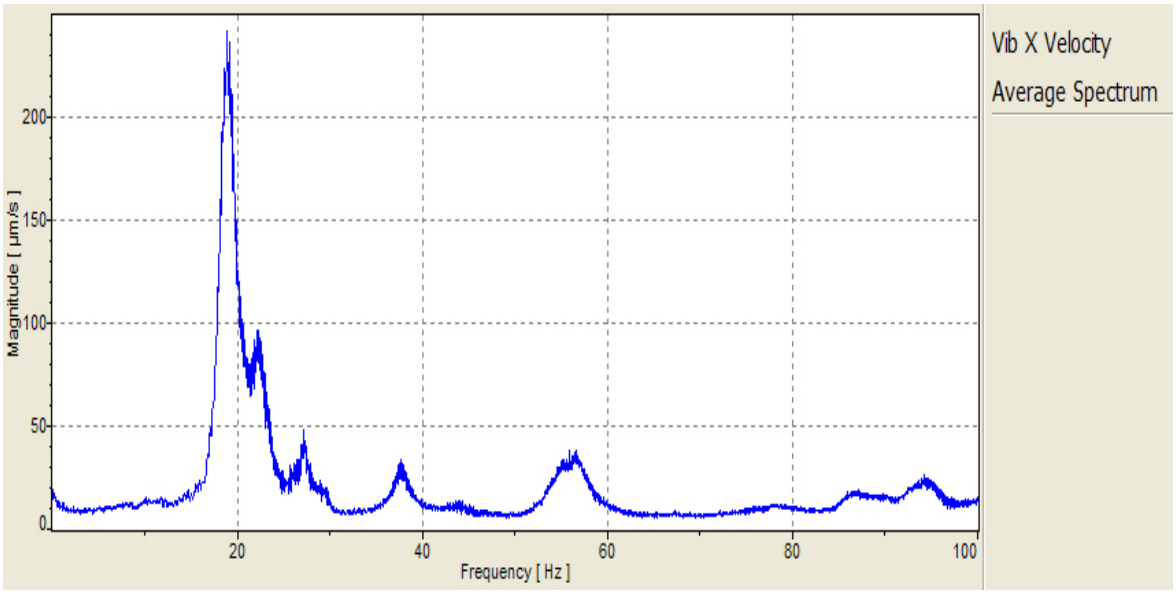

Figure 52: Test 2, Right Span, Average Spectrum, Vib X Velocity

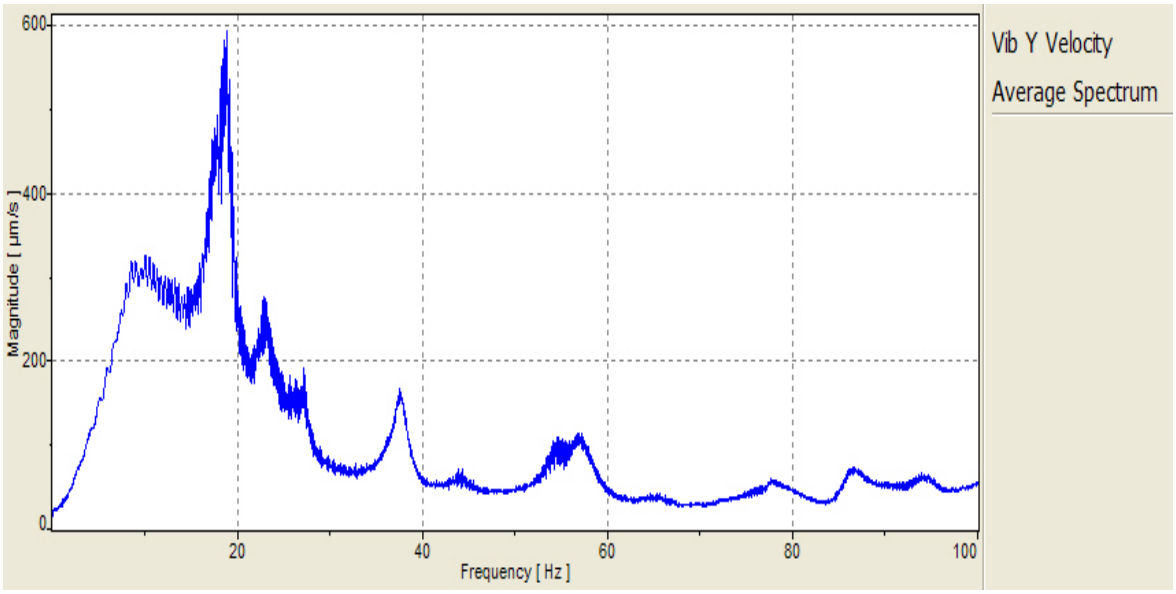

Figure 53: Test 2, Right Span, Average Spectrum, Vib Y Velocity

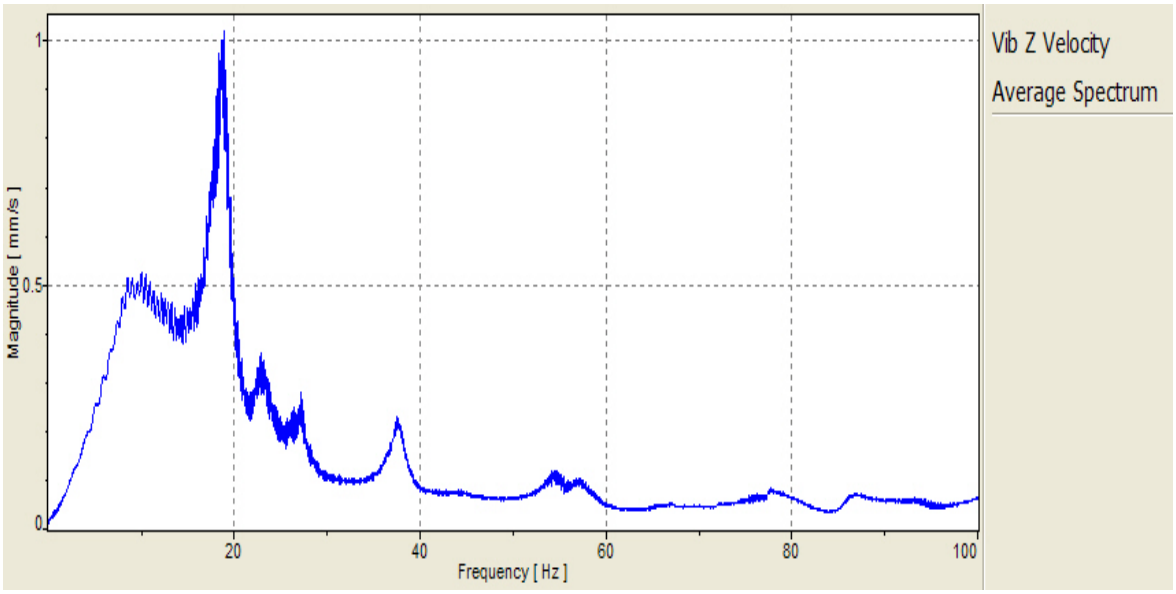

Figure 54: Test 2, Right Span, Average Spectrum, Vib Z Velocity

B.5 Index 4 Average Spectrum Graphs

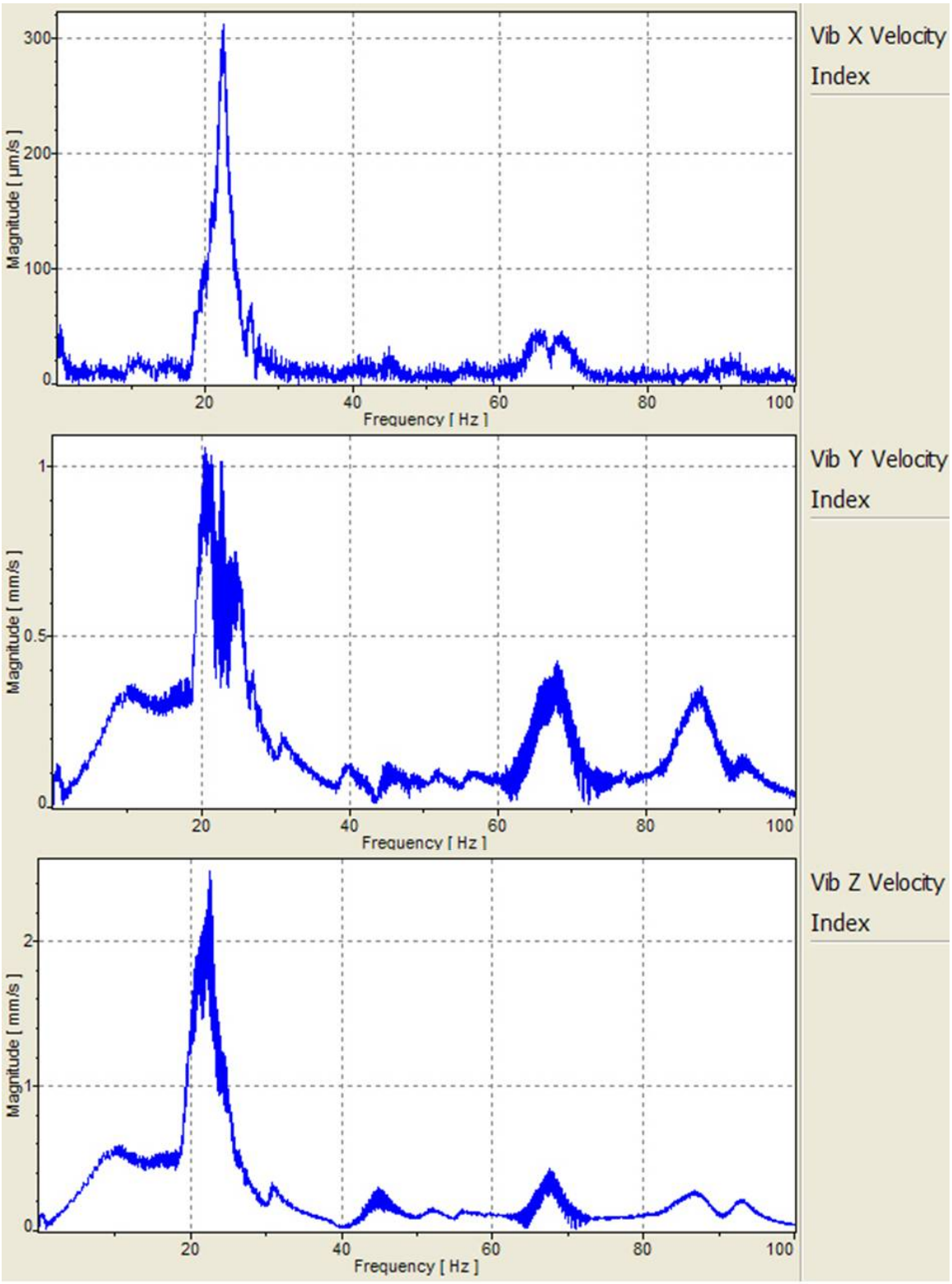

Figure 55: Index 4 Test 1, X, Y, Z Average Spectrum Graphs

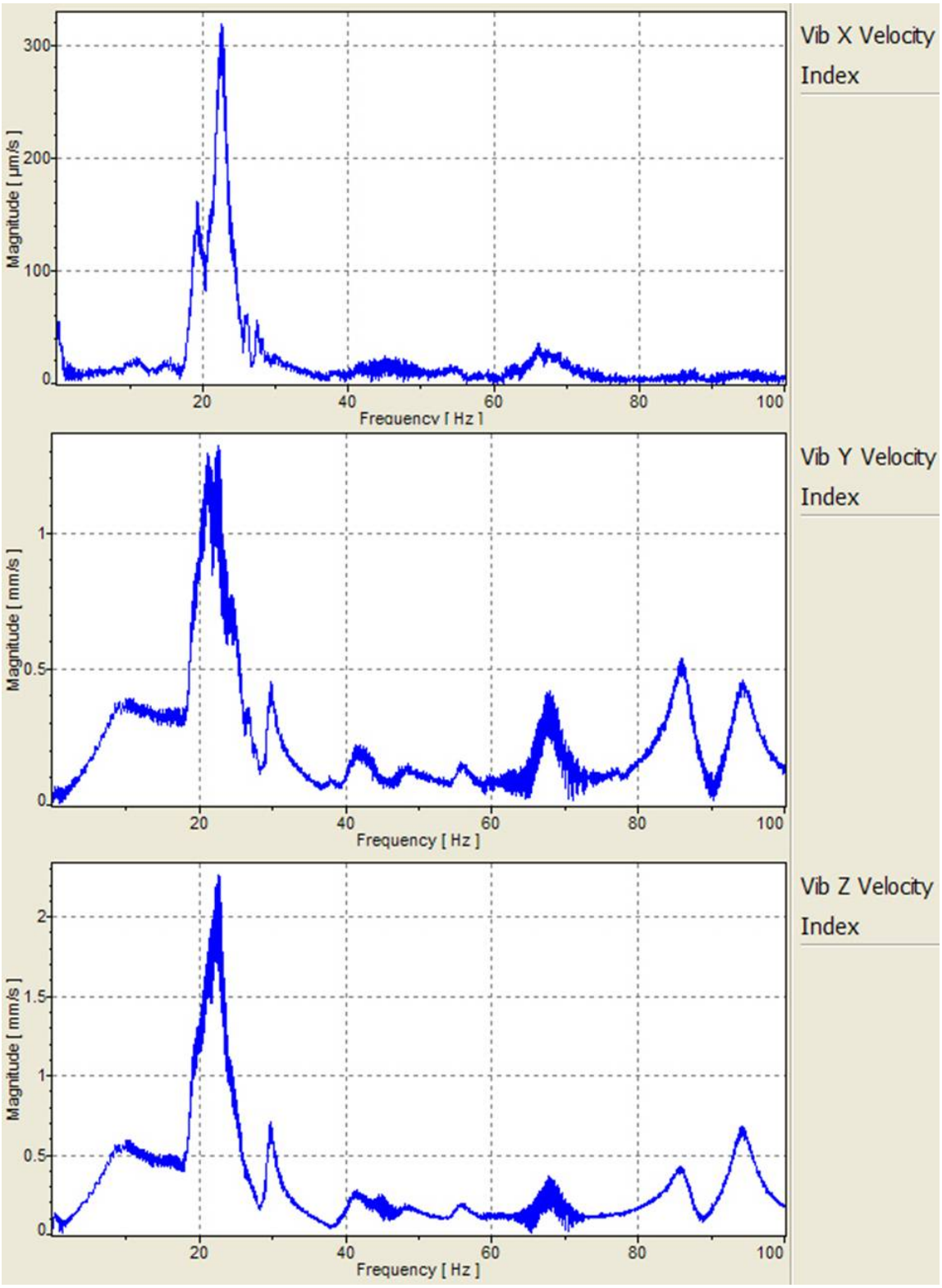

Figure 56: Index 4 Test 2, X, Y, Z Average Spectrum Graphs

B.6 Index 76 Average Spectrum Graphs

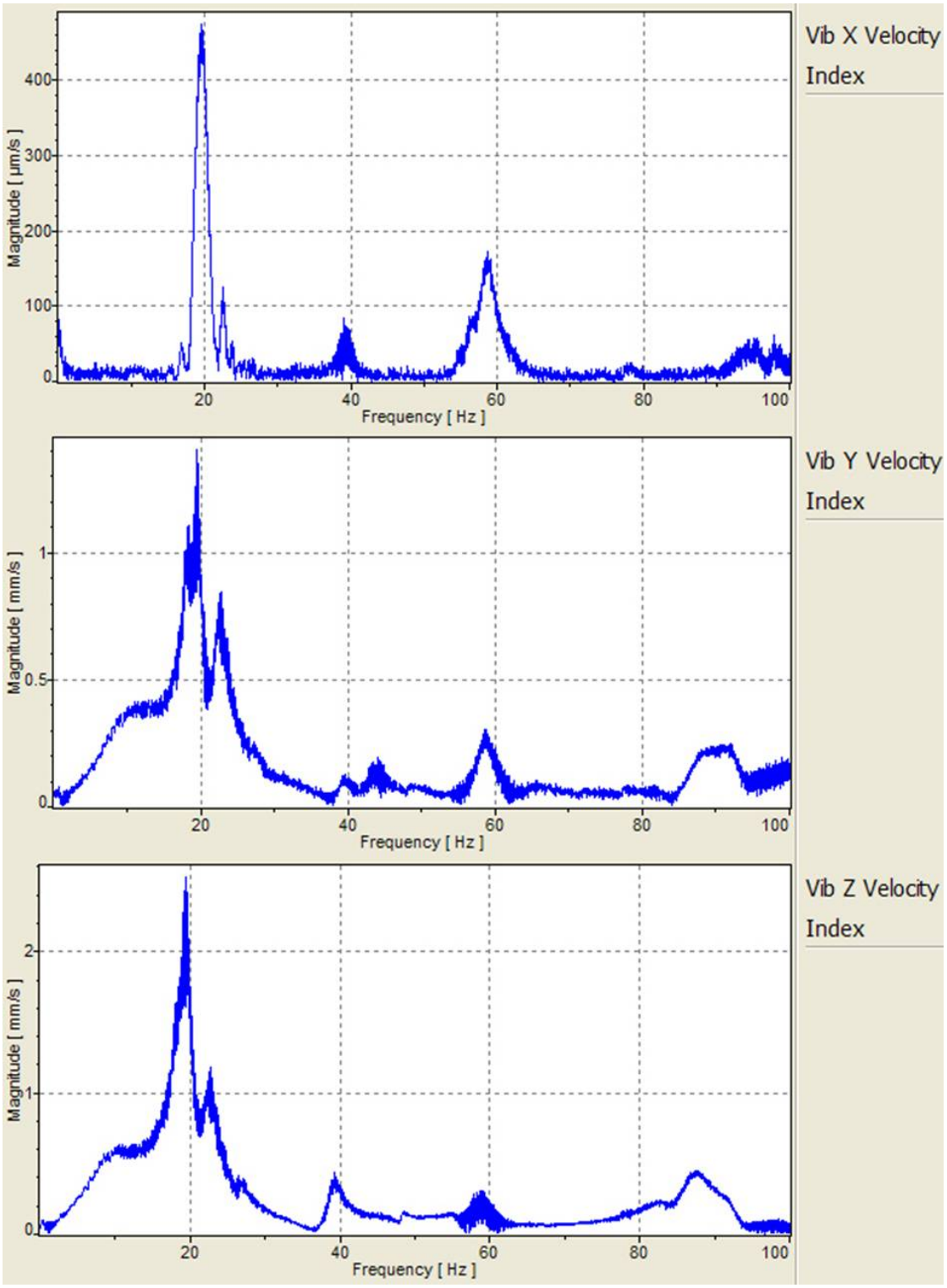

Figure 57: Index 76 Test 1, X, Y, Z Average Spectrum Graphs

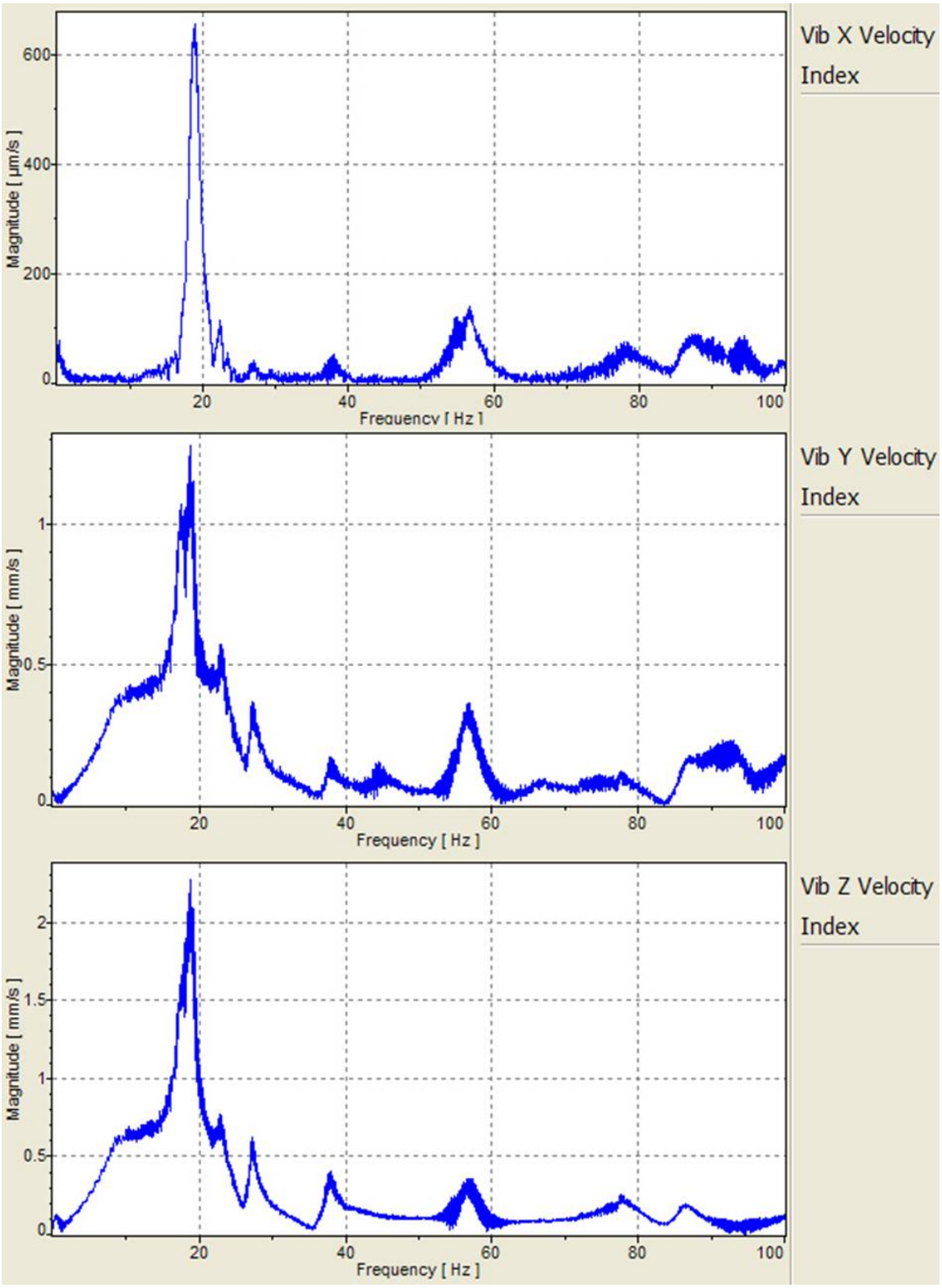

Figure 58: Index 76 Test 2, X, Y, Z Average Spectrum Graphs

B.7 Index 103 Average Spectrum Graphs

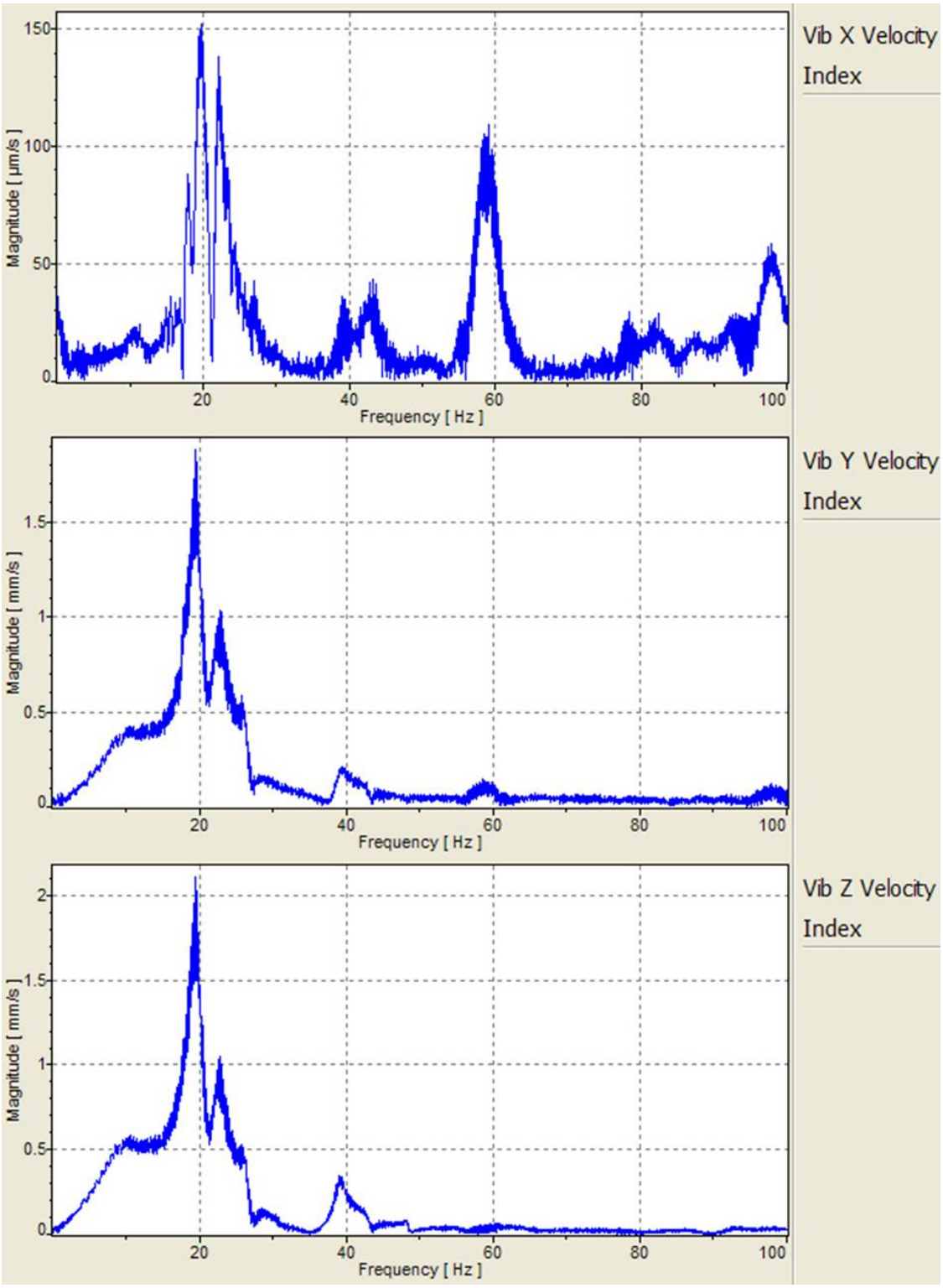

Figure 59: Index 103 Test 1, X, Y, Z Average Spectrum Graphs

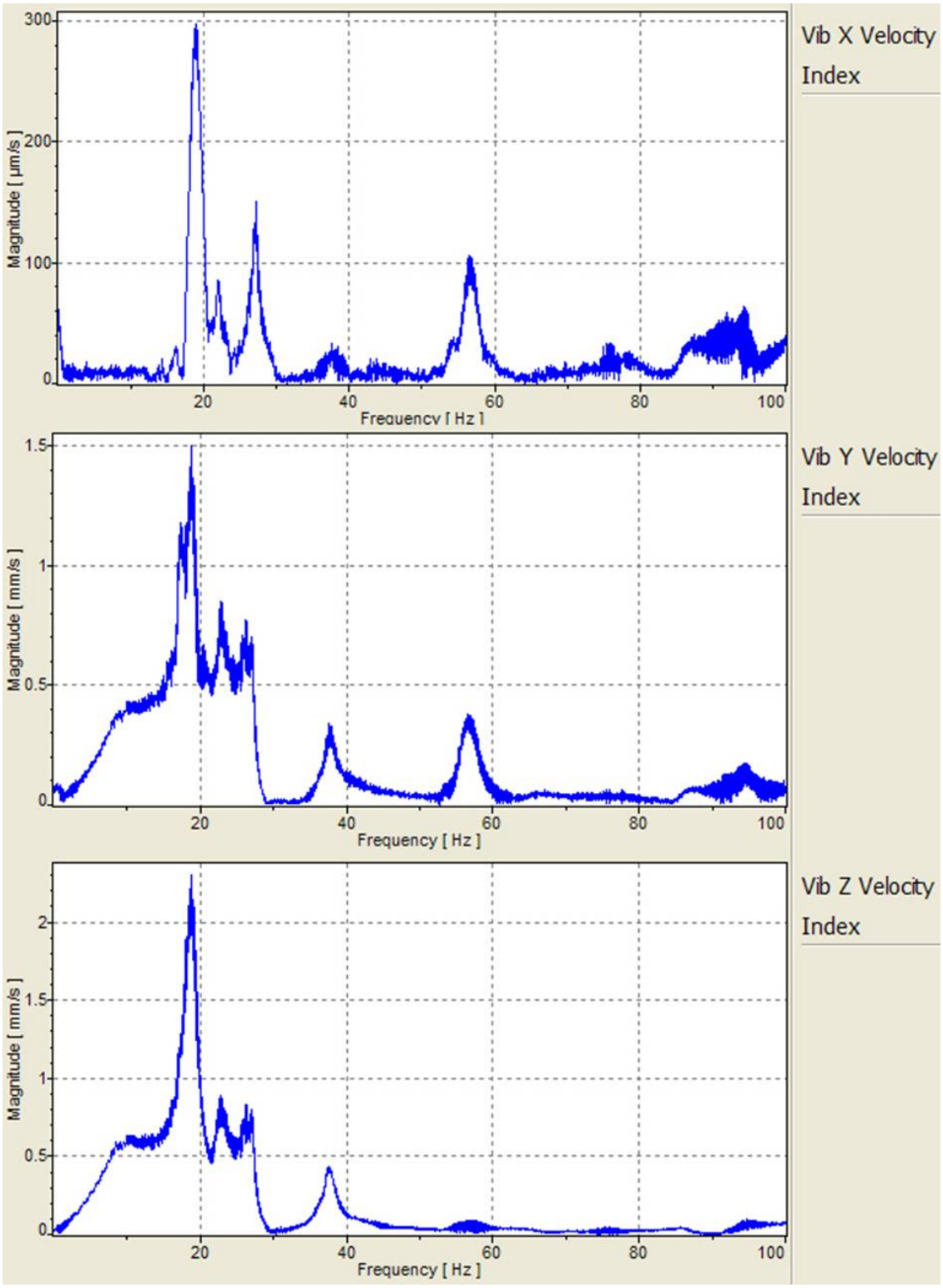

Figure 60: Index 103 Test 2, X, Y, Z Average Spectrum Graphs

B.8 Index 147 Average Spectrum Graphs

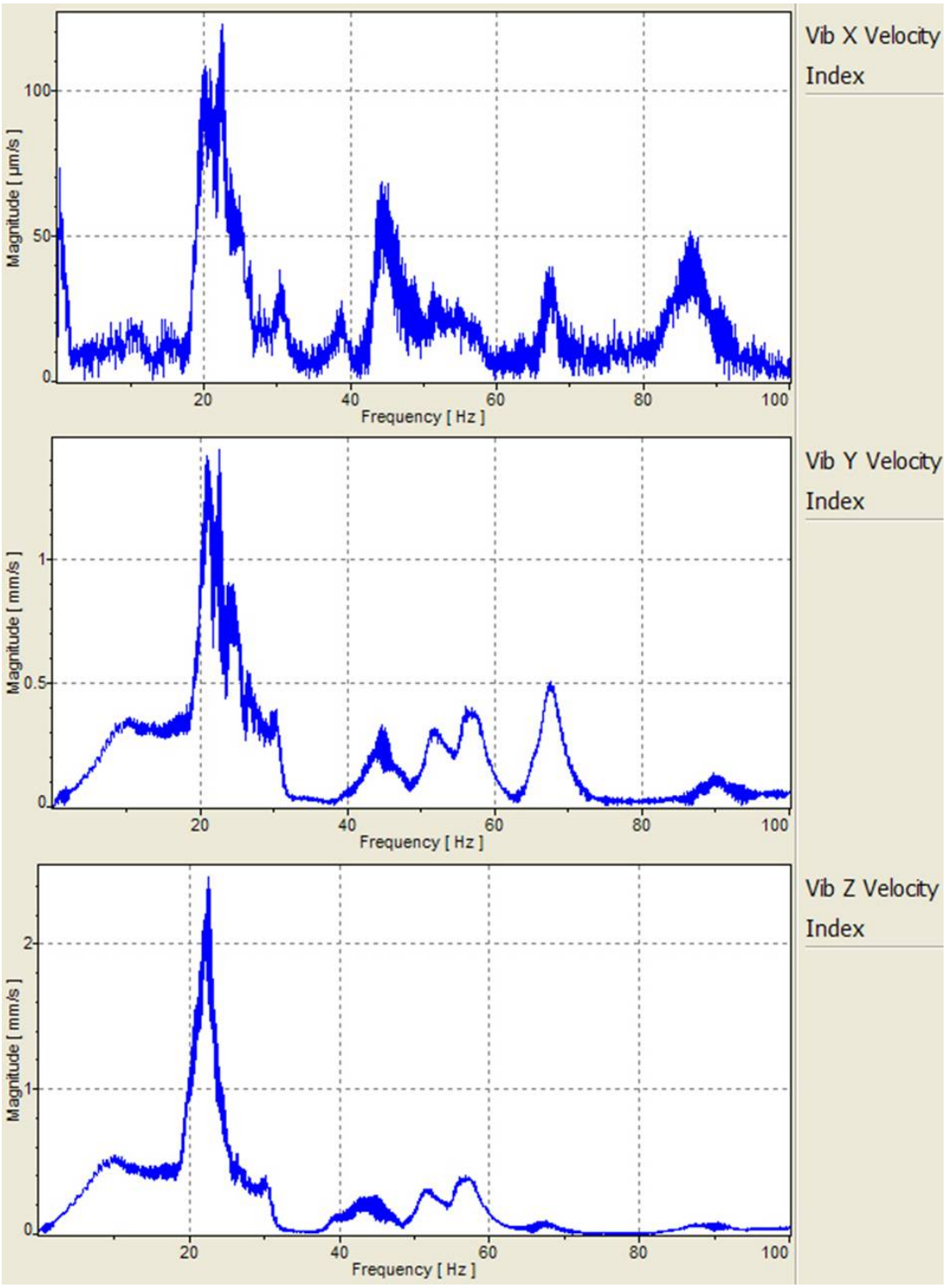

Figure 61: Index 147 Test 1, X, Y, Z Average Spectrum Graphs

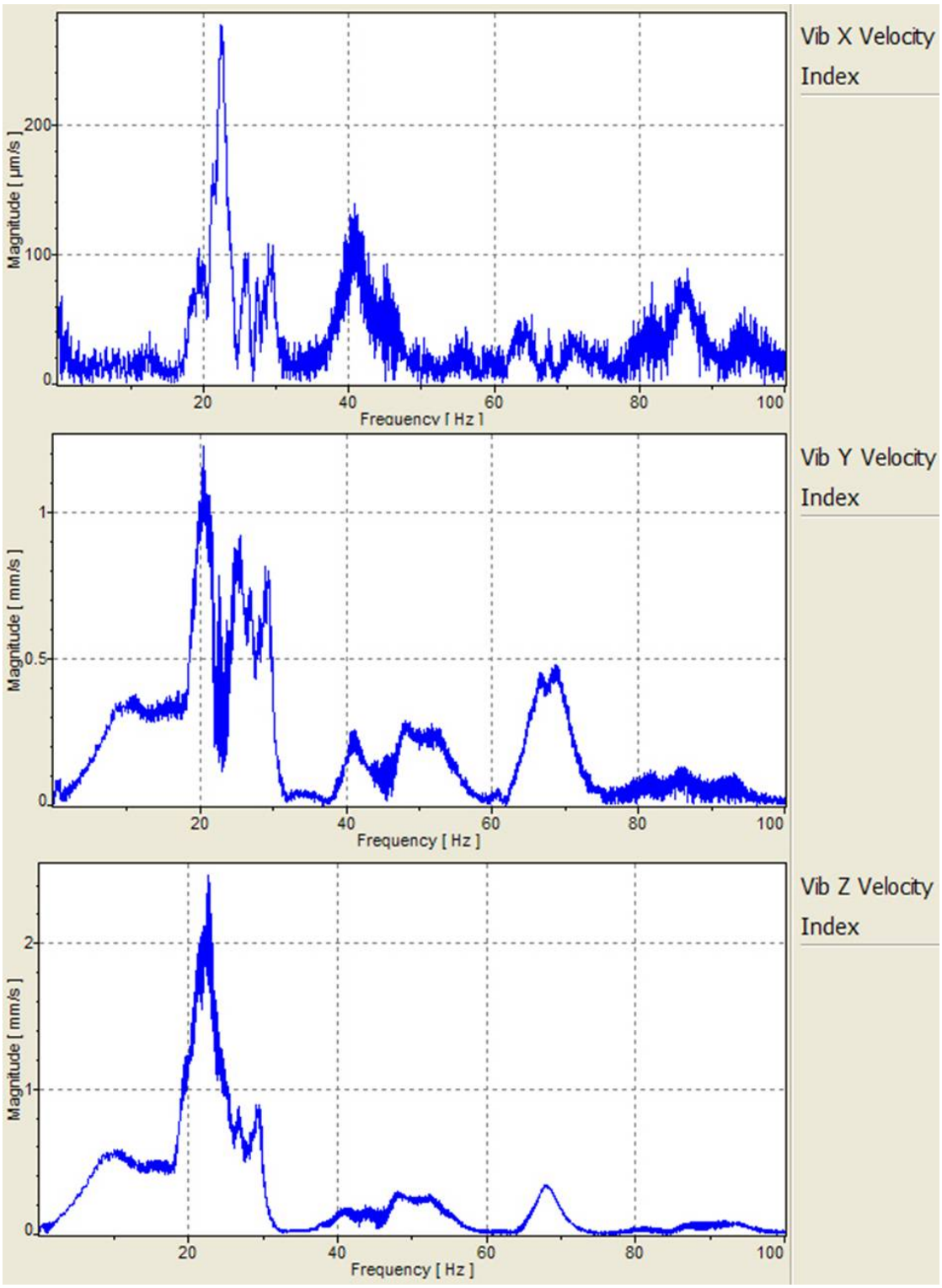

Figure 62: Index 147 Test 2, X, Y, Z Average Spectrum Graphs

Appendix C

The following methods put forth are derived from instructions written by Capt. Adam Tobias, suggestions and recommendations from Polytec employees, and personal experience. The Polytec Hardware, Software, and Theory manuals are highly recommended for reference.

Beginning a Test

1. Turn on PSV computer.
2. Turn on the 3 vibrometer controller boxes.

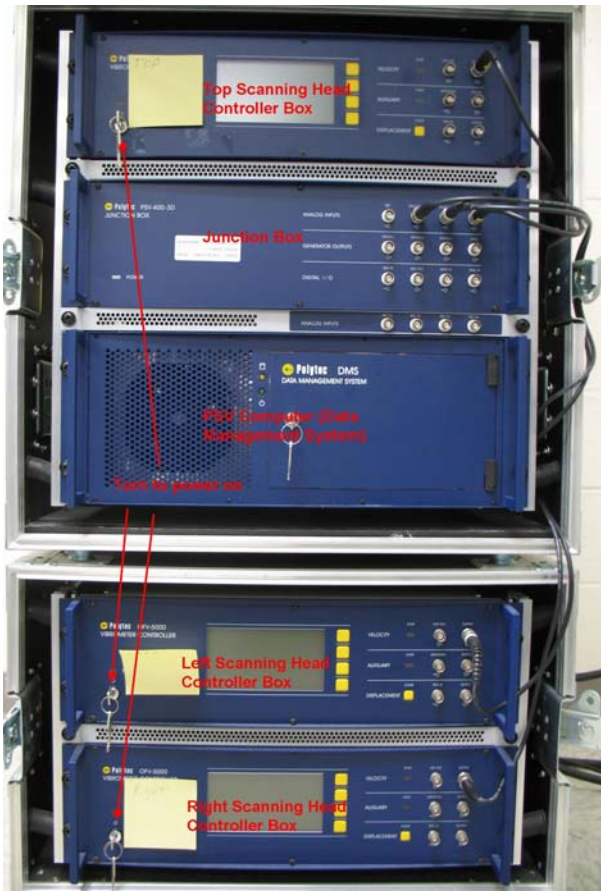

Figure 63: Setup 1

3. Open PSV 8.41 Program using icon on the desktop.
4. Open the laser and camera lens covers on all three vibrometer scanning heads.
5. Set up vibrometers to a height approximately level with the object being tested.
6. The scanning head with the operating video camera should be positioned in the center.
7. Select *Acquisition Mode* (a red starburst icon) in the PSV Program.

8. Verify the *Toggle Scanning Head* icon to the right of *Acquisition Mode* is selected.
9. On the far right of the screen is the optics toolbox, verify that all 3 lasers are checked on.
10. Click the center button in the optics toolbar to center the laser's position.

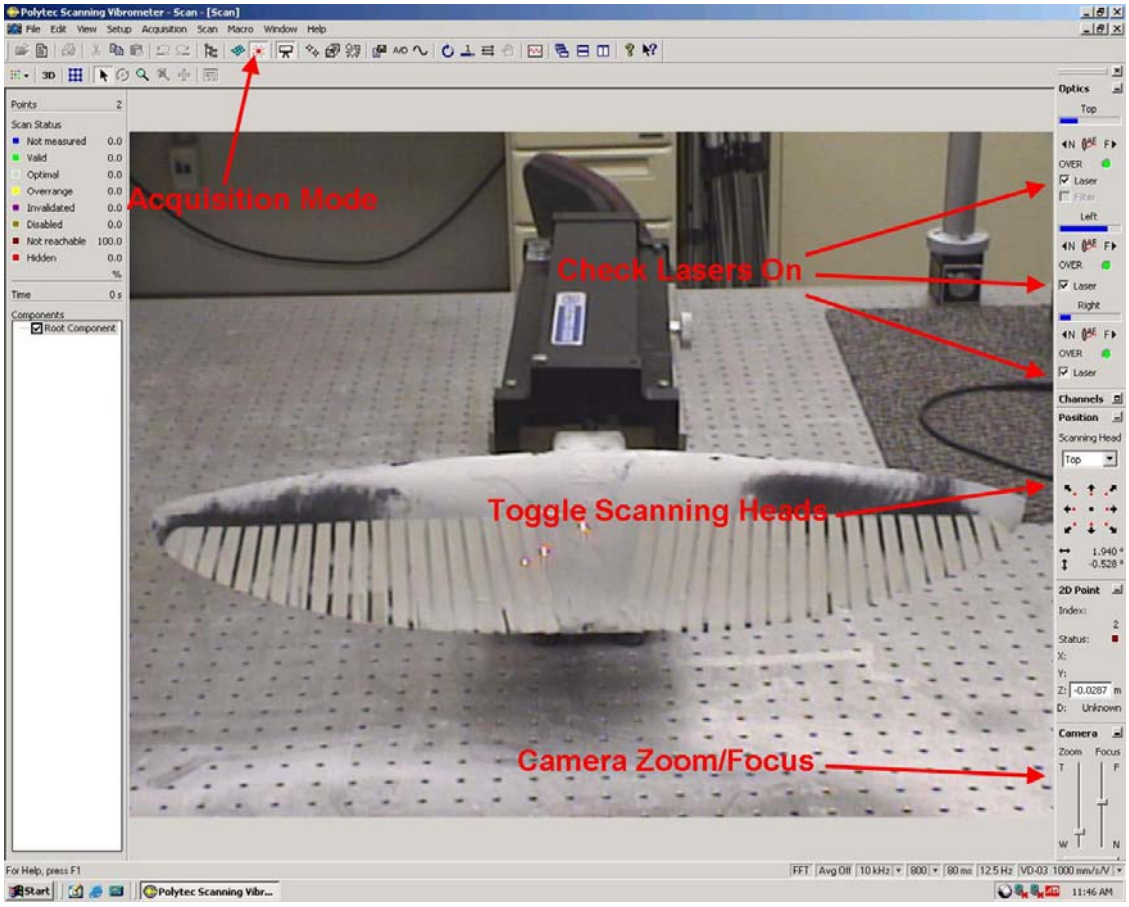

Figure 64: Setup 2

11. Adjust all 3 scanning heads manually so that the lasers point to the center of the object being tested.
12. Make sure the *top* scanning head camera is zoomed out completely and the object to be scanned is in the center of the picture on the monitor, then autofocus the camera using the button in the optics toolbox.
13. Now zoom in the focus of the camera using the *focus* bar in the optics toolbox, so that the object being tested now takes up the full area (width and/or height) of the monitor picture.
14. Autofocus the camera.
15. Ensure that all 3 lasers are still positioned in the center of the object being tested.
16. Click the autofocus button for each of the lasers (designated *AF* in the optics toolbox). To select each laser to autofocus one at a time, you must use the *Scanning Head* pull down menu in the optics toolbox and choose Top, Left, and Right. You may also autofocus all 3 lasers at once by holding down the *Shift* key and left clicking on *AF*.
17. If you would prefer to zoom in further at this point to a specific area of the item being tested, you may use the zoom "magnifying glass" icon. You can zoom in and out with the

magnifying glass icons without affecting the focus of the camera. This zoom feature is similar to the one in Microsoft Word.

18. The basic setup is complete

2-D Alignment

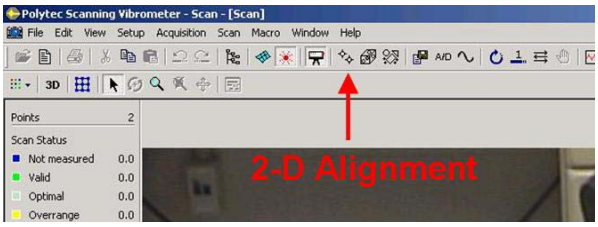

Figure 65 - 2-D Alignment Button

1. 3-D testing requires you do a 2-D Standard Alignment
2. Right click on the screen and select *Delete All* to delete all previously stored alignment points
3. Decide on 4-10 alignment points for each head. If the object is relatively basic, such as a flat beam or plate, 4-6 points may be used. If it is complex, such as a 3-D wing, 15-25 points should be used. Verify the laser head can quickly find the point on the video image. If the laser head cannot quickly find the point after 25 points continue until the laser head can easily identify the point.
4. Now shut off 2 of the 3 lasers by unchecking the respective *Laser* box in the optics toolbox
5. Verify the remaining "on" laser is the one toggled in the *Scanning Head* pull down menu
6. Use the center button on the mouse to move the laser to the first alignment point
7. Autofocus the laser and then left click with the cursor centered exactly over the laser spot
8. Repeat steps 6 and 7 for the other two Scanning Heads (remember to switch lasers by using the *Scanning Head* pull down menu)
9. Now repeat steps 6-8 for all remaining alignment points
10. Once you have defined all of your 2-D alignment points, select the 2-D alignment icon again to close the alignment. If the alignment is successful, it will close uneventfully; otherwise you will receive a message stating the alignment did not succeed. Redefine 2-D alignment points or add more alignment points.

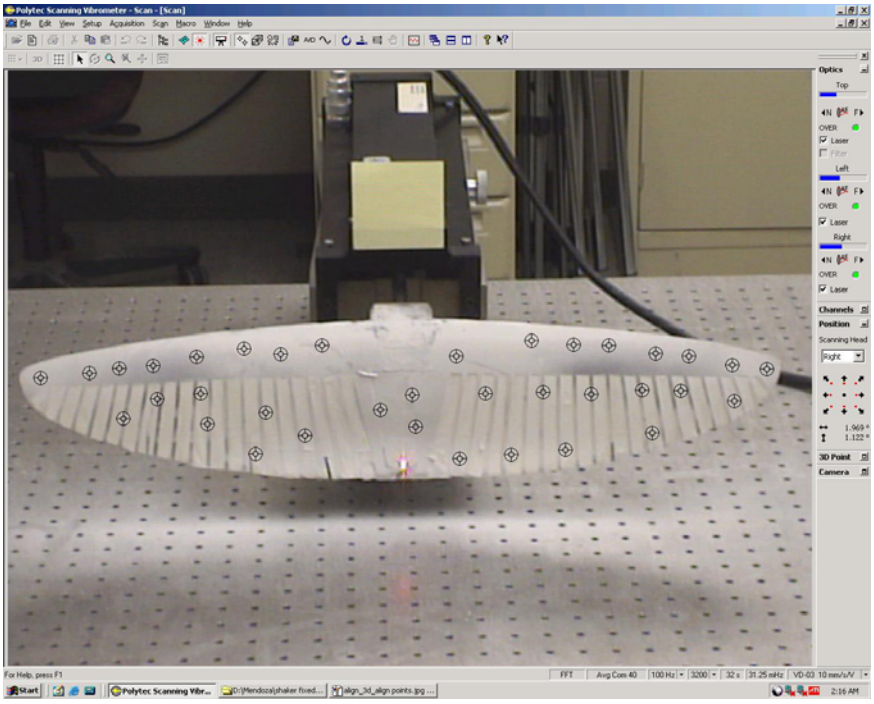

Figure 66 - Example 2-D Alignment

3-D Alignment

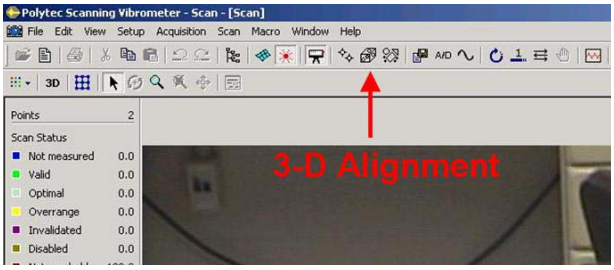

Figure 67: 3-D Alignment Button

1. Determine the coordinate system you would like to use. For example:

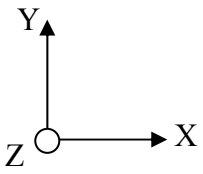

x+ to the right, y+ to the ceiling, z+ to the camera

2. Click on the *3-D Alignment* icon on the top toolbar.
3. Make sure *Auto* is checked "on" in the 3-D Alignment toolbox.

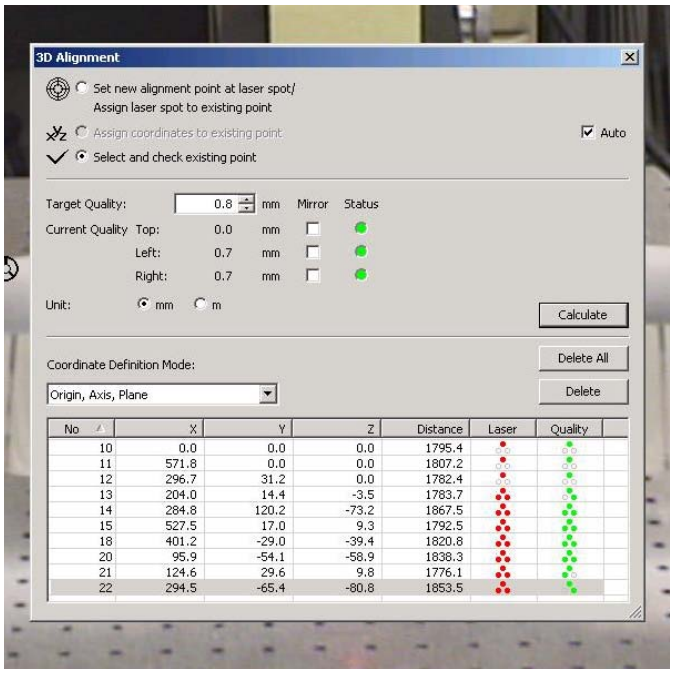

Figure 68: 3-D Alignment Dialog Box

4. Choose *Origin, Axis, Plane* as the Coordinate Definition Mode in the 3-D Alignment toolbox and make sure *Auto* is checked.
5. Set the target quality to 1.0 mm.
6. Choose *Set New Alignment Point* in the toolbox.
7. The first three points that will be made are the origin, a point on the +x axis, and a point on the x/+y plane. Only the top scanning head is required to make these three points.
8. Switch off the Left and Right lasers and select the Top Scanning Head.
9. Move the laser to the point you would like to make the origin and auto focus the laser.
10. Click on top of the point and a point should be made. Right click on the point and select *Origin.*
11. Repeat steps 9 and 10, except now when selecting the points, make them *Point on +x axis*, and *Point on x/+y plane.*
12. The coordinate system has now been defined by the three selected points.
13. Four to seven alignment points now need to be made using all three lasers. These alignment points determine the position of the three scanning heads relative to each other.
14. Using the green glasses allows you to see the laser more clearly. Use the remote control to position all 3 lasers on exactly the same spot.
    a. In *Grid Mode* use *up* arrow to switch laser; In *Free Mode* use the four directional arrows to move the selected laser. When in *Grid Mode* the selected scanning head will be shown in the *Toggle Scanning Head* box.
15. Once all 3 lasers are at the same point, click on top of the point and do so for every scanning head.
16. Repeat this process with a minimum of 4 and maximum of 7 total alignment points. Similar to the 2-D alignment, the number chosen depends upon the complexity of the object being tested. When the complexity of the object is unknown choose 7 total alignment points.
17. All remaining alignment points should be labeled *Alignment Point* when defined by step 13

18. Once all alignment points have been defined, select *Calculate* on the 3-D Alignment toolbox. If the target quality is not within your chosen desired quality, do either of the following:
    a. Redefine alignment points. Verify alignment is accurate, reduce exterior lighting, and coat the testing object to reduce surface effects.
    b. Increase the value of the target quality and re-click *Calculate*
19. Return to the top menu bar *Setup* and click *Align 3D Coordinates* to complete.

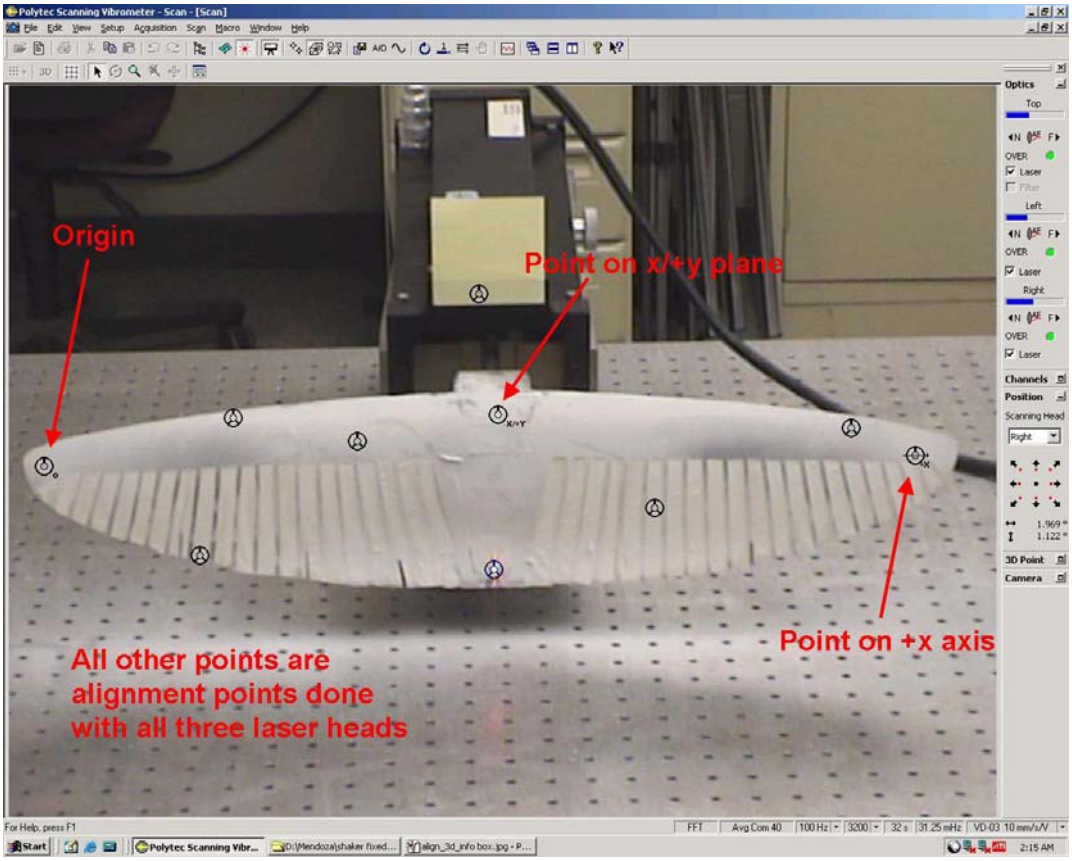

Figure 69: 3-D Alignment Points

Creating a Grid/Scan Points

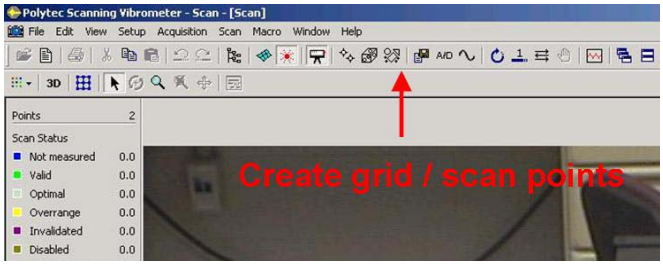

Figure 70: Create Grid Button

The grid establishes the grid points across the entire shape of your object. In the 3-D laser scan, all of the points that you have defined will be used. The more grid points, the longer the duration of a test scan, but the better your results will be.

1. Select the grid creation icon to use the grid creation toolbar.
2. Select the *Professional* icon.
3. Determine which shape to use to define the grid for your object.
4. Experiment with all the shapes to learn how to create different grids.
5. If your object is not perfectly level, rotate the grid object.
6. Change the density of the grid points as desired.
7. Once you have created a grid, uncheck the grid creation icon.

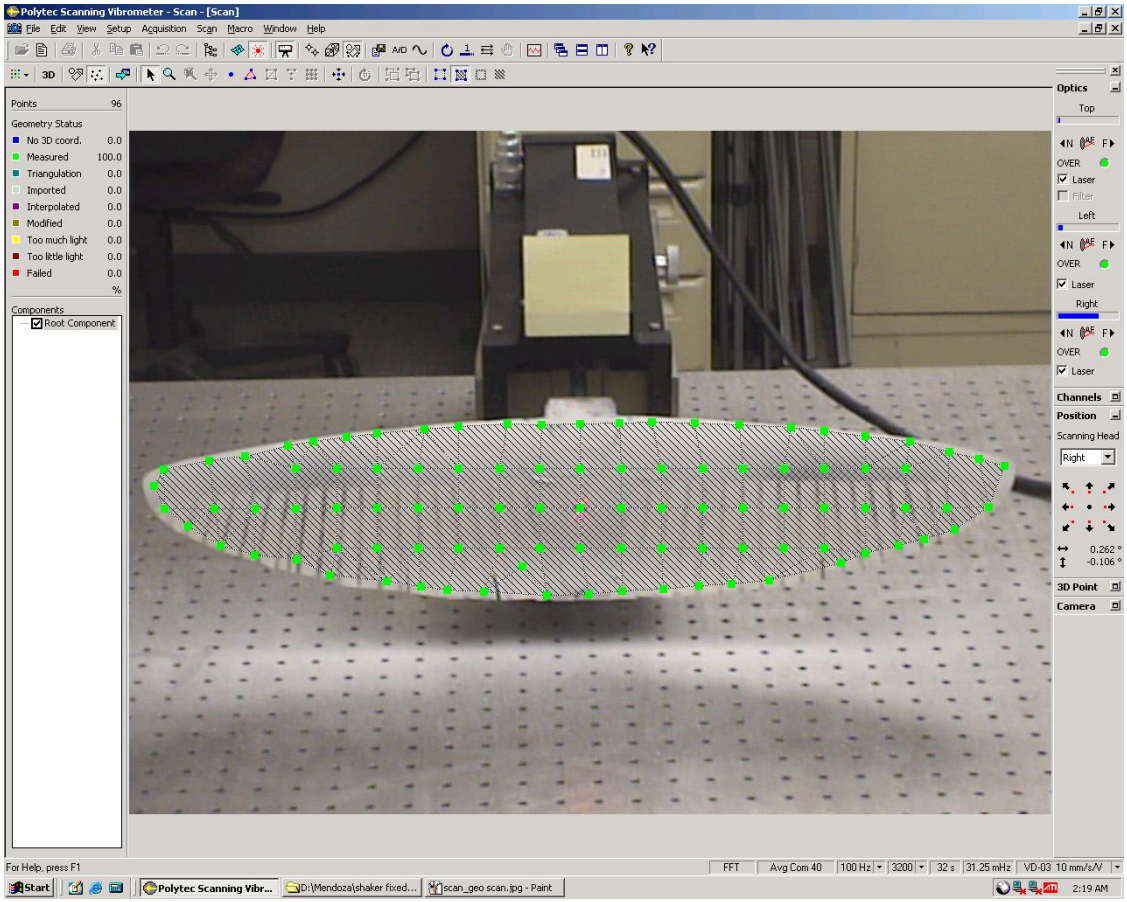

Figure 71: Example of Grid

Geometry Scan

1. Go to the scan menu and choose *Geometry Scan.*
2. A laser will jump to all grid points to scan the item's geometry.

3. A message stating *Geometry Scan Succeeded* will appear if the test is successful. Otherwise, return to the grid creation tool and make any necessary changes such as shifting or deleting scanning points.
4. When finished with the geometry scan, select *Assign Focus Fast* or *Assign Focus Best* depending upon which you prefer
    a. Use *Assign focus fast* for simple planar objects that are made of the same material, such as an aluminum plate
    b. Use *Assign focus best* for an object that has multiple surface properties and/or is a complex 3-D shape.

Acquisition Board Settings and Testing

A basic introduction into some common A/D settings will be provided in these instructions. This software offers many features and one should consult the PSV Software and Theory Manual as needed to determine the features most appropriate for their testing.

1. Connect the amplifier to your tester (shaker table or horn). Use the blue sided APS Dynamics amplifier for the shaker table.
2. Turn on the amplifier, verity the switch is on voltage and the small dial is turned counterclockwise until it stops.
3. Click the A/D icon on the computer.
4. There are 9 different tabs ranging from *General* to *Generator*, begin with *General.*

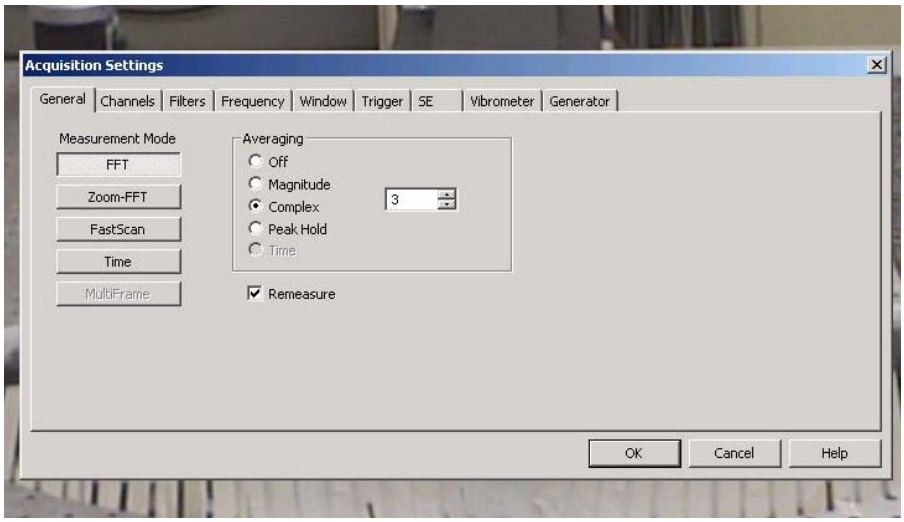

Figure 72: Acquisition Settings General Tab

5. For an initial test, always choose the measurement mode *FFT.*
6. If complex averaging is used, begin with 3 complex averages. Increasing the number of averages can be used to improve data if desired.
7. In the *Channels* tab, make sure the channels *Vibrometer 3D* and *Reference 1* are checked *active.*

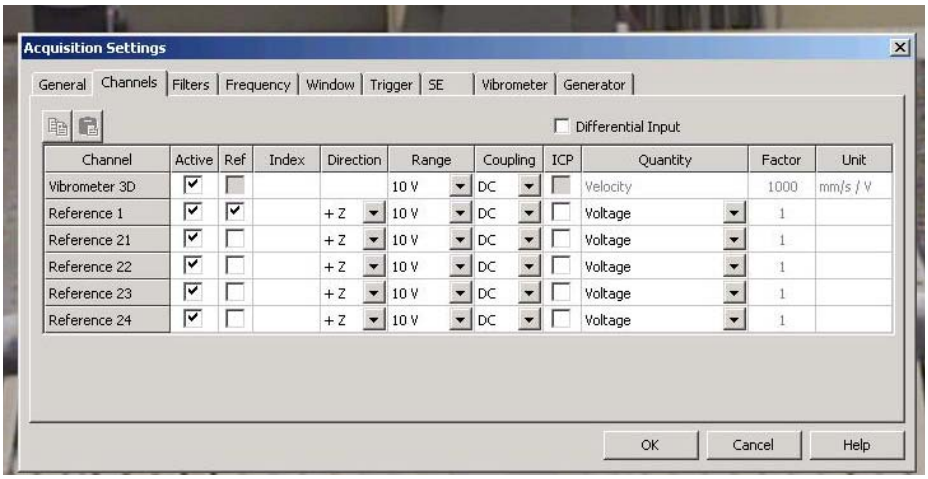

Figure 73: Acquisition Settings Channels Tab

8. In the *Filters* tab, if you do not want to use a filter, select *no filter.*

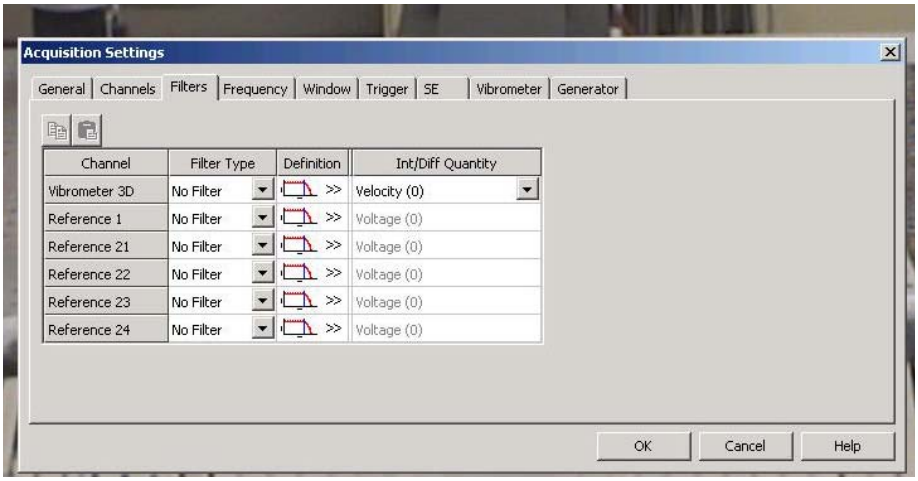

Figure 74: Acquisition Settings Filters Tab

9. In the *Frequency* tab, select the desired Bandwidth and range, the smaller the bandwidth the more precise the test. Use a range corresponding to the frequency range you will be testing.

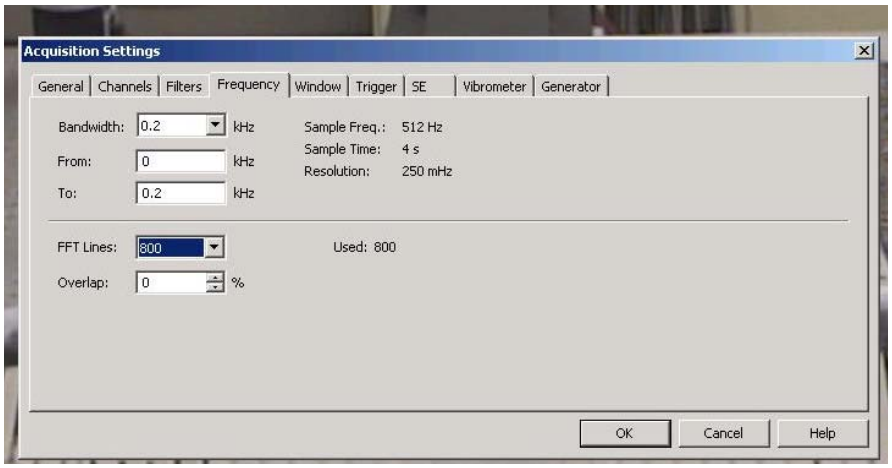

Figure 75: Acquisition Settings Frequency Tab

10. The FFT lines improve test results. Increasing the number of FFT lines will increase scanning time.
11. The *Window* tab may be left at *Rectangle Functions* if desired.

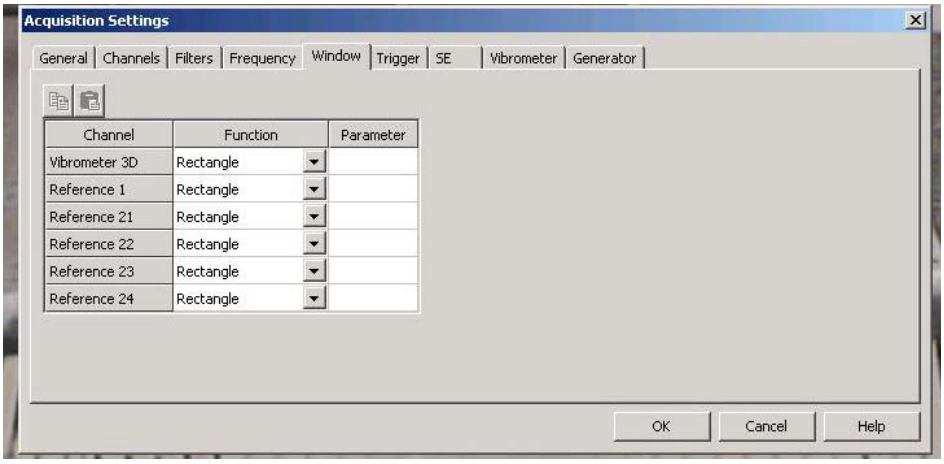

Figure 76: Acquisition Settings Window Tab

12. The *Trigger* tab may be left off.
13. *SE* tab is speckle tracking, select it on and choose Fast.
14. The *Vibrometer* tab defines the velocity range. If the amplitude is too great, the software will indicate *over range*. Also, there is a light on the front of all 3 control boxes that must be watched for over ranging as well. Adjust the velocity range so that no over ranges occur. If the max velocity range is chosen and the test still over ranges, you must reduce the test amplitude.
15. The *Filters* tab may be left as Off/1.5MHz/Off.

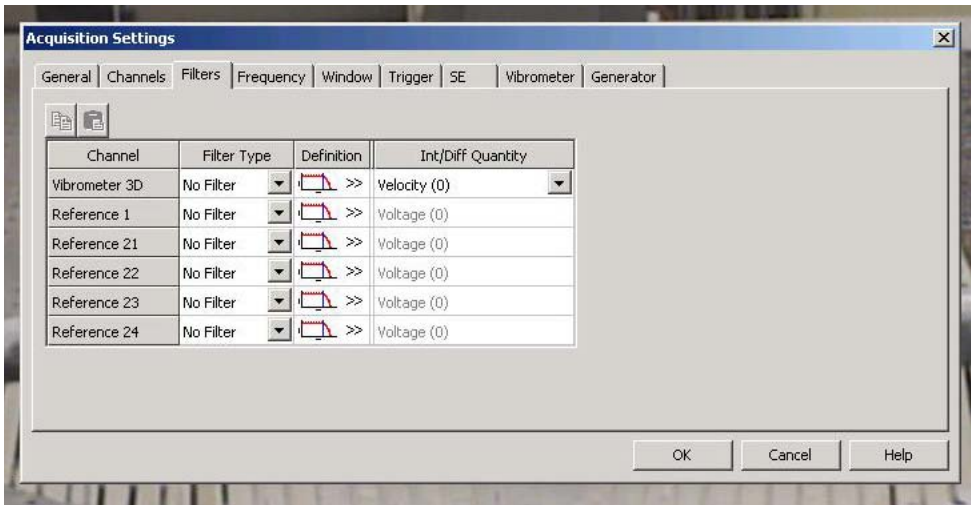

Figure 77: Acquisition Settings Filters Tab

16. Select the *Generator* tab.

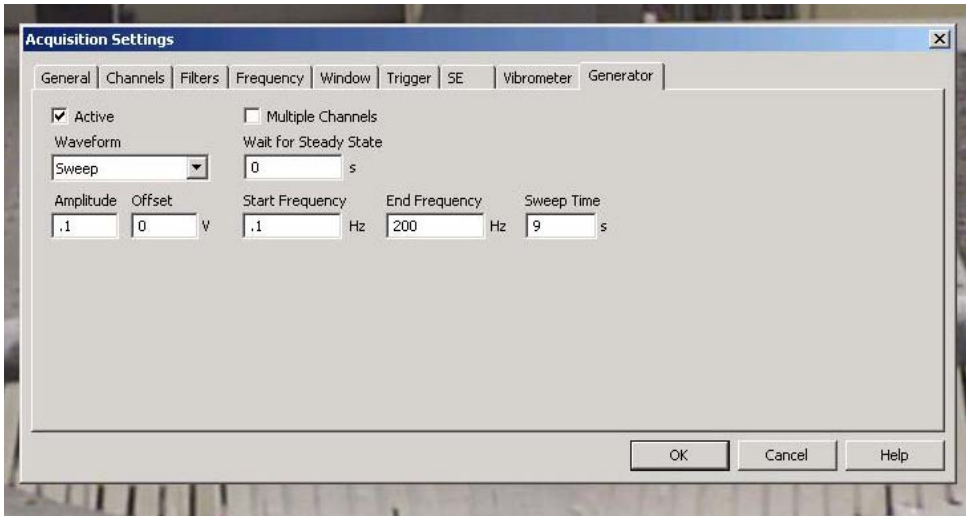

Figure 78: Acquisition Settings Generator Tab

17. Check the box *Active* and choose the waveform desired. For initial scans, a sweep or chirp waveform are common, but many others are available.
18. If applicable, define the *Start* and *End frequency range* and the *Sweep Time*. The Sweep Time may be kept similar to the sample time found in the *Frequency* tab.
19. Choose the lowest possible amplitude of 0.05V initially, and increase from there. Remember that you have turned the amplitude dial off on the amplifier and when you turn the generator on you must increase the amplification, otherwise nothing will happen.
20. When changes to the Acquisition Settings are complete, select *OK*.
21. Turn on the generator using the sine wave icon. Increase the amplitude on the amplifier to the desired amplitude.
22. To perform sample tests, turn on the *Continuous* icon. An analyzer window will appear displaying a graph of velocity vs. time.

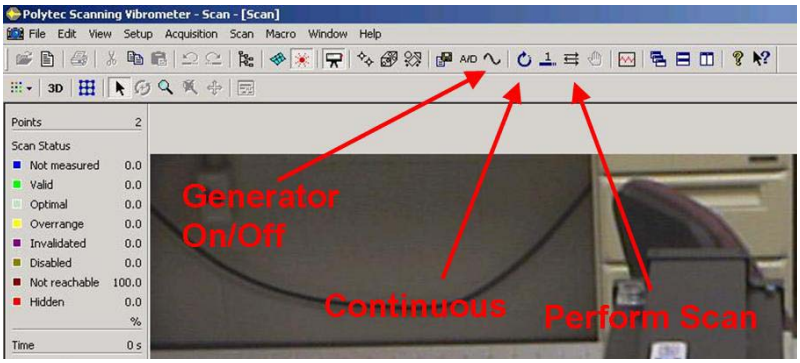

Figure 79: Continuous Scan, Perform Scan Options

23. To see velocity vs. frequency (FFT), select the far left icon in the analyzer window and choose *FFT*.
24. Experiment with the different icons in the analyzer to see what is available.
25. The far right icon is an *Auto Scale* feature that will zoom in/out your graph to create the best fit.
26. When you are satisfied with your scan samples, you are ready to run a scan test
27. Choose either the *Single Shot* or the *Scan* icon.
    a. Single Shot only looks at one specific point and provides the same results you see in the continuous scan sampling done previously.
    b. Scan tests all grid points for the desired frequency or frequency range.
28. When scanning is complete, a message will appear stating the scan is complete and the duration of the scan.
29. Now you may go to the presentation mode to see the results of your scan.

Presentation Mode

1. Toggle into presentation mode by selecting the *Presentation* icon.
2. Experiment with the choices in presentation mode.
3. To see the frequencies of the different modes for your object, select the top left *Change View* icon and choose *Average Spectrum*.
4. To choose only the frequency peaks, select the *Frequency Bands* icon.
5. Using the mouse, drag and select a tight range around each given frequency peak.
6. The peaks will be automatically calculated in a *Frequency Band Definition* toolbox
7. When the calculation is complete, click the top right *X* on that toolbox to close it.
8. A message will appear stating "Band Definition Changed", select *Yes*.
9. The pull down *Frequency Band* toolbar will have the peaks that you found. Select the frequency you wish to view.
10. The animation may be played to see what happens at the respective frequencies. Observe the *X, Y, Z* directions together or separate. You may also zoom and rotate the animation as desired.
11. Animations and graphics may be saved using the *File* pull down menu. To see raw data for all frequencies tested, you may export an ASCII or Universal file. Here you will see all velocity magnitudes and their corresponding frequencies.

Vita

Ensign Leo L. Mendoza Jr. graduated from Old Dominion University in Norfolk, Virginia in May 2006 with a Bachelor of Science degree in Mechanical Engineering. In June 2006, he entered the Graduate School of Engineering and Management, Air Force Institute of Technology. Upon graduation, he will be assigned to NAS Pensacola where he will undergo training as a student naval aviator.

REPORT DOCUMENTATION PAGE

Form Approved
OMB No. 074-0188

1. REPORT DATE *(DD-MM-YYYY)*	**2. REPORT TYPE**	**3. DATES COVERED** *(From – To)*
14 Jun 2007	Master's Thesis	Jun 2006 – Jun 2007

4. TITLE AND SUBTITLE

Damage Considerations of a Flexible Micro Air Vehicle Wing Using 3-D Laser Vibrometry

5a. CONTRACT NUMBER

5b. GRANT NUMBER

5c. PROGRAM ELEMENT NUMBER

6. AUTHOR(S)

Mendoza, Leo L. Jr., Ensign, USN

5d. PROJECT NUMBER

5e. TASK NUMBER

5f. WORK UNIT NUMBER

7. PERFORMING ORGANIZATION NAMES(S) AND ADDRESS(S)

Air Force Institute of Technology
Graduate School of Engineering and Management (AFIT/EN)
2950 Hobson Way
WPAFB OH 45433-7765

8. PERFORMING ORGANIZATION REPORT NUMBER

AFIT/GAE/ENY/07-J13

9. SPONSORING/MONITORING AGENCY NAME(S) AND ADDRESS(ES)

AFRL/VASD
Attn: Dr. Phillip Beran
Bldg 146, 2210 8th St
WPAFB OH 45324 DSN: 785-6645

10. SPONSOR/MONITOR'S ACRONYM(S)

11. SPONSOR/MONITOR'S REPORT NUMBER(S)

12. DISTRIBUTION/AVAILABILITY STATEMENT

APPROVED FOR PUBLIC RELEASE; DISTRIBUTION UNLIMITED.

13. SUPPLEMENTARY NOTES

14. ABSTRACT

In recent years there has been a major push towards a new class of unmanned aerial vehicles: micro air vehicles. A great amount of research has been done towards the aerodynamics, aeroelasticity, construction, and flight characteristics of flexible wing micro air vehicles. However, there has not been much research done regarding possible structural deficiencies of a flexible micro air vehicle wing. The focus of this research is to evaluate the effects of damage on a flexible micro air vehicle wing, particularly its natural frequencies and mode shapes, using three dimensional laser vibrometry. The flexible micro air vehicle wing studied was based on a University of Florida micro air vehicle wing design and was examined using measurements from the Polytec 400-3D Scanning Vibrometer. Comparisons of the wing's natural frequencies and displacements were made between the wing's undamaged and damaged states.

15. SUBJECT TERMS

Micro Air Vehicle, Flexible Wing, Damage, Laser Vibrometry

16. SECURITY CLASSIFICATION OF:			**17. LIMITATION OF ABSTRACT**	**18. NUMBER OF PAGES**	**19a. NAME OF RESPONSIBLE PERSON**
REPORT	**ABSTRACT**	**c. THIS PAGE**			Anthony N. Palazotto, PhD
U	**U**	**U**	**UU**	94	**19b. TELEPHONE NUMBER** *(Include area code)* (937) 255-6565, ext 4599; anthony.palazotto@afit.edu

Standard Form 298 (Rev: 8-98)
Prescribed by ANSI Std. Z39-18